Evaluating the use of Low-Cost Technologies for Pavement Surface Evaluations

by Werner Visser Hattingh

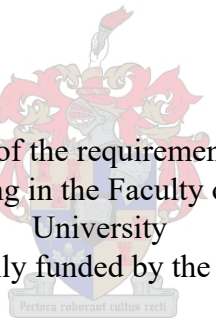

Thesis presented in fulfilment of the requirements for the degree of Master of Engineering in Civil Engineering in the Faculty of Engineering at Stellenbosch University
Partially funded by the NRF

Supervisor: Mr Christiaan Johannes Jurgens

December 2020

Abstract

South Africa has the tenth largest road network in the world, with a total road network of 750 000 kilometres. The Provincial governments are responsible for the regional roads, while local municipalities are responsible for local roads and city streets. Both these management authorities monitor road conditions through a time-consuming visual inspection and reporting process as per the TMH 9 manual.

Current road surface inspection methods used by the South African provincial governments include a two-phase visual inspection. This method can be time-consuming, resulting in increased inspection and maintenance costs. Visual inspections rely on the trained perspective of the assessor. This may lead to inconsistencies between assessors or inspections. Provincial governments in South Africa perform the routine surface inspections on an annual basis which result in high ongoing costs of pavement surface inspections. Alternative pavement inspection methods with low-cost hardware could, therefore, reduce the cost of pavement surface inspections and improve data accuracy and safety.

This thesis evaluates different inspection platforms based on their time, cost and quality performance. The three platforms evaluated include traditional inspection methods (TMH 9), as well as UAV platforms and ground-based vehicle platforms fitted with different low-cost technology types. The investigated technology types include a digital camera, thermal device and LIDAR device.

The evaluation includes the testing of technology types and vehicle platforms to determine the data collection speed limit, the ability of the technology to capture different crack widths and the sensitivity to changing light conditions. The testing highlighted that the digital camera required additional lighting to reduce the sensitivity to changing light conditions.

The required inspection time depends on the maximum platform travel speed until one image pixel becomes blurry. The image blur depends on the shutter speed, field of view, height above the pavement surface and the time-lapse speed of the device. It was determined at two meters above the pavement surface, that the thermal SeekShot Pro (9Hz) can collect data at 68 km/h compared to 19.5 km/h for the GoPro Hero 8 digital camera.

The total cost includes variable costs such as the operator cost, vehicle running cost and exchange rate. A Monte Carlo analysis was followed to determine the most probable cost for each platform and technology type based on different distribution models developed for the cost evaluation. Thermal devices fitted to the different platforms resulted in a lower operating cost for each platform. It was found that the UAV platform has the lowest operating cost, followed by a ground-based vehicle platform and the traditional inspection method.

The quality of each platform is measured via a comparison of the pavement assessment list provided in the TRH 22 manual. The ability of each technology type to identify different distress mechanisms depended on the ability to measure distance and identify different crack widths accurately. It was determined that the thermal device could identify 73.03% of the different distress mechanisms, while the digital camera and LIDAR device could identify 68.54% and 38.58% respectively.

Ultimately the ground-based vehicle platform fitted with a combination of a thermal and LIDAR device proved to be the most suitable for pavement surface evaluations. Using a combination of devices will increase the number of different distress mechanisms identified to 86.14%.

Opsomming

Suid Afrika het die tiende langste pad netwerk in die wêreld met ‘n totale pad netwerk van 750 000 kilometer. Die provinsiale regering is verantwoordelik vir die provinsiale en streeks paaie terwyl die plaaslike munisipaliteit verantwoordelik is vir die stedelike paaie. Beide hierdie entiteite monitor plaveisel kondisies met ‘n tydsame visuele inspeksie proses soos voorgeskryf in TMH 9.

Huidige plaveisel inspeksie metodes wat deur die Suid-Afrikaanse provinsiale regerings gebruik word, sluit 'n twee-fase visuele inspeksie in. Hierdie metode kan tydrowend wees, wat lei tot verhoogde inspeksie- en onderhoudskostes. Beide hierdie visuele inspeksies maak staat op die opgeleide perspektief van die assessor. Dit kan moontlik lei tot teenstrydighede tussen assessore of inspeksies. Provinsiale regerings in Suid-Afrika voer jaarliks die roetine plaveisel inspeksies uit, wat hoë plaveisel inspeksie kostes tot gevolg het. Alternatiewe plaveisel inspeksie metodes met lae-koste tegnologie kan dus die koste van plaveisel inspeksies verlaag en die akkuraatheid van inspeksies verbeter.

Hierdie tesis het verskillende inspeksie platforms geëvalueer volgens hul tyd, koste en kwaliteit. Die drie platforms wat geëvalueer word, sluit in tradisionele inspeksie metodes (TMH 9), UAV-platforms en grondgebaseerde voertuig platforms wat met verskillende lae-koste tegnologieë toegerus is. Die tegnologie tipes het 'n digitale kamera, termiese toestel en LIDAR-apparaat ingesluit.

Die evaluering sluit die toets van tegnologie-soorte en voertuig platforms in om die spoed van data-insameling te bepaal, die vermoë van die tegnologie om verskillende kraak wydtes te identifiseer en die sensitiwiteit vir veranderende lig toestande te bepaal. Die toetse het gewys dat die digitale kamera addisionele beligting benodig om die sensitiwiteit vir veranderende lig toestande te verminder.

Die totale inspeksie tyd hang af van die maksimum spoed wanneer een pixel vaag word. Die maksimum spoed word beïnvloed deur die sluiter spoed van die toestel, die sig wydte van die toestel, die hoogte van die toestel bo die plaveisel oppervlak en die tydsverloop tussen foto’s van die toestel. Dit is bepaal dat op twee meter bokant die sypaadjie kan die termiese SeekShot Pro (9Hz) data teen 68 km/h versamel in vergelyking met 19.5 km/h van die GoPro Hero 8 digitale kamera.

Die koste evaluering sluit veranderlike kostes soos die operateur koste, lopende voertuig koste en wissel koers in. 'n Monte Carlo-analise is gevolg om die mees waarskynlike koste vir elke platform en tegnologie tipe te bepaal, gebaseer op verskillende verspreidings modelle wat ontwikkel is vir hierdie tesis. Die tesis vind dat termiese toestelle wat op die verskillende platforms gemonteer word het gelei tot 'n laer bedryfskoste vir elke platform. Die UAV-platform het die laagste bedryfskoste gevolg deur 'n grond voertuigplatform en die tradisionele inspeksie metode.

Die kwaliteit van elke platform word gemeet aan die lys van plaveisel inspeksies wat in die TRH 22-handleiding voorsien word. Die vermoë van elke tegnologie tipe om verskillende defekte te identifiseer, hang af van die vermoë om afstand akkuraat te meet en verskillende kraak wydtes te identifiseer. Dit is bepaal dat die termiese toestel 73,03% van die verskillende defekte identifiseer, terwyl die digitale kamera en die LIDAR-toestel onderskeidelik 68,54% en 38,58% identifiseer.

‘n Grond voertuigplatform met 'n kombinasie van 'n termiese en LIDAR-apparaat sal die geskikste wees vir die evaluering van plaveisel oppervlaktes. Dit sal die aantal verskillende defekte wat geïdentifiseer kan word, verhoog na 86,14%.

Acknowledgements

I want to acknowledge the exceptional leadership of my research supervisor, Mr C. Jurgens and Co-supervisor, Prof. J.A. Wium, for their diligent efforts to ensure that this thesis is completed.

I would like to thank and record my deep appreciation to my family. First, to my parents - JP Hattingh and Ria Hattingh - who have unconditionally supported me financially; helped with the collection of data and testing of devices during the lockdown; and encouraged me throughout my studies. To my brother Johan who supported me in making this journey more worthwhile. To my fiancé Carla for motivating and supporting me throughout this thesis project.

I would like to acknowledge the financial support from the Department of Civil Engineering at Stellenbosch University and the National Research Fund (NRF) that made it possible to complete this thesis.

My gratitude extends towards Stephan Olivier who provided and helped me with the UAV operations, Sarel van den Berg who lend me his thermal device and all my friends who remained steadfast and supportive and all the industry professionals who provided valuable inputs towards this thesis.

Finally, my greatest thanks go to the Lord God Almighty for His motivation, guidance, gifts and the opportunities He has given me during this thesis.

List of Abbreviations

km – Kilometre

SANRAL- South African National Roads Agency Limited

UAV- Unmanned Aerial Vehicle

AS- Asphalt surfacing

SE- Seal

CS- Cape seal

SL – Slurry

Pixel- Picture element

DTM – Digital Terrain Model

MST – Minimum Spanning Tree

3D – Three Dimensional

DHDV – Digital Highway Data Vehicle

WMA – Warm Mix Asphalt

HMA – Hot Mix Asphalt

GPU – Graphics Processing Unit

Fps – Frames per second

TP – True Positive

FP – False Positive

TN – True Negative

FN – False Negative

GUI – Graphical User Interface

VCI – Visible Condition Index

IPP – Image Processing Program

Table of Contents

List of Tables

List of Figures

List of Equations

Chapter 1: Introduction and Overview

1.1 Background

South Africa has the tenth largest road network in the world, with a total road network of 750 000 kilometres (Department: National Treasury of South Africa, 2014; Kannemeyer, 2016). The road network consists of the following (Department: Transport, 2018; SANRAL, 2019):

- 163 472 kilometres of paved roads,
- 586 528 kilometres of gravel roads of which
- 168 000 km is urban roads
- 366 872 km is non-urban roads.

The occurrence of distress in the pavement surface is inevitable due to the number of load combinations travelling over the road during its useful life. Areas of distress are typically identified through road surface inspections and recorded through manual data entries. Pavement inspections and manual data entries can, however, be a costly and unsafe procedure to ensure road maintenance management.

Regular inspections to evaluate road surface conditions is often the most efficient and cost-effective way to maintain good road standards (Gavilán *et al.*, 2011). Distress measurements' main attributes are the type of distress, the degree of distress and the extent of the distress (Roads Coordinating Body, Committee of Transport Officials; and Road Asset Management Systems Subcommittee, 2016). Cracking of the road surface occurs during the first stages of worsening road conditions. The detection and monitoring of cracks can, therefore allow appropriate maintenance, resulting in large savings compared to rebuilding a road section (Gavilán *et al.*, 2011).

In South Africa, the provincial government is responsible for the regional roads, while the local municipalities are responsible for local roads and city streets. Both these management authorities monitor road conditions through a time-consuming visual inspection and reporting process, as stated according to the TMH 9 manual. The national government is responsible for the national roads and monitor its road conditions with a vehicle using laser and ultrasonic sensors to capture road information. The devices can be complex to operate and, coupled with expensive calibration, results in expensive road measurements (SANRAL, 2014).

Visual inspections and checklists for each road section need to be completed during the road surface inspections procedure. The road evaluation is performed from two perspectives the first, a road user perspective, this includes the drivability of the road. The second from an engineering perspective, this includes the usability of the road's structure and surface (TMH 9, 2016).

The monitoring of road conditions requires intensive professional expertise (Zhang *et al.*, 2016). Remote sensing offers pavement managers a cost-effective method to assess large areas in little time (Schnebele *et al.*, 2015). However, current remote sensing inspections include expensive hardware which requires experienced personnel to operate these systems.

1.2 Problem Statement

The current road surface inspection methods used by the South African provincial governments include a two-phase visual inspection. Phase one is the preliminary network analysis to obtain an overview of the condition of the road network. Phase two is a walkthrough inspection of the problem sections using the traditional visual inspection method with a checklist. This method can be time-consuming, resulting in high inspection costs. Both visual inspections rely on the trained perspective of the assessor. This may lead to inconsistencies between assessors or inspections. The completed checklists of visual inspections are electronically processed for record-keeping. This could lead to human errors in the process.

Automated systems to detect cracks as used in many parts of the world are typically only suitable for detecting wide cracks in pavements with thick asphalt surfacing, and are, therefore, not generally suitable for use in South Africa (SANRAL, 2014). Provincial governments in South Africa perform the routine surface inspections on an annual basis which result in high costs of pavement surface inspections. Alternative pavement inspection methods with low-cost hardware could reduce the cost of pavement surface inspections and reduce inspection inconsistencies. Automated systems have the potential to be developed for South African pavement types, and typical distresses.

1.3 Purpose of the Thesis

Automating the process of distress detection and monitoring could improve the effectiveness and efficiency of pavement management by reducing the time professionals spend during road inspections and monitoring areas of distress. This thesis evaluates different low-cost technology

types fitted to an Unmanned Aerial Vehicle (UAV) and ground-based vehicle platform to identify pavement surface defects.

1.4 Aims and Objective

This thesis aims to evaluate low-cost technology alternatives for pavement inspections at a network level that can be used by provincial governments to improve their Pavement Management System (PMS). The research will improve upon the current visual inspections and manual data entry methods used by visual inspectors. This will improve the efficiency and cost-effectiveness of distress management on road networks.

The aim of this research is reached through the following objectives:

- Research current pavement inspection techniques
- Developing an image processing program to evaluate collected test data
- Collecting test data with different technology types and data collection platforms
- Evaluate available technology types and data collection platforms based on time, cost and quality
- Determining the requirements and limitations of the different data collection platforms

1.5 Scope and Limitations

In this thesis, cost-effective technologies are evaluated for the use of pavement inspections at a network level in Pavement Management Systems. The network-level analysis serves as a preliminary evaluation of the entire road network to identify possible problem areas in road sections.

The evaluation will include a semi-autonomous distress identification program based on image thresholding techniques. The image processing program will be used to evaluate various technology platforms. This thesis will focus on distresses during the road life-cycle use and not distresses during the road's construction. Rigid pavements are not readily used in South Africa; therefore, will this thesis focus on flexible pavement surfaces.

This thesis is subjected to various limitations. The researcher is limited to only obtain data from a specific road section. The COVID-19 pandemic resulted in limited access to roads for defect identifications and traditional inspection method evaluations. The road section only contained a limited number of distress mechanisms.

Digital cameras will be tested using a GoPro Hero 8 Black and thermal devices using a Major Tech MT 2005. Limited funding resulted in the theoretical evaluation of LIDAR technologies.

1.6 Thesis Methodology

The activities listed in this section show the procedure followed to complete all tasks required in the thesis to perform the research and reach a proper conclusion. The project roadmap can be seen in Figure 1.

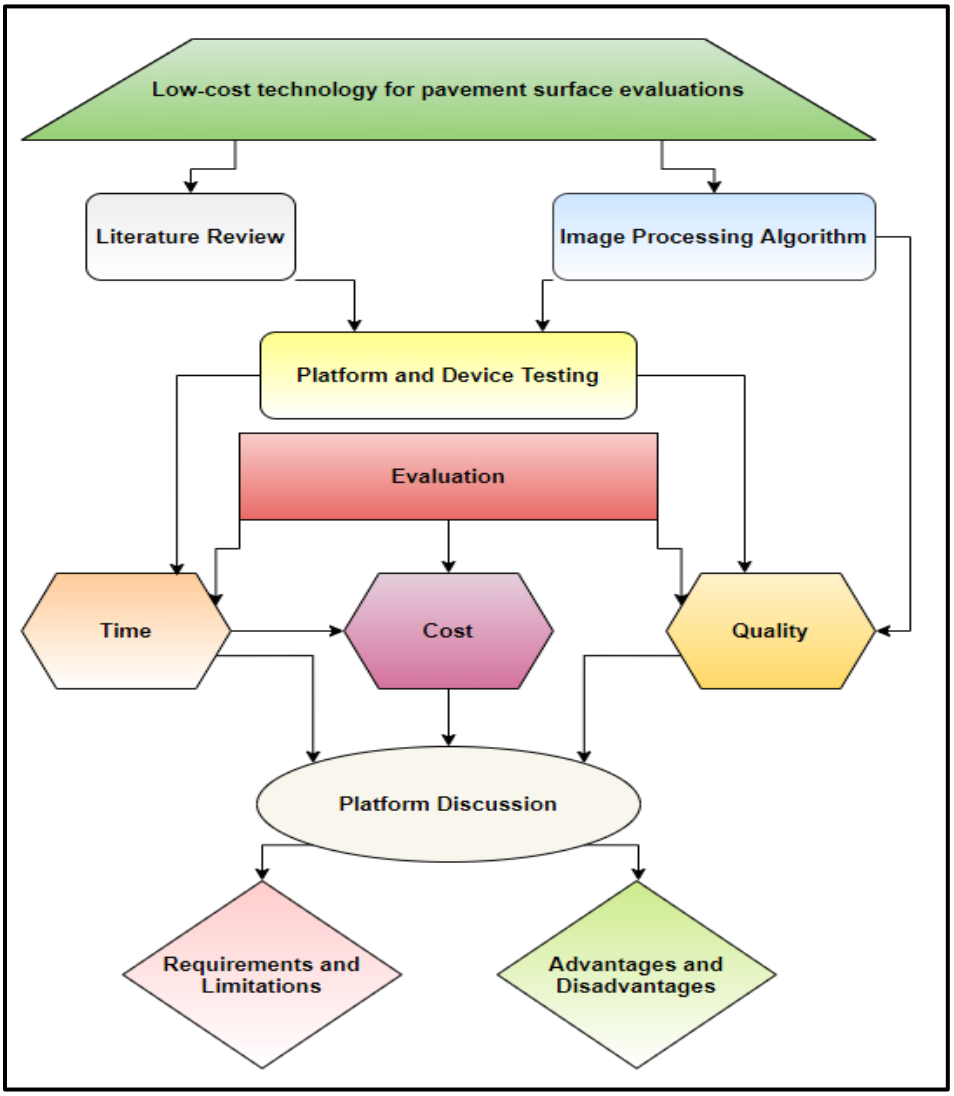

Figure 1: Research Roadmap

This thesis evaluates the use of low-cost technologies for pavement surface evaluations in terms of time, cost and quality. The steps in Figure 1 are followed to evaluate the technologies and provide valuable recommendations for future work. Throughout the thesis, there will be a continuous collaboration with industry professionals to gather information, data and industry viewpoints regarding Figure 1.

This thesis's literature study investigates the South African road network and its pavement classifications, inspection methods, distress mechanisms, distress identification techniques for each platform, technological devices available for inspections, and different distress identification software. The literature review determines the devices and tests required to evaluate the platforms and devices.

A semi-autonomous distress identification program is developed to help the user consistently evaluate the use of low-cost technologies for pavement surface inspections. The program will be used during testing of the technology types and platforms, and the quality evaluation of the low-cost technologies.

The different pavement inspection platforms are evaluated according to time, cost and quality. Each platform's quality will be measured through the pavement assessment list provided in the TRH 22 manual. The three platforms to be evaluated include traditional inspection methods, UAV platforms and moving vehicle platforms fitted with different low-cost technologies.

The platform discussion includes the requirements and limitations of each technology determined through the technology evaluation and the advantages and disadvantages of each technology and platform. The requirements for each technological platform to perform the most accurate and efficient pavement surveys will be determined. This will ensure efficiency and cost gains in pavement management systems.

1.7 Thesis Layout

Chapter 1: Chapter 1: Introduction and Overview – This chapter includes the background of the thesis, problem statement, purpose of the thesis, aims and objectives, scope and limitations, ethical considerations and the thesis layout.

Chapter 2: Overview of the South African Road Network and Current Inspection Systems – This chapter focuses on the broader research of the South African road network, pavement classifications, typical distress mechanisms in road surfaces and current inspection systems

Chapter 3: Existing Literature on Pavement inspections - This chapter focuses on the research of pavement inspection methods, inspection platforms, distress identification techniques for each platform, technology types available for inspections and different distress identification software.

Chapter 4: Image Processing Program Development – This chapter discusses the program structure, class development, general operation and output of the image processing program developed.

Chapter 5: Testing of platforms and technology types – This chapter discusses the preliminary platform tests to identify problem areas and solutions before the technology evaluation commences.

Chapter 6: Time, Cost and Quality Evaluation – This chapter evaluates the use of digital cameras, thermal cameras and LIDAR devices fitted to different platforms for pavement surface inspections in terms of time, cost and quality.

Chapter 7: Discussion of Evaluation Results - This chapter discusses the vehicle and UAV platform fitted with different technology types. The discussion will include general remarks on each platform, advantages and disadvantages.

Chapter 8: Conclusions and Recommendations – This chapter will conclude the thesis and provide recommendations for future work.

Chapter 2: Overview of the South African Road Network and Current Inspections Systems

South Africa has an extensive road network ranking tenth-largest in the world. South Africa's road network comprises a total length of 750 000 kilometres, with 163 472 kilometres of paved roads and 586 528 kilometres of unpaved roads (Kannemeyer, 2016). Both the paved and unpaved roads require maintenance and management. This thesis focuses on the evaluation of paved road surfaces only.

The road network management is divided into four spheres: The South African National Roads Agency Limited (SANRAL), the Provincial governments, district municipalities, and local municipalities, including the 8 Metropolitan Municipalities. SANRAL is responsible for the national roads, which include 22 197 kilometres of paved roads. The provincial government is responsible for the provincial and regional roads, including 48 988 kilometres of paved roads, and metropolitans are responsible for the municipal roads within the metropolitan boundaries, including 51 682 kilometres of paved roads. The District and Local municipalities are responsible for all the municipal roads, including 40 648 kilometres of paved roads(SABITA, 2018)(Western Cape Government, 2019). The distribution of the paved road network in South Africa can be seen in Figure 2.

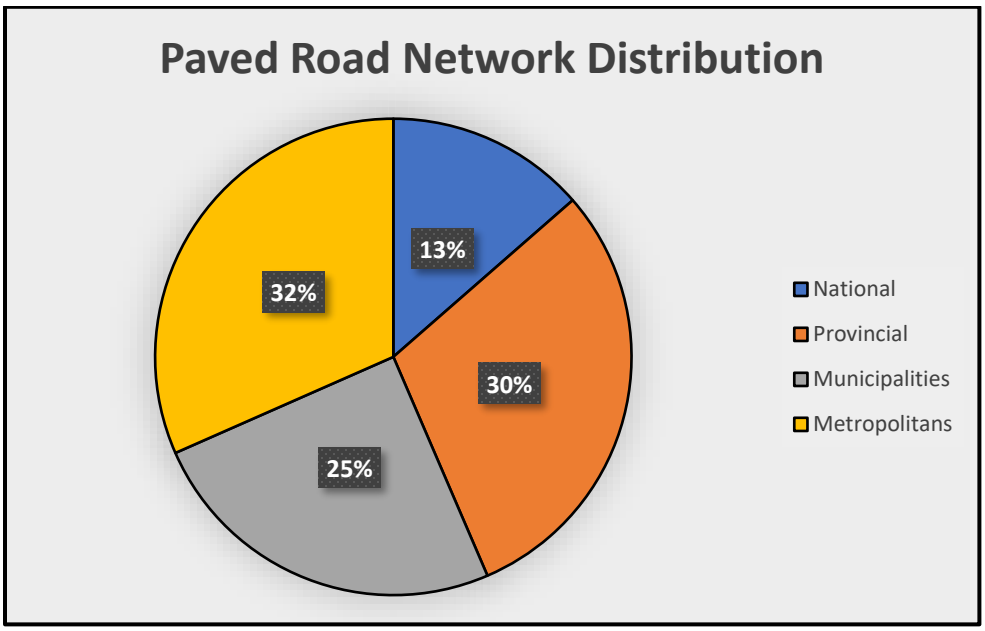

Figure 2: Paved Road Network Distribution of South Africa(Carter *et al.*, 2018; SABITA, 2018)

South Africa has nine provinces, each province with its own government responsible for maintaining and managing the road network. The provincial roads link towns to the national road network and are indicated with an R prefix in the route number.

The paved road distribution per province can be seen in Figure 3 (SABITA, 2018). From Figure 3, it can be seen that KwaZulu-Natal has the longest paved provincial road network in South Africa, while the Western Cape province has the second-longest provincial road network.

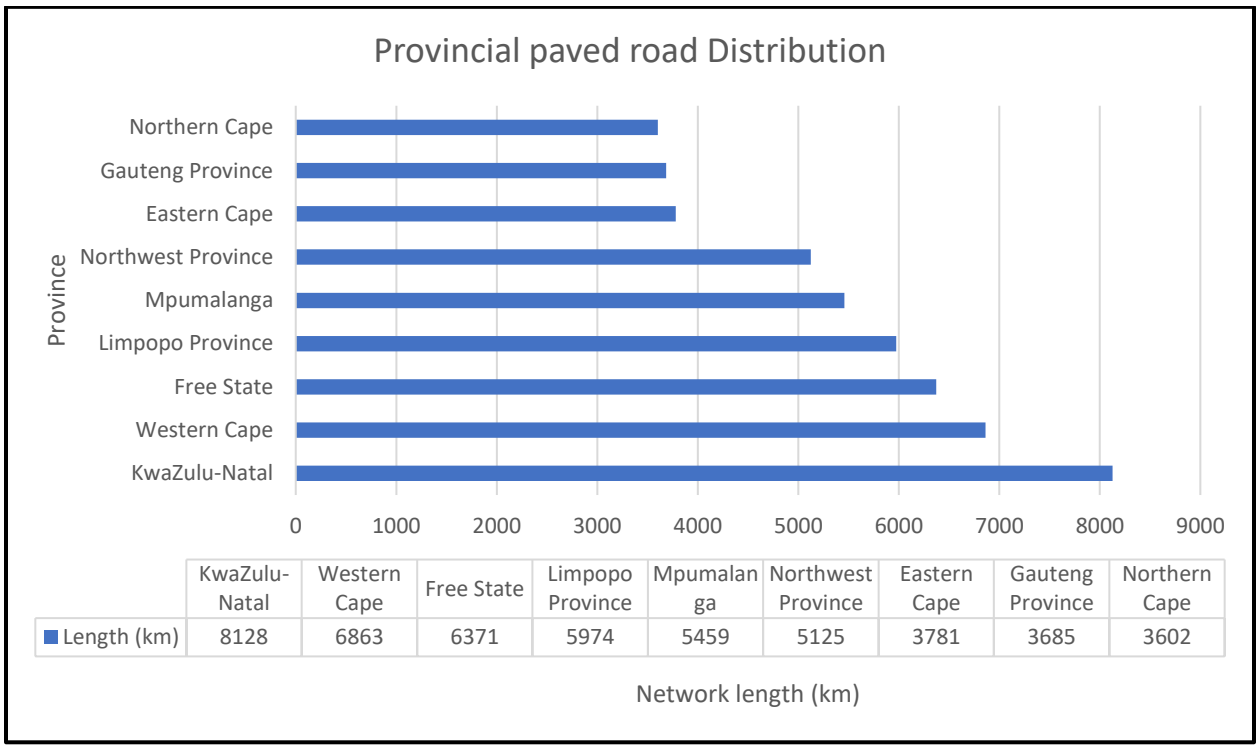

Figure 3: Provincial Paved Road Distribution of South Africa (SABITA, 2018)

The visual condition index (VCI) is calculated as a combination of all the destresses on the road section and can be categorised as one of the following (Western Cape Government, 2019):

- Very good (VCI between 85 and 100%)
- Good (VCI between 70 and 85%)
- Fair (VCI between 50and 75%)
- Poor (VCI between 30 and 50%)
- Very poor (VCI between 0 and 30%)

Figure 4 indicates the overall condition of the provincial road network of South Africa, according to the 2017 VCI results (Ross and Townshend, 2018). Figure 4 indicates that 49% of the provincial road network across South Africa is poor or fair, with 40% of the network in a good or very good condition. This indicates that the provincial governments are struggling to maintain the road network and that the provincial road network's general road condition is concerning (Department: National Treasury of South Africa, 2014; Ross and Townshend, 2018).

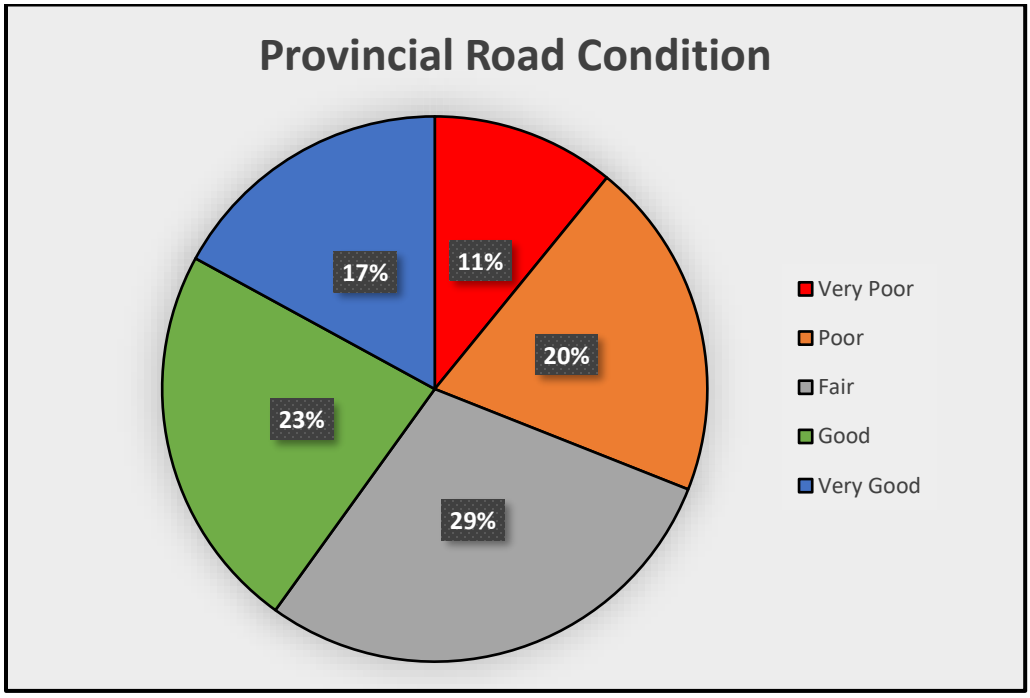

Figure 4: Overall provincial road conditions in 2017 (Carter et al., 2018; Ross and Townshend, 2018)

According to the 2017 visible condition index (VCI), the condition of the provincial road networks can be seen in Table 1 (Ross and Townshend, 2018). Table 1 indicates that the Limpopo and Gauteng Provinces had the best maintained provincial road network, while the Free State and Northwest have the worst provincial road networks in South Africa. Northwest Province has the highest percentage of the road network in a very poor condition.

Table 1: Provincial Road Network Condition (Ross and Townshend, 2018)

Provincial Pavement Condition						
Authority	**Very Poor (1)**	**Poor (2)**	**Fair (3)**	**Good (4)**	**Very Good (5)**	**Total**
Free State	33,0%	33,0%	27,0%	6,0%	1,0%	2,09
Northwest	39,6%	11,5%	15,6%	21,2%	12,0%	2,54
Eastern Cape	6,0%	35,7%	36,3%	21,8%	0,2%	2,75
Mpumalanga	6,0%	28,0%	35,0%	21,0%	10,0%	3,01
KwaZulu-Natal	7,0%	29,0%	34,0%	16,0%	14,0%	3,01
Northern Cape	1,0%	13,0%	32,0%	32,0%	22,0%	3,61
Western Cape	2,0%	11,0%	29,0%	36,0%	22,0%	3,65
Gauteng	0,8%	9,3%	33,5%	26,3%	30,1%	3,76
Limpopo	2,5%	10,6%	18,0%	26,8%	42,1%	3,95

2.1 Pavement classification

A road or pavement is designed with four primary functions in mind. The four functions provide a reasonably smooth riding surface, provide waterproofing, protect the subgrade, and provide adequate skid resistance (Adlinge and Gupta, 2013).

Adlinge and Gupta (2013) describe a pavement as any surface which is paved; "a floor or covering of solid material, laid to make a hard and convenient surface for travel; a paved road or sidewalk; a decorative interior floor of tiles coloured bricks." Pavements can be categorised into the three following categories: unpaved, rigid and flexible pavements (Adlinge and Gupta, 2013). Unpaved roads are predominantly gravel roads

A paved road can be any road that is surfaced to be waterproof and improve the road's riding quality. Paved roads have either rigid or flexible road surfaces. **Rigid pavements** can be placed on top of weaker supporting layers due to the concrete top layer's high stiffness. Rigid pavements are not readily used in South Africa. Reinforcing steel bars can reduce the number of joints (Adlinge and Gupta, 2013).

Figure 5 shows that a rigid road comprises of the normal layer works of a pavement, surfaced with a concrete top layer. This pavement type is more rigid than flexible pavements due to the high modulus of elasticity of the concrete material (Adlinge and Gupta, 2013).

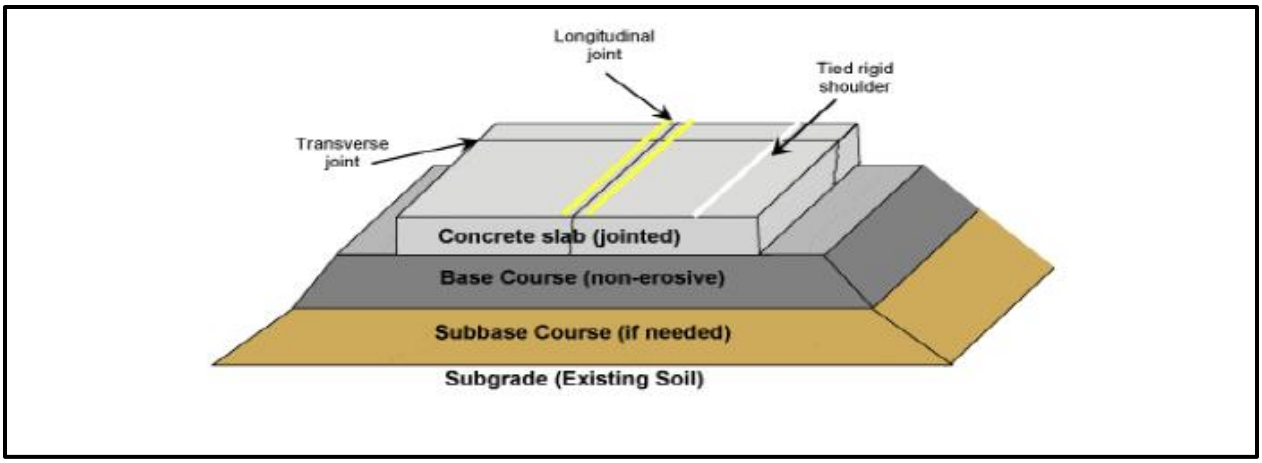

Figure 5: Rigid pavement structure (Mishra, 2019)

The performance of rigid pavement structures can be affected by environmental factors like temperature and moisture, the structure's material characterisation, the elastic model of the structure, and the traffic contact pressures.

Distress mechanisms present in rigid pavements include (Bhattacharjee, 2015):

- Slab cracking
- Faulting
- Spalling
- Longitudinal cracks
- Durability cracks
- Pumping and bleeding
- Shrinkage cracks
- Pop-outs

Flexible pavements are designed to flex under the axle load of a vehicle. Flexible pavements consist of multiple granular material layers topped with one or more bituminous surface layers. Figure 6 shows the typical structure of flexible pavements. The surface course is typically the waterproof bituminous surface. The load spreading pattern changes from one layer to another, allowing the pavement to flex under load (Adlinge and Gupta, 2013). The most rigid material will be in the top layers, while the most flexible material will be in the lower layers.

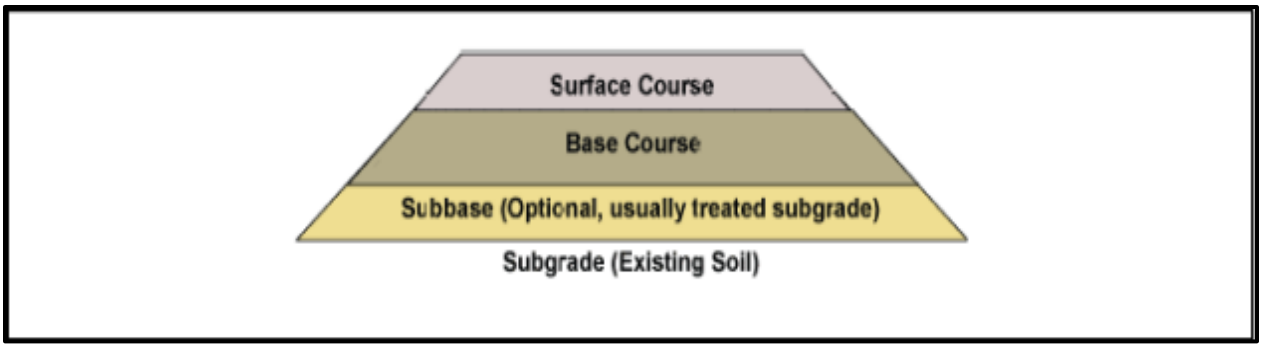

Figure 6: Flexible pavement structure (Mishra, 2019)

2.1.1 Flexible Pavement Assessment List

Flexible pavement structures should be evaluated according to the different distress mechanisms in Figure 7. Trained visual assessors in South Africa currently use the assessment list in Figure 7.

Figure 7 indicates the essential and desired distress mechanisms in traditional inspection methods (TMH 9, 2016). The low-cost technology types fitted to different vehicle platforms must identify the essential items in Figure 7. Pavement network analysis focuses on the structural assessment of pavement surfaces.

VISUAL ASSESSMENT ITEM		ASSESSMENT REQUIREMENTS	
		ESSENTIAL	DESIRABLE
SURFACING ASSESSMENT			
Texture			X
Voids			X
Surfacing failure		X	
Surfacing cracks		X	
Aggregate loss		X	
Binder condition		X	
Bleeding/flushing		X	
STRUCTURAL ASSESSMENT			
Block/stabilisation cracks		X	
Longitudinal/slip cracks		X	
Transverse cracks		X	
Crocodile cracks		X	
Pumping		X	
Rutting		X	
Undulation/settlement			X
Patching		X	
Failures/potholing		X	
FUNCTIONAL ASSESSMENT			
Riding quality			X
Skid resistance			X
Drainage:	Surface		X
	Side		X
Shoulders:	Unpaved	X	
	Paved		X
Edge breaking		X	
OVERALL CONDITION		X	

Figure 7: Visual assessment items for flexible pavements from TMH 9, (2016)

2.2 Flexible Pavement Distress Mechanisms

Flexible pavement distress mechanisms can be extremely complex and varying. Describing each distress has been simplified by only recording the main characteristics of a distress mechanism. The main characteristics of distress mechanisms are the degree of distress, the extent of the distress and the type of distress (TMH 9, 2016).

2.2.1 Degree of the Distress Mechanism

The degree of distress should be recorded as the best average of the severity of distress in a road section with varying distresses (TMH 9, 2016). The degree can be classified within the range of 1-5. One is a slight degree; this is typically the start of distress. Five being severe distress, this will typically be the worst degree possible.

Table 2 provides guidelines according to TMH 9 to determine the degree of a distress mechanism. The degree of distress is primarily marked either a 1, 3 or 5; if uncertain, a 2 or 4 can be marked (TMH 9, 2016).

Table 2: Description of Degree classification (TMH 9, 2016)

Degree	Severity	Description
0	-	Distress not present
1	Slight	First signs of distress visible
2	Slight to warning	
3	Warning	Distress is distinct. Requires maintenance
4	Warning to severe	
5	Severe	Distress is extreme. Immediate attention required

2.2.2 Extent of the Distress Mechanism

The extent of distress can be a measure of how common the distress appears on the road section. The extent of distress should be recorded in the traffic lane where the most significant distress will be possible. Distress occurrence is most probable in the slow-moving lanes due to the high number of axle-loads carried in the slow lane. The extent of distress can be classified within the range of 1-5. One being a limited occurrence, three being scattered occurrence and five indicating the extensive occurrence of distress over the road section (TMH 9, 2016). Table 3 provides guidelines according to TMH 9 to determine the extent of a road segment's distress.

Table 3: Description of extent classification (TMH 9, 2016)

Extent	Description
0	No distress present
1	Limited occurrence.
2	Scattered occurrence over parts of the road segment
3	Scattered occurrence over most of the road segment
4	Frequent occurrence over a large road segment
5	Extensive occurrence

2.2.3 Types of Distress

Types of distress can be categorised into three categories: surfacing distress, structural distress and functional distress. Detailed descriptions of each distress can be found in the TMH 9 manual; a summary of each distress category is highlighted in this thesis (TMH 9, 2016).

I. Pavement Surfacing Defects

Paved roads can be surfaced by the following flexible surfaces: asphalt surfacing (AS), seal (SE), cape seal (CS) and slurry (SL). Visually distinguishing between the different types of surfaces can be a difficult task. Therefore, a database containing the actual surfacing types is kept in the maintenance files. Common surface distress mechanisms can be classified using the six following items (TMH 9, 2016):

- Texture
- Voids
- Surface failures
- Surface cracks
- Aggregate loss
- Binder condition and
- Bleeding
- Surface deformation

The surface texture mainly depends on the amount of binder and the aggregate size present in the surface layer. The voids in the road surface describe the open spaces between aggregates in the road surface. The amount of surface voids is influenced by the aggregate size and the amount of binder present. Surface failures occur due to the loss of binder and aggregates in the surfacing layer, exposing the underlying layer. The difference between surface failure and aggregate loss is during aggregate loss; the binder remains on the surface. Surface cracks occur due to aged binders where the binder has lost the binding ability it was designed for. Surface cracks form by shrinkage of the bituminous surface due to decreased binder volume on the surface. Aggregate loss occurs due to the abrasive action of traffic on the road surface. In severe cases of aggregate loss, the underlying layer can be exposed; this could result in surfacing failures (TMH 9, 2016). A description of aggregate loss for different pavement surfaces can be seen in Table 4.

Table 4: Aggregate loss description for different surfaces (TMH 9, 2016)

Degree	**Description**		
	Asphalt surfacing	**Slurry seal**	**Stone seal**
5	Disintegrating asphalt layer over large areas	Slurry loss over large areas	Loss of stone over large patches
3	Disintegrating asphalt layer over small areas	Aggregate loss over small areas which is visible from a moving vehicle	Stone loss over a small area
1	Little loss of aggregate, which is difficult to identify	Little aggregate loss, which is only visible from a close distance	Little stone loss, which is difficult to identify from a vehicle

Binder conditions can be assessed through the colour and the stickiness of the binder. It is required to remove some aggregate from the road surface to assess the binder condition and better understand the binder itself. Bleeding occurs when the binder passes through the aggregates towards the road's surface, reducing the voids and texture depth of the surface (TMH 9, 2016).

II. Structural Pavement Defects

Structural defects normally occur near the end of pavement service life due to the number of axle load passes over the road surface. Structural defects decrease the design strength of the road, therefore decreasing the design life. Structural defects are visible on the road surface through the following (TMH 9, 2016):

- potholes
- patching
- undulation
- rutting
- pumping
- crocodile cracks
- transverse cracks
- longitudinal cracks
- block cracks

Potholes are bowl-shaped holes in the road surface which start in the top layer and progress through to the lower layers. Potholes occur due to disintegrating pavement layers under the loading of traffic. A patch is a block of pavement surface that has been replaced. Patches are used to repair distress areas and, in some cases, cause distress for surrounding pavement areas. Rutting can be described as the displacement of surface materials to create a channel in the wheel path. Rutting occurs when the underlying layers of the pavement structure have failed. The width of the rut can determine the layer of failure. Pumping occurs after water ingress in the pavement's underlying layers when fine materials are pumped to the surface through existing cracks (Adlinge and Gupta, 2013; TMH 9, 2016).

Crocodile cracks are interconnected, irregular shaped small pieces of the pavement caused by the base layers' failure due to repetitive traffic loading. Crocodile cracks can be the start of rutting and finally result in potholes. Transverse cracks are typically perpendicular across the road's surface and are regularly spaced over a road section. Transverse cracks occur due to shrinkage of the stabilised cemented layers. Longitudinal cracks are normally parallel to the centreline of the road and not in the normal wheel path. Longitudinal cracks can occur due to embankment failure or active clay in the subgrade layers, resulting in the slip of underlaying road layers.

Block cracks are a crack pattern in the surface dividing the pavement surface into rectangular blocks, which can occur due to the lack of compaction of the underlying layers during construction (MTAG, 2003; Adlinge and Gupta, 2013).

III. Functional Pavement Defects

The functional evaluation of a road surface includes factors governing travel speed, safety, and comfort of the road. The factors include edge braking, shoulder conditions, surface drainage, skid resistance and riding quality (TMH 9, 2016).

Riding quality can be defined as the general extent to which a road user experiences a ride that is either smooth or comfortable or bumpy and unpleasant. The unevenness of the road profile can determine the riding quality. Problems contributing to poor riding quality can include (TMH 9, 2016):

- Corrugation
- Patching
- Potholes
- Undulation
- Rutting

Skid resistance is the general ability of the pavement surface to prevent skidding when the surface is wet. The surface texture or roughness predominantly determines skid resistance. Skid resistance can be described as either very poor, fair or very good. Bleeding and polished aggregates can result in poor skid resistance (TMH 9, 2016).

Surface drainage is the measure of the road's ability to clear the riding surface of water or liquids. Surface drainage only includes the area up to two meters from the outside yellow line; this does not include side drains. Surface drainage can be described as either inadequate, warning or adequate. Horizontal and vertical alignment, road shoulder and rutting can contribute to inadequate surface drainage (TMH 9, 2016).

The surface breakaway causes edge breaking at the outside edge of the paved surface. Edge breaking can be due to poor or no management of the unpaved shoulders. Edge breaking is measured as degree 1 where slight edge breaking occurs, degree 3 where significant edge breaking occurs and degree 5 where severe edge breaking occurs, which is a safety hazard (TMH 9, 2016).

2.3 Inspection methods

Various road inspection methods are used to monitor road conditions' degradation through cracks, potholes, and other distress mechanisms. Road conditions are considered from the road user viewpoint and the road engineer viewpoint (TMH 9, 2016). The Western Cape provincial government uses a two-phase approach to visual inspections. The visual pavement inspection process can be seen in Figure 8. Phase one of the visual pavement inspection commences by dividing the road network into sections of two kilometres, followed by the network analysis.

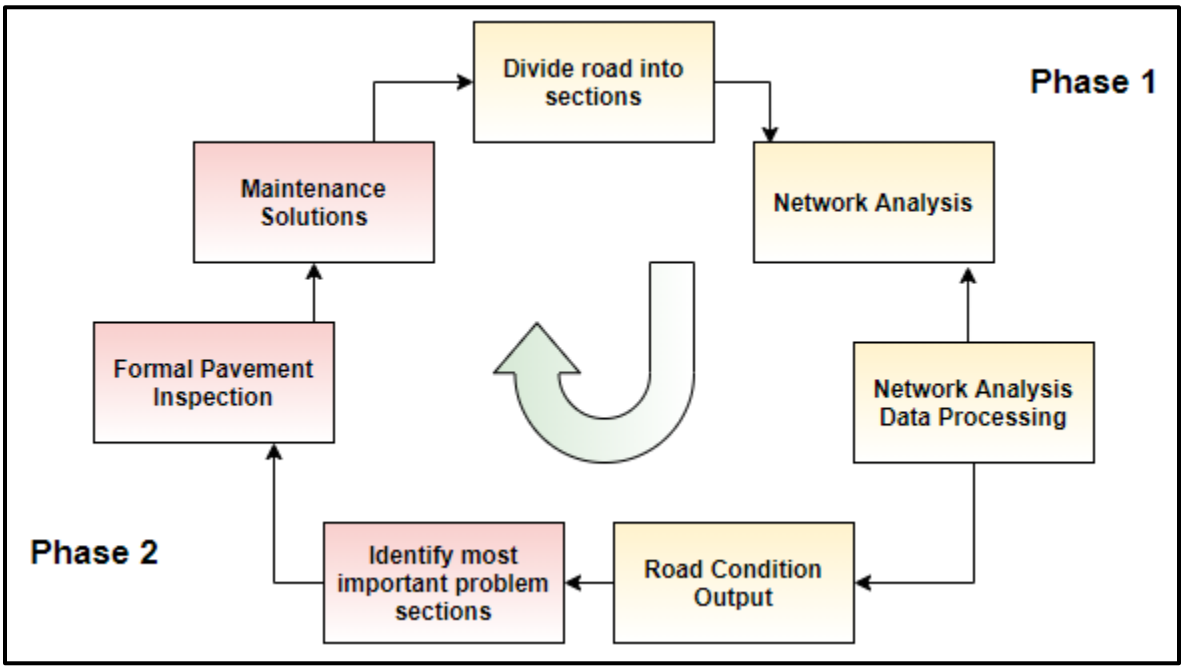

Figure 8: Pavement Surface inspection process (Adapted from (SANRAL, 2018)*)*

The network analysis serves as a preliminary evaluation to identify possible problem areas in road sections. The network analysis comprises of a formal drive-through evaluation of the road section to identify possible problem areas on the road surface. The trained assessor is required to indicate problem areas on a specific form for each section according to the TMH 9 manual (TMH 9, 2016).

The completed forms are processed once the road evaluation is finished. The typical output from the network analysis indicates the overall road condition as a percentage value using Equation 1.

Equation 1: Visible Condition Index

$$Visible\ Condition\ Index\ (\%) = (1 - x) \times 100$$

Where x is the value of problem areas of the road surface.

The network data is processed to determine a Visible Condition Index (VCI) for each road section. Phase two commences by identifying the problem sections in the road network; this will be sections with very poor, poor or fair VCI's. Once the network analysis is completed, the lowest road condition areas are assessed through a formal pavement surface inspection procedure focusing on repair and design requirements. The formal inspection is done through contracted personnel with the required expertise and training to perform an in-depth assessment and provide maintenance solutions for each road section.

Chapter 3: Existing Literature on Pavement Inspections

Formal pavement inspections in South Africa are done according to the visual evaluation guidelines for flexible paved roads documented in the TMH 9 manual. The road conditions are evaluated according to condition indices, maintenance and rehabilitation, and network-level priorities (TMH 9, 2016). Traditional road inspections are performed by trained visual assessors who travel the road segments and perform a visual evaluation of the road surface. The assessors are trained and calibrated annually to minimise subjectivity during assessments (TMH 9, 2016).

The TMH 9 manual states visual assessments of roads should be done towards the end of the rainy season or in cooler months (TMH 9, 2016). This ensures good visibility of distress conditions on the surface. Assessments are limited to be completed within three months; daily road sections should not exceed 130 kilometres, inspections need to be performed at the maximum speed of 20 km/h and inspectors should drive on the road shoulder where possible. Therefore, visual inspections can be time-consuming and expensive to complete for large road networks like the South African road network.

The visual assessment should be independently checked to ensure the visual evaluation is correct. The sample should include approximately 10% of all the roads assessed by the specific assessor. Visual inspection data is processed using a computer and ranked according to the highest priority (TMH 9, 2016).

The most common inspection method used is human visual inspections, where the inspector is driving the section of the road doing the inspection (Medina, Gómez-García-Bermejo and Zalama, 2017). While performing the visual inspection, the inspector can be exposed to high safety risks and concentrate on different areas simultaneously while driving. Distress areas can, therefore, be omitted due to different areas of concentration.

Figure 9 is an example of the visual assessment checklist to be completed by a trained assessor. The checklist is completed for each road segment where after the checklist is processed by a computer. The accuracy of the visual assessment depends on the frequency of stops to examine the road surface. The frequency depends on the road condition and variability of distress over the road segment (TMH 9, 2016).

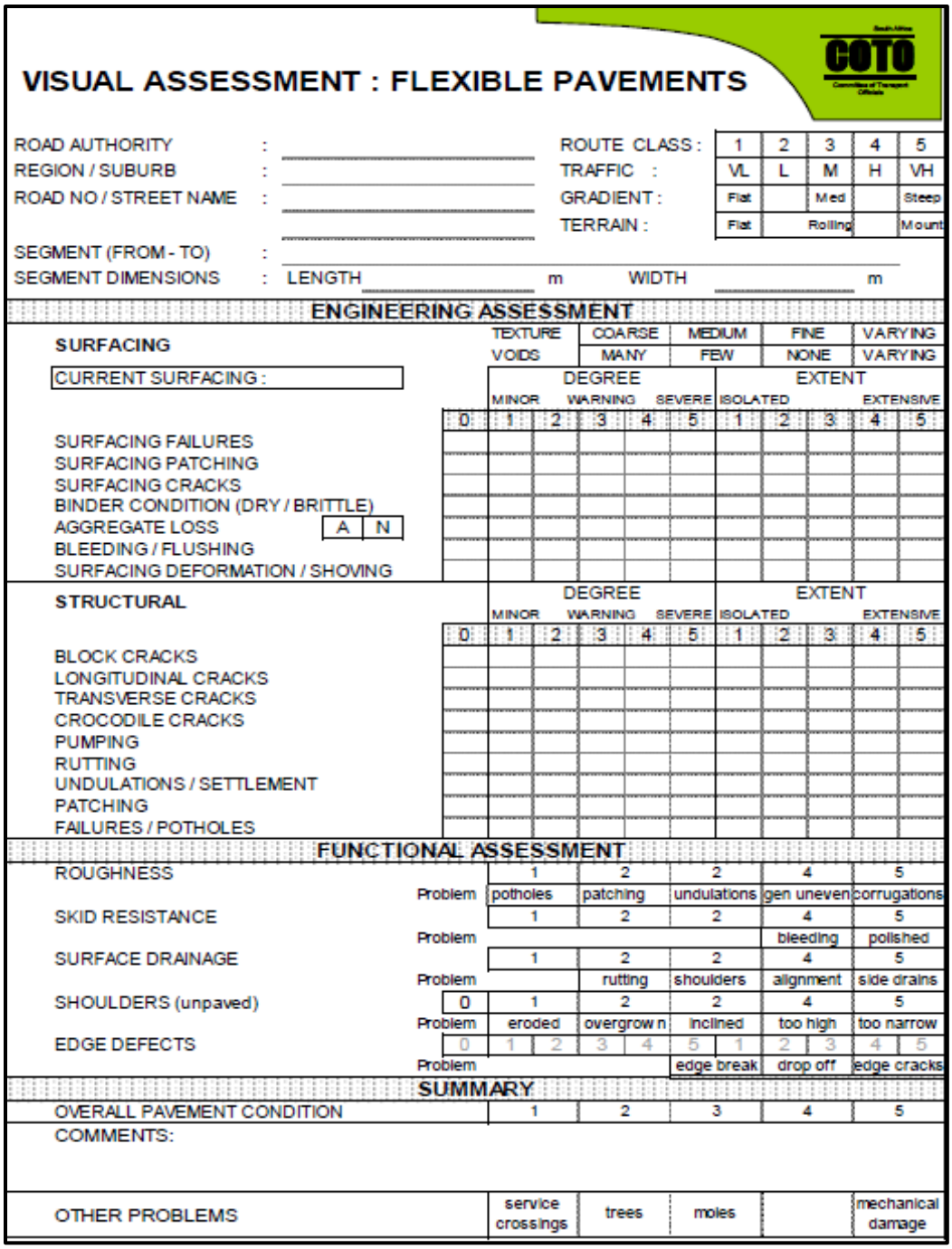

VISUAL ASSESSMENT : FLEXIBLE PAVEMENTS

COTO

ROAD AUTHORITY :
REGION / SUBURB :
ROAD NO / STREET NAME :
SEGMENT (FROM - TO) :
SEGMENT DIMENSIONS : LENGTH m WIDTH m

ROUTE CLASS :	1	2	3	4	5
TRAFFIC :	VL	L	M	H	VH
GRADIENT :	Flat		Med		Steep
TERRAIN :	Flat		Rolling		Mount

ENGINEERING ASSESSMENT

SURFACING — TEXTURE: COARSE / MEDIUM / FINE / VARYING; VOIDS: MANY / FEW / NONE / VARYING

CURRENT SURFACING :

	DEGREE: MINOR 0	1	2	WARNING 3	4	SEVERE 5	EXTENT: ISOLATED 1	2	3	EXTENSIVE 4	5
SURFACING FAILURES											
SURFACING PATCHING											
SURFACING CRACKS											
BINDER CONDITION (DRY / BRITTLE)											
AGGREGATE LOSS (A / N)											
BLEEDING / FLUSHING											
SURFACING DEFORMATION / SHOVING											

STRUCTURAL

	DEGREE: MINOR 0	1	2	WARNING 3	4	SEVERE 5	EXTENT: ISOLATED 1	2	3	EXTENSIVE 4	5
BLOCK CRACKS											
LONGITUDINAL CRACKS											
TRANSVERSE CRACKS											
CROCODILE CRACKS											
PUMPING											
RUTTING											
UNDULATIONS / SETTLEMENT											
PATCHING											
FAILURES / POTHOLES											

FUNCTIONAL ASSESSMENT

ROUGHNESS		1	2	2	4	5
	Problem	potholes	patching	undulations	gen uneven	corrugations
SKID RESISTANCE		1	2	2	4	5
	Problem				bleeding	polished
SURFACE DRAINAGE		1	2	2	4	5
	Problem		rutting	shoulders	alignment	side drains
SHOULDERS (unpaved)	0	1	2	2	4	5
	Problem	eroded	overgrow n	inclined	too high	too narrow
EDGE DEFECTS	0	1	2	3	4	5
	Problem			edge break	drop off	edge cracks

SUMMARY

OVERALL PAVEMENT CONDITION	1	2	3	4	5

COMMENTS:

OTHER PROBLEMS	service crossings	trees	moles		mechanical damage

Figure 9: Pavement Visual Assessment Form (TMH 9, 2016)

3.1 Alternative Inspection platforms

Alternative Inspection platforms can include satellites, aeroplanes, UAVs and moving vehicles fitted with data capturing technology (Schnebele *et al.*, 2015). Such methods typically use remote sensing to survey broad areas to identify problems rapidly. Currently, available technology does

not allow remote sensing to replace traditional pavement inspection methods. Remote sensing identifies problem areas where specific distress areas can be evaluated using traditional methods.

Remote sensing provides a contactless non-destructive pavement evaluation method. Schnebele *et al.* (2015) described semi-autonomous and autonomous pavement evaluation methods as inevitable; these methods will likely be faster to conduct inspections over a larger area, be more consistent, and less expensive than traditional methods. Remote sensing methods for pavement surveys provide results consistent with traditional survey methods while being safer and less labour intensive (Schnebele *et al.*, 2015; Petkova, 2017).

3.1.1 Aeroplanes and Satellites

Aeroplane and satellite platforms can provide aerial images for pavement surface inspections at a high level above ground. These platforms possess limited manoeuvrability, which can limit the available image data, especially in urban environments (Petkova, 2017). Satellites and aeroplanes can be associated with high operating costs and are limited in spatial resolution, resulting in distress mechanisms like cracks and rutting to be undetected (Zhang, 2010).

3.1.2 Unmanned Aerial Vehicles (UAVs)

UAV platforms for remote sensing have been gaining popularity in logistics, surveillance, agriculture, and search and rescue operations (Petkova, 2017). UAV's have quick response times and good manoeuvrability. UAV's can produce near real-time images with high resolution at minimal expense (Schnebele *et al.*, 2015). UAV platforms can be fitted with GPS systems that allow the operator to program a pre-selected flight path which the UAV can follow to acquire pavement surface data autonomously. UAV platforms can be fitted with a diversity of sensors and imaging devices but can be limited by payload capabilities (Petkova, 2017).

3.1.3 Ground-based Vehicles

Ground-based vehicles can be fitted with different sensors or cameras using specifically designed mountings on the vehicle. Technology that can be fitted on ground-based vehicles can include (Petkova, 2017):

- Light Detection and Ranging (LIDAR)
- Microsoft Kinect
- Ground Penetrating Radar (GPR)
- Digital camera
- Accelerometer

Ground-based vehicles possess the potential to perform remote sensing of pavement surfaces at highway speeds, given no traffic congestions. Vehicles can collect data continuously under bridges or trees with no obstructions (Petkova, 2017).

Sensors using vibration-based measurements to determine pavement surface defects are prone to measurement deficiencies reducing data reliability. These sensors can incorrectly diagnose high energy events, which include hard braking, manholes and road joints; this can result in false positives (Eriksson *et al.*, 2008). The vehicles should be calibrated for variables like tire pressure to ensure comparable data readings. Vehicle tyres only have contact with the pavement surface in the wheel paths. Pavement areas outside the wheel paths remain unevaluated (Koch and Brilakis, 2011). The shortcomings suggest that sensor-based data which requires accelerometer vibration readings to obtain data, lack reliability and accuracy and should be used for rough pavement condition surveys or preliminary surveys only (Koch and Brilakis, 2011).

3.2 Current Identification Platforms used

3.2.1 UAV Platforms

UAVs are flexible platforms that allow custom configurations with a range of different remote sensing technologies and sensors. The most common technology used is digital images; other sensors include LIDAR.

3.2.1.1 Types of UAV's

An unmanned aerial vehicle (UAV) is an aerial vehicle without an onboard human pilot. UAV's can be autonomously operated through onboard computers or by remote control from a grounded pilot (Martin and Rapp, 2017). Unmanned Aerial Vehicles (UAV's) can be categorised into three categories. A fixed-wing system; multi-rotor system; and a hybrid system. The fixed-wing system is a smaller version of an aircraft. The multi-rotor system uses four and more rotors to operate, much like a helicopter.

UAV advantages include safe and easy launch and landing, operation in any weather conditions, easy manoeuvring and low cost (Tahar and Ahmad, 2013). Disadvantages of UAVs include geometric image distortion, a large number of images to be processed, limited image coverage area and payload limitations (Tahar and Ahmad, 2013).

When deciding on a UAV, important considerations are the camera that acquires the necessary data, the battery life between charges, the quality of the Global Positioning System (GPS) and safety sensors to protect the UAV (Abbie, 2018).

I. Fixed-Wing UAV

A Fixed-wing system refers to a type of aircraft, commonly known as an aeroplane, that generates lift using the forward motion of the aircraft and wings. The wings do not rotate around a central axis but are fixed to the fuselage of the aircraft (Law Insider, 2018).

Fixed-wing systems can have one or more propellers which generate the forward motion of the system. Control surfaces within the wing and tail rudder direct the drone to the intended path. Due to the shape of the fixed-wing system, it possesses natural gliding capabilities. This can reduce the amount of power required to operate the system and increase the flight time or flying distance (Abbie, 2018). Figure 10 shows a picture of a typical fix-wing UAV with one propeller. This type of fixed-wing UAV is streamlined for gliding in a straight direction. The camera is fitted at the nose of the UAV to ensure a wide camera view. Fixed-wing UAV's are typically used for aerial mapping, construction, security and surveillance (Herrick, 2017).

Figure 10: Fixed-wing UAV (González-Jorge, Higinio; Martínez-Sánchez, Joaquin; Bueno, Martín; Arias, 2017)

Table 5 lists some of the advantages and disadvantages of fixed-wing UAV's (Chapman, 2016; Herrick, 2017).

Table 5: Advantages and disadvantages of fixed-wing UAV's

Advantages	Disadvantages
Ability to carry a high payload compared to multi-rotor UAV's	Can only move in one direction
Can fly at high altitude	Requires a large landing area
Long flight time	Training is required to operate the UAV
Can glide naturally	Requires a launcher aid
	Expensive

II. Multi-Rotor UAV

Multirotor or rotary-wing UAV's are the most common type of UAV used; this is due to the portability of the UAV. Multirotor UAV's have four or more propellers used for linear propulsion, lift, and steering. Multirotor UAV's are not designed to glide and rely on the battery power and motors for manoeuvrability. The UAV's are fragile and a loss of battery power can result in UAV damage (Abbie, 2018). Multirotor UAV's are typically used for video and photogrammetry, search and rescue, package delivery and monitoring. Multirotor UAV's can land and take off vertically resulting in launches from anywhere. Figure 11 is examples of multi-rotor UAV's available from DJI. Multirotor UAV's are typically used in construction, safety, agriculture and photo and aerial video inspections (Chapman, 2016).

Figure 11: Multirotor UAV examples (Drone Deploy, 2017)

Table 6 lists some of the advantages and disadvantages of multi-rotor UAV's (Chapman, 2016; Herrick, 2017).

Table 6: Advantages and disadvantages of multi-rotor UAV's

Advantages	**Disadvantages**
Easy to control and manoeuvre	Limited flight time per battery
Very stable in the air	The UAV uses most of the energy to counter gravity and stabilise the UAV
Take off and land vertically	Small payload capability
Ability to hover in the air	
Autonomous operation	

III. Single Rotor UAV

Single rotor UAV's are similar in design to a helicopter. This type of UAV is strongly built, with one long-bladed rotor acting as a spinning wing and a small rotor at the tail end of the UAV used for directional changes and steering (Herrick, 2017). Figure 12 is an example of a single rotor UAV. Single rotor UAV's are typically used for aerial LIDAR laser scanning (Chapman, 2016).

Figure 12: Single-rotor UAV

Table 7 lists some advantages and disadvantages of single-rotor UAV's (Chapman, 2016).

Table 7: Advantages and disadvantages of single-rotor UAV's

Advantages	Disadvantages
Vertical take-off and land	Expensive
Heavier payload capabilities	Training needed to operate
Strong and durable construction	Dangerous
Longer flight time	Higher complexity

3.2.1.2 UAV and Digital Image uses

Shatnawi (2018) developed a method of automatic crack detection in pavement surfaces with the use of neural networks to process images obtained from a UAV. The method removes noise from the image and applies a digital image recognition algorithm to identify different types of cracks on a pavement surface. This method can calculate the orientation and length of the surface crack.

The study used 80 images to validate the method through the sensitivity, specificity, accuracy, and precision. The method returns the results in Table 8. Shatnawi (2018) recommended additional research in image acquisition and accurate assessments of the method.

The parameters in Table 8 were determined with true positives, false positives, true negatives and false negatives (Shatnawi, 2018):

Table 8: Case Study results: Automatic Pavement Cracks Detection using Image Processing Techniques and Neural Network (Shatnawi, 2018)

Parameter	**Result (%)**
Specificity	60
Sensitivity	90
Precision	87
Accuracy	82.5

Specificity is the number of true negatives that were correctly identified by the image processing method. The sensitivity of the data is a measure of how the method is effected by changing variables. Precision indicates the repeatability of the method to identify true positives, false positives, true negatives and false negatives. Accuracy indicates the ability to identify cracks on images correctly.

3.2.1.3 UAV and LIDAR use

Light Detection and Ranging (LIDAR) can directly obtain three-dimensional spatial information on the pavement surface. The three-dimensional information allows the measurement of pavement distress dimensions and simple monitoring of the entire pavement surface. LIDAR is independent

of lighting conditions and is not influenced by the illumination differences of the pavement surfaces caused by the sun. LIDAR can be used during the day or night due to the independent nature of lighting conditions (Li *et al.*, 2019).

Li *et al.* (2019) studied the feasibility to use a LIDAR sensor fitted to a single rotor low-altitude UAV and random forest classification (RFC) to identify distress on a pavement surface. The study used a flexible pavement surface in Shihezi City, China. The system achieved an overall accuracy of 95.86% of cracks correctly identified.

Li *et al.* (2019) used the single rotor UAV in Figure 13 to capture the point cloud data of the road section.

Figure 13: LIDAR data collection UAV (Li *et al.*, 2019)

The UAV was fitted with a RIEGL VUX-1LR LIDAR scanning device. The specifications of the LIDAR scanner can be seen in Table 9.

Table 9: RIEGL VUX-1LR specifications (RIEGL, 2015)

RIEGL VUX-1LR	
Range	1350 m
Accuracy	15 mm
Measurement speed	750 000 measurements/s
Field of view	330^0

Li *et al.* (2019) obtained the point cloud data using the UAV at an altitude of 30 metres above the pavement surface. The UAV travelled at a set speed of 5 m/s with the LIDAR sensor field of view set to 55^0. The experiment with the mentioned variables managed to obtain a point cloud density of 40 points/m^2.

3.2.2 Current Ground-based Platforms

3.2.2.1 Vehicle and Digital Image uses

Koch and Brilakis (2011) developed a method to automatically detect potholes from images of an asphalt pavement surface with the use of image processing in MATLAB. The researchers tested the method with 70 images; most of the images were obtained using a robot vehicle fitted with a high-speed camera. Figure 14 shows the robotic vehicle used for pavement surface sensing. The high-quality camera reported an average image resolution of 640 by 480 pixels. The method can identify and extract the shape of the potholes with a precision of 82% and an accuracy of 86%. The validation of the method was performed using the TP, FP, TN, FN numbers to determine accuracy and precision.

The alternative to moving vehicle data collection for pavement surfaces in the form of low-cost UAV systems has been explored by research. Petkova (2017) emphasised previous studies focused on the evaluation of unpaved road inspections using UAV platforms. The bulk of the vision-based algorithms currently in use had been developed using dedicated vehicles with specially designed sensor stands. This requires many funds to be devoted to purchase and set up the vehicles before data collection can commence. The use of vehicle requires trained technicians to operate the data collection systems (Petkova, 2017).

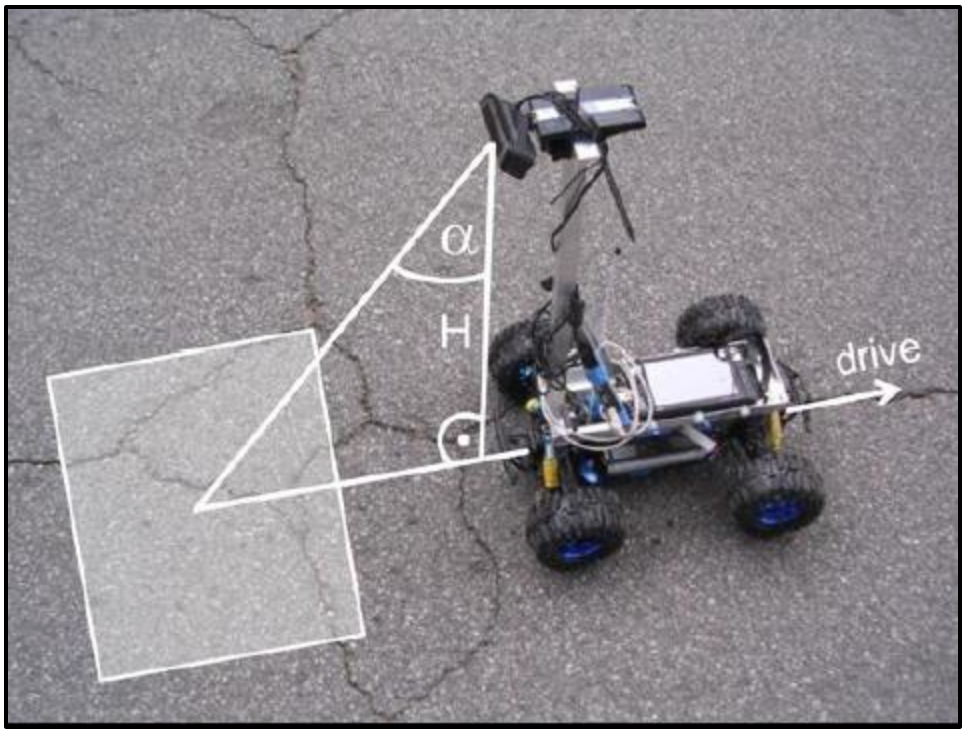

Figure 14: Robot vehicle with a high-speed camera (Koch and Brilakis, 2011)

The South African National Roads Agency Limited (SANRAL) pavement management system includes all national routes as well as specific high traffic routes across the country. The road network under the jurisdiction of SANRAL equals 16 170 kilometres of two-way roads. This equals 32 340 kilometres of paved lanes to be managed (Van Zwieten, 2010). SANRAL uses a specially designed and equipped road survey vehicle fitted with distance measuring systems, video cameras, a differential GPS unit, gyros, accelerometers, and numerous laser devices to acquire pavement data. The vehicle in Figure 15 can record the road surface data, the vertical and horizontal alignment of the road, road cross-sections, and roadside furniture while driving at normal traffic speeds. The survey vehicle can cover an average of 500 lane kilometres of road per day, given favourable weather and traffic conditions (Van Zwieten, 2010).

Wet rainy conditions can scatter the laser beams resulting in unacceptable data, while the position of the sun needs to be accounted for when capturing road signs and markings. Other challenges include (Van Zwieten, 2010):

1. Keeping the survey equipment working when rough road conditions occur. Excessive vibrations can cause seizures to the system, as the system requires the simultaneous operation of all sensors.
2. Traffic congestion can result in an unacceptable survey due to the travelling speed of the vehicle going below the minimum of 25 km/h

Figure 15: SANRAL Road Survey Vehicle (SANRAL, 2014)

3.2.2.2 Vehicle and LIDAR uses

The traffic can influence LIDAR technology mounted on vehicles moving in the normal traffic stream. The LIDAR point cloud data can measure the traffic instead of the road surface. This happens especially when slow-moving traffic occurs and following distances are short. It is difficult to ensure full sampling of the pavement surface and monetary and resource costs are high. Vehicle-mounted LIDAR platforms will not effectively and comprehensively assess the conditions of the pavement surface (Li *et al.*, 2019).

3.3 Overview of technology types used for inspections

Continuous innovation and improvements to technology in the last decade have resulted in a revolution in civil engineering (ILSI Engineering, 2019). Various types of technology are used in quality monitoring and surveying of civil engineering projects. Technology not previously used

for road surface monitoring are also discussed. The identified technological systems will be discussed according to the application, as well as various advantages and disadvantages. The identified technological systems are as follows:

- Digital images
- Laser scanners
- Accelerometers
- GPS devices
- Thermal Imaging

3.3.1 Digital Cameras

Digital images of a surface are captured using a digital camera. Digital cameras use the light rays streaming into the lenses of the camera and convert the incoming analogue rays into digital electronic signals through image sensors. The digital image quality is determined by the quality of the lenses and sensors used in the camera (Peterson, 2005).

A digital image is a discrete representation of intensity and spatial information represented as data (Solomon and Breckon, 2011). A digital image comprises of a large number of small dots, each dot is called a picture element (pixel) (Christenssoon, 2006). The quality of a digital image can be determined by the number of pixels present in the image. A digital image is divided into thousands of matrices of pixel determining the image quality (Christenssoon, 2006).

A pixel is a combination of three different colours red, green and blue and each colour is represented in three dimensions through XYZ (Saravanan, 2010). The x and y values of a digital image are all discrete integer values ranging between 1 and 256. The brightness of a digital image also ranges from 0 to 255, with 0 being black and 255 being white (McAndrew, 2005).

True colour or RGB images can be described as three-dimensional arrays which conceptually contains three different two-dimensional planes, one plane corresponding to the red (R), green (G), and blue (B) colour spectrums. The RGB spectrums are used as either the primary colours or mixed colours to represent the displayed digital image (Solomon and Breckon, 2011).

RGB images can be simply transformed into greyscale image conversions contained reduced amounts of image information. Grey scaled images are used in many image analysis algorithms. This is due to the image preserving important feature related information in a simplified format (Solomon and Breckon, 2011).

The biggest benefit of digital images is the low-cost hardware required to capture the images. Digital images provide lasting evidence of a pavement surface. Digital images can be stored and opened on any suitable electronic device. UAV platforms fitted with a digital camera can assess large areas relatively quickly compared to ground surveying methods (Colorado Department of Transportation, 2015).

Disadvantages of digital Images is that the image quality is light-dependent, therefore should special care be given to which lighting conditions will provide the best road surface image. The shadows of trees and the vibration of the UAV platform can result in low-quality images. It is difficult to obtain accurate height measurements using digital images (Cao *et al.*, 2019). The system accuracy is dependent on the image quality and the flying height (Colorado Department of Transportation, 2015).

The digital camera devices in Table 10 are cameras designed with different primary objectives in mind. There are much more different types of cameras. The Unibrain Firewire-800 and Fuji XT2 DSLR have high shutter speed rates but are not fitted with a GPS device to know the exact location of each image. When these cameras are used, a separate GPS will be required to record the pavement surface data.

Table 10: Digital Camera devices

Device	**Price**	**Shutter Speed (Seconds)**	**Source**
Unibrain Firewire-800	R78 000.00	5/1000 000 - 3600	(Unibrain, 2010)
Fuji XT2 DSLR	R21 495.00	1/32000	(DPReview, 2016)
GoPro Hero 8 Black	R8 000.00	1/2500	('Hero 8 Black Manual', no date)
DJI Osmo Action	R7 000.00	1/8000	(DJI, no date)

The GoPro Hero 8 Black and DJI Osmo Action have slow shutter speed values compared to the more expensive alternatives but are fitted with GPS and electronic image stabilisation software. This allows the ability to know the exact location of images without external GPS systems. The Unibrain Firewire-800 cameras are currently used in pavement monitoring systems. The systems operate with four synchronised cameras allowing a maximum data collection speed of 100 km/h.

3.3.2 Laser scanners

Laser scanners are a contactless form of remote sensing performing measurements and documentation through three-dimensional (3D) laser scanning. Scanners can collect between 250,000 and 976,000 data points per second (Podges, 2017). Laser scanner devices emit laser beams over the entire field of view of the device. The emitted laser beams are reflected from the surface back to the receiving scanner. The reflected laser beams are received as point cloud data which represents points with spatial information in the form of x, y and z coordinates (Podges, 2017; Surface and Edge, 2018).

Short-range and medium or long-range laser scanners are currently available. Short-range laser scanners function at less than 1 meter between the scanned object and laser scanner. Short-range scanners utilise either Structured Light technology or Laser triangulation to obtain data (EMS USA, 2016). Medium or long-range laser scanners function at more than 2 meters between the scanned object and laser scanner. Medium or Long range scanners have two formats, Pulse based lasers or Phase shift lasers, both formats can scan large objects like buildings (EMS USA, 2016). Figure 16 shows a typical long-range laser scanner.

Figure 16: Long-range laser scanner (Du and Teng, 2007)

Pulse based laser scanners use the time of flight to calculate the point cloud data. The concept uses the known value for the speed of light (299 792 458 m/s) to calculate the distance between the scanner and the scanned object (Fowler, 1962). The time the laser beam takes to travel from the scanner to the object and reflect is used to calculate the distance. These types of scanners can rotate via a mirror to scan the full 360 degrees around the scanner (EMS USA, 2016). Phase shift laser scanners work similarly to pulse-based laser scanners and additionally modulate the power of the laser beam. Phase shift scanners are limited to a scanning distance of 300 meters, while a pulse-based scanner can identify objects up to 1000 meters (EMS USA, 2016).

The following procedure is used for laser scanners to perform object measurements (Du and Teng, 2007; Podges, 2017):

1. Set up the laser scanner to scan the required surface
2. Convert the point cloud data to a Digital Terrain Model (DTM) with computer software
3. Transfer or analyse the data with the AutoCAD environment

Laser scanners provide great benefits for surveying. The scanners can scan millions of points in a single scan. Provide safe and contactless scanning of objects (EMS USA, 2016). The point cloud data can provide accuracies within 2mm from a scanning distance of 25 meters (Surface and Edge, 2018). Laser-based scanners are less sensitive to changing light.

Disadvantages of laser scanners include training on how to operate the laser scanners and how to use the software to transfer point cloud data to CAD data. Laser scanners are expensive to use and are prone to high noise levels, especially long-range laser scanners (3D Systems Inc., no date; Podges, 2017). Limitations of laser scanners include discontinuity of spatial information, scanning range and sensor calibrations (Mani, Feniosky and Savarese, 2009).

3D laser scanners are used for different applications in civil engineering. The applications include surveying, construction quality control, and as-built documentation development. In surveying are lasers used to create accurate 3D profile models and topographical maps. The maps can be used to measure distance, areas, and volumes. A Building Information Model (BIM) could be created from 3d laser scanner data (Podges, 2017; Surface and Edge, 2018).

Laser scanners used in pavement surface evaluations are used as part of a series of laser scanners. The series of laser scanners are surface profilers which measure accurate surface measurements to an accuracy of 1mm. The road profilers use many point laser devices spaced at a required spacing (Technologies, no date; Dynatest, 2020). The point lasers continuously record the distance between the laser and the road surface.

Pavemetrics (no date) developed a Laser Crack Measurement System (LCMS) using two 2D laser scanners fitted on a vehicle. The system can produce 0.25mm accuracy at speeds up to 100 km/h. LCMS can measure cracking, rutting, potholes, patching, lane marking and other functional pavement characteristics (Pavemetrics, no date). The system can be seen in Figure 17.

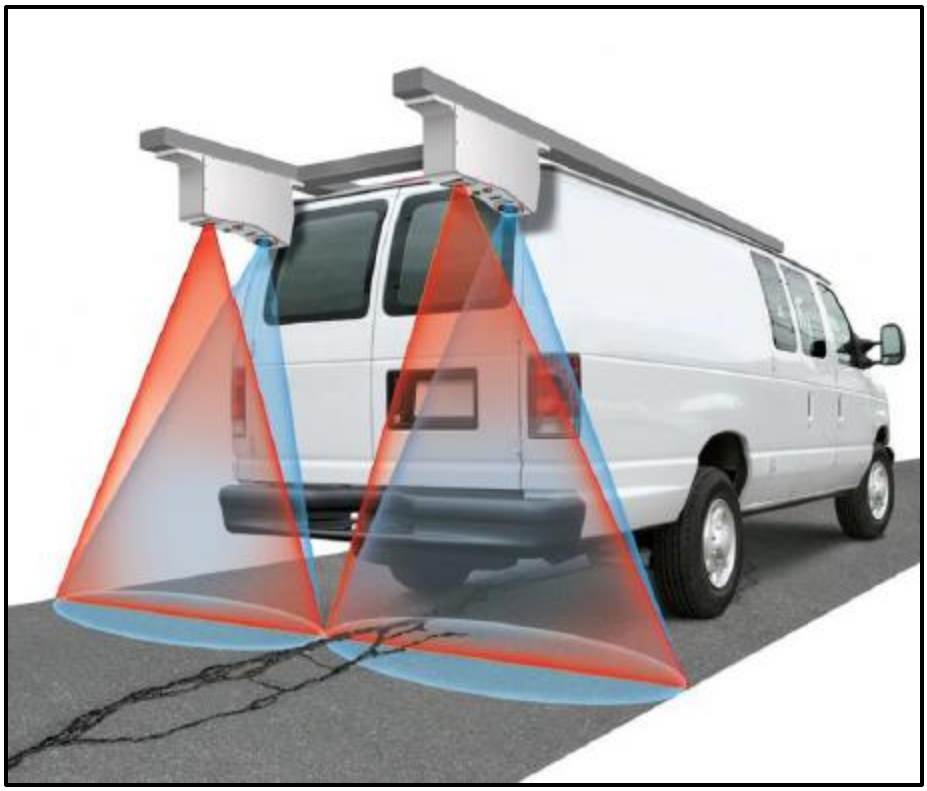

Figure 17: Pavemetrics' LCMS (Pavemetrics, no date)

3.3.3 LIDAR Devices

LIDAR is a remote sensing technique used to determine measure distance between the sensor and an object. LIDAR devices are used in many applications with different priorities. LIDAR emits a laser beam travelling at the speed of light which reflects the sensor to determine distance. The applicability of a LIDAR sensor in pavement surface evaluations is the accuracy of the device.

Table 11 include LIDAR devices with a range of accuracies.

Table 11: LIDAR Devices

Device	Accuracy	Field of View (degrees)	Price	Source
RIEGL VMZ Hybrid	5mm	360	$73 300.00	(RIEGL, 2015a; Horts, 2020)
RIEGL VUX-1UAV	10 mm	75	$186 300.00	(RIEGL, 2015b; Horts, 2020)
Livox Mid-40	20mm	38.4	$599.00	(Livox Lidar, 2019; DJI Store, 2020b)
Livox Mid-100	20mm	98.4	$1499.00	(Livox Lidar, 2019; DJI Store, 2020a)
Quanergy M8	38mm	360	$1499.97	(Doug Deals, 2020; LiDAR USA, 2020)
Baumer OM70-P/L Distance sensor	0.6mm	Point	R33 500.00	(Baumer, 2009; RS Online, 2020)

The Quanergy M8, Livox Mid-40 and RIEGL VUX-1UAV are LIDAR sensors that can be fitted on a UAV, while the RIEGL VMZ Hybrid, Livox Mid-100 and the Baumer OM70 devices are designed to be mounted on vehicles. The Baumer OM70 is a point laser which requires a system of multiple devices to be mounted on the vehicle to capture data of the whole pavement surface.

3.3.4 Accelerometers

An accelerometer is an electromechanical device that measures the physical acceleration forces experienced by an object. An accelerometer uses a damped mass connected on a spring element when the mass is displaced due to acceleration the displacement of the mass is measured to obtain the acceleration of the object (Andrejašicˇ, 2008).

When an object accelerates a force equal to the mass time acceleration is exerted on the mass resulting in the deflection of the mass. The amount of deflection of the mass is sensed and converted to an electrical signal. The electrical signal is used to determine the acceleration of the object.

The following are different types of accelerometers (Longoria, 2014):

- Piezoresistive accelerometer
- Capacitive accelerometer
- Piezoelectric accelerometer

The different types of accelerometers use different techniques to convert the mechanical motion of the mass into an electrical signal (Longoria, 2014). Piezoelectric accelerometers are used for upper-frequency ranges, have a low weight and can resist high temperatures. Piezoresistive accelerometers are used in high shock applications. Capacitive accelerometers are used in low-frequency ranges and have high stability (Andrejašicˇ, 2008).

Some advantages of accelerometers, and especially piezoelectric accelerometers include a wide range of dynamic measurements where shock has little influence on the measurements. Accelerometers are compact, lightweight sensors with no moving parts. Accelerometers are self-generating sensors that require no external power supply (MMF, no date).

Disadvantages of accelerometers, and especially piezoelectric accelerometers include the requirement of high expertise to operate the sensors. Accelerometers are not robust sensors that are sensitive to dirt on the connectors. Accelerometers can be sensitive to noise (Instruments, no date).

3.3.5 Global Positioning System

The Global Positioning System (GPS) is a global navigation system developed by the U.S Department of Defence. The GPS can provide accurate position, time and velocity information to anyone free of charge. The GPS can provide information on the ground, sea, air and outer space (Abulude, Akinyinka and Adeyemi, 2015).

A GPS functions through the use of a GPS receiver and satellites. The GPS satellites transmit signals to the GPS receiver which solve equations to determine the position, time and velocity information of the receiver. The GPS receiver must have an unobstructed view of at least four GPS satellites simultaneously. Three of the GPS satellites are positioning co-ordinates and one satellite for clock deviation from satellite time (Hoque, 2016).

Different satellite networks have been developed by various countries and states to fulfil the needs of specific countries. The different navigation systems are used in different regions of the world to navigate the specific region. Different satellite networks can be seen in Table 12 (Hoque, 2016).

Table 12: Different navigation satellite systems

Navigation system	Developer	Region available
QZSS	Japanese	Asia and Oceania
IRNSS	India	India and Northern Indian Ocean
COMPASS	China	Worldwide
BEIDOU	China	Asia and Western Pacific
GALILEO	European Union	Worldwide
GLONASS	Russia	Worldwide
NAVSTAR	United States	Worldwide

3.3.6 Thermal Imaging

Commercial thermal imaging devices were first sold in 1965 to be used for high voltage power line inspections. The technology of thermal imaging has progressed considerably since the first stages. Thermal imaging devices have become compact in shape and size to look similar to digital cameras. The current technology provides easy to use, high-resolution and real-time images that can be used by different industrial applications (Rai, Maity and Yadav, 2018).

Thermal imaging cameras provide a non-intrusive method to scan and visualize temperature distributions on surfaces to accurately identify anomalies that can be invisible to the human eye. Thermal imaging is used mainly in the electrical and mechanical industries to determine maintenance requirements and save cost and time across the world (Rai, Maity and Yadav, 2018).

Thermal imaging use infrared (IR) wavelengths that are invisible to the human eye to detect the heat of objects. Infrared wavelengths are part of the electromagnetic spectrum humans perceive as heat. Every object or surface with a temperature above absolute zero (-273.15 ^{0}C) will emit heat. The thermal imaging devices can detect three different wavelengths of infrared: the short-wave (SW) are wavelengths between 0.9 and 1.7 μm; the mid-wave (MW) are wavelengths between 3 and 5 μm; the long-wave (LW) are wavelengths between 8 and 14 μm (Vollmer and Möllmann, 2018). Thermal imaging devices detect the three different infrared wavelengths which are emitted from a surface and converts the temperature information into an image. The image will represent the temperature range and distribution of the object or surface (Davis Instruments, no date).

Advantages of thermal imaging include fast and accurate measurements of surfaces or objects from a distance away. The thermal image is available in seconds. Thermal imaging can record data while the object is moving (Davis Instruments, no date). Some critical thermal imaging specifications that are required to ensure the most accurate and efficient use of thermal imaging for the specific application include the temperature range of the device, the thermal sensitivity of the device, and the resolution of the images. The higher the image resolution, the greater the image detail and accuracy will be (Davis Instruments, no date).

Thermal imaging is used in many different industries for different applications. The main uses of thermal imaging are in the security and surveillance industry, agricultural industry, medical industry, electrical and mechanical industry. Finland uses thermal imaging cameras to determine the pavement conditions and identify moisture ingress in pavement surface layers (Heijsman, 2014).

Figure 18 is a typical example of pavement failure identified through thermal imaging (Heijsman, 2014). The crack failures in the pavement surface can be identified in the image on the left, while the cracks in the pavement surface are more difficult to identify using a normal digital image.

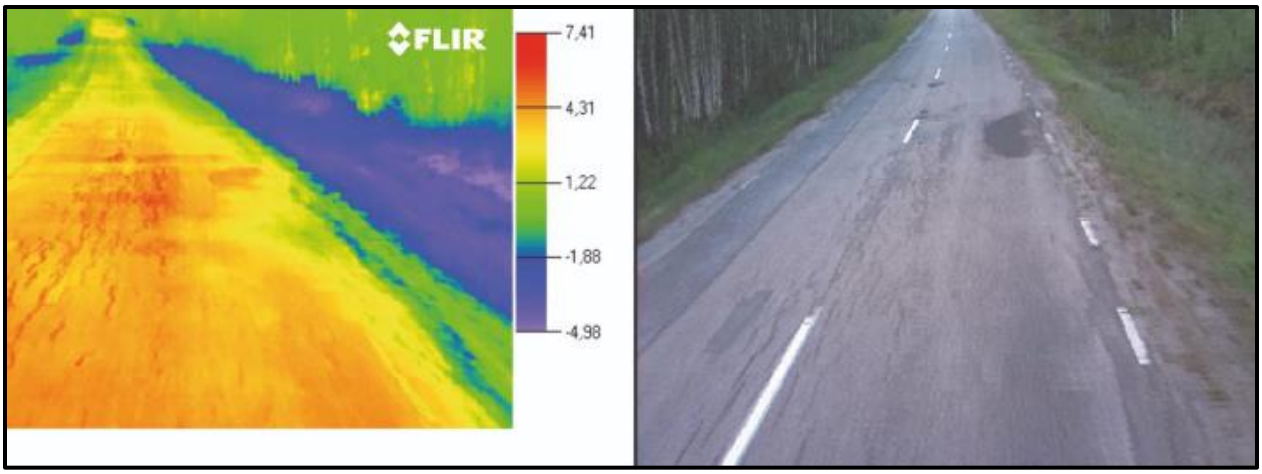

Figure 18: Thermal pavement surface image (Heijsman, 2014)

Thermal cameras are used to determine the temperature variance between objects in a digital image. Two different types of thermal cameras are available. The first is a camera with a cryocooler, which lowers the sensor temperature to cryogenic temperatures inside the detector. The second is an uncooled camera with no cooling of the detector.

The cooled detector cameras allow fast image capture rates (FLIR Systems, 2015). Cooled thermal cameras have an integration time of 1-1.5 milliseconds which allow sharp images with little image blurring. An uncooled microbolometer has an integration time of 10-12 milliseconds which may result in significant image blurring (Oswald-Tranta *et al.*, 2017). Cooled thermal cameras are expensive devices and will not be researched. Table 13 includes a range of uncooled thermal cameras.

Table 13: Thermal devices

Device	**Detector**	**Sensor**	**Price**	**Source**
FLIR TG267	Uncooled	160 x 120	R8 750.00	(Go Thermal, 2020a)
FLIR E95	Uncooled	464 x 348	R197 000.00	(Go Thermal, 2020b)
RS Pro 730	Uncooled	160 x 120	R26 681.04	(RS Pro, 2020)
FLIR Duo Pro R640	Uncooled	640 x 512	R106 299.00	(Go UAV, 2020)
FLIR Vue Pro	Uncooled	640 x 512	R64 999.00	(Go UAV, 2020)
Seek Shot Pro	Uncooled	320 x 240	R10 500.00	(Makro, 2020; Seek Thermal, 2020)
Major Tech MT 2005	Uncooled	80 x 80	R19 159.00	(Major Tech, 2020)

The FLIR Duo Pro and Vue Pro devices are devices specifically designed for UAV operations and are compatible on the DJI Phantom 4 UAV. The other FLIR, Seek and RS devices are handheld devices primarily used for electrical and building inspections.

3.4 Current Distress Identification software

Image processing provides an economical and efficient system to detect pavement cracks; therefore, various image-based processing methods have been developed and investigated over the past 20 years. Most of the developed methods are based on the general assumption that the crack intensity will be lower than the surrounding environment resulting in the use of an intensity thresholding method to identify cracks.

The intensity along the crack is non-homogeneous, resulting in these methods to produce fragmented crack identification results. The pavements surface is often covered by unwanted shadows from overhanging branches which may affect the results. Low contrast between the cracks and surrounding environment contribute to the difficulty of crack detection using image processing (Zou *et al.*, 2012). Alternative methods for automatic crack detection have been developed to improve on the results of the thresholding method.

3.4.1 CrackTree

Zou *et al.* (2012) developed a fully automatic crack detection method called CrackTree. The method uses standard pavement images to identify pavement surface cracks through three steps. The first step is to remove the unwanted shadows on the pavement surface using a geodesic shadow removal algorithm developed by the authors. The results of the shadow removal algorithm can be seen in Figure 19.

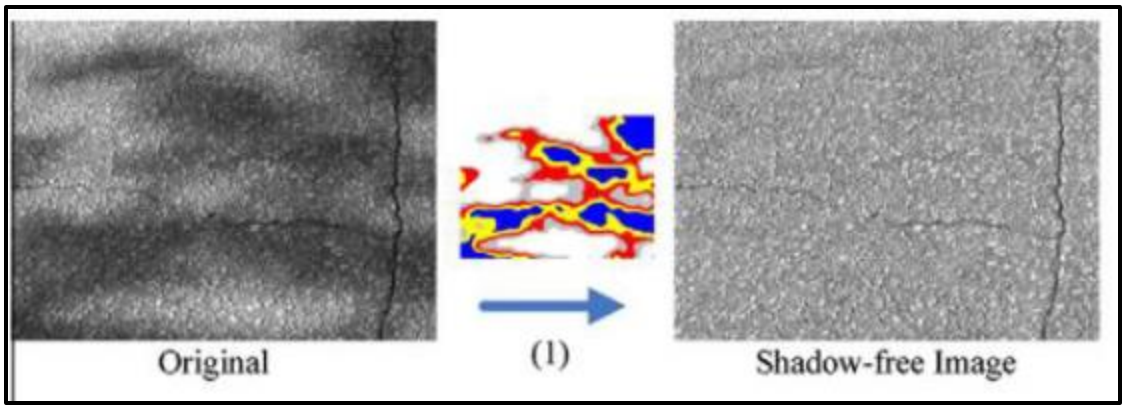

Figure 19: Geodesic shadow removal results (Zou *et al.*, 2012)

The second step is to use tensor voting to develop a crack probability map. Tensor voting extracts edges by detecting delicate local changes in the image intensity and linking the locations based on the noisy image response of the intensity (Medioni and Lee, 2000). Tensor voting augments the crack fragment connections with good curve continuity and proximity. The crack probability map results can be seen in Figure 20. The crack pixels are identified using the local image intensity analysis method, where after the tensor voting is used to develop the crack probability map (Zou *et al.*, 2012).

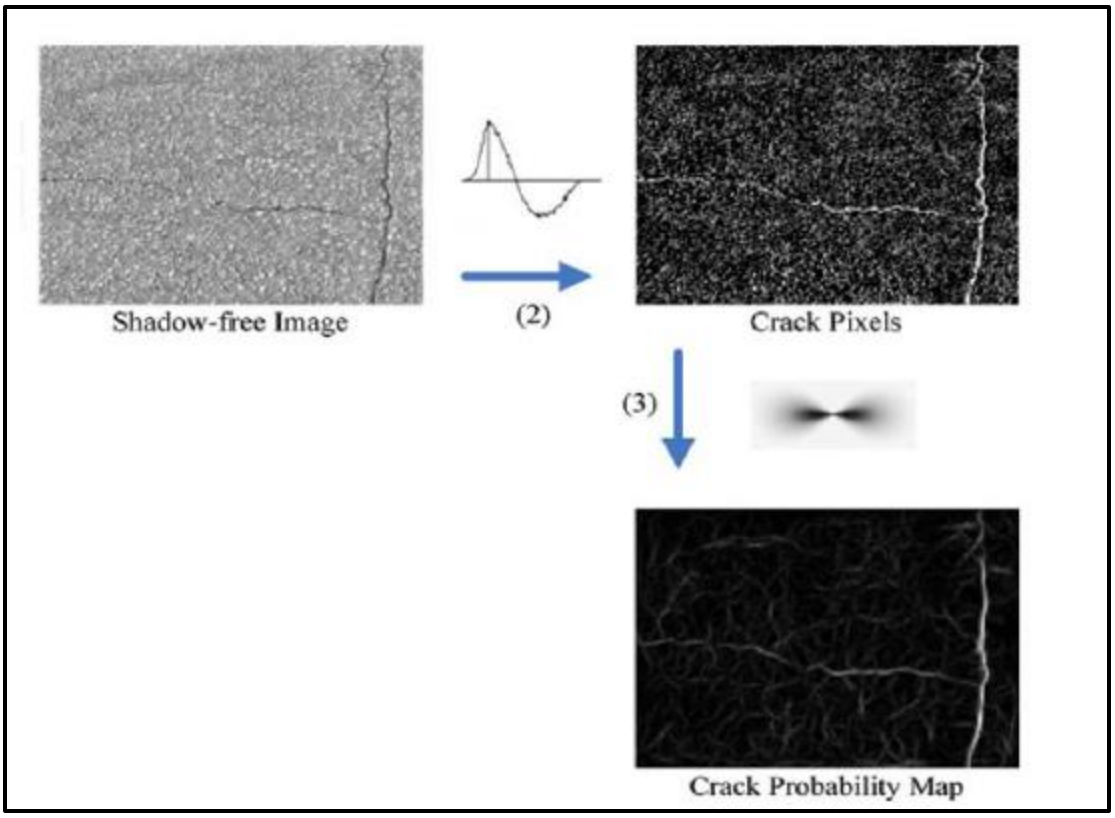

Figure 20: Crack probability map development results (Zou *et al.*, 2012)

The final step is to develop a crack seed sampling graph model from the crack probability map. The graph model is used to construct the minimum spanning tree (MST) of the graph. Recursive edge pruning of the MST is used to identify the final crack curves. The final crack curve results can be seen in Figure 21. In Figure 21 is the crack seed sampling process represented by a number (4) and number (5) represent the minimum spanning tree construction and edge pruning process (Zou *et al.*, 2012).

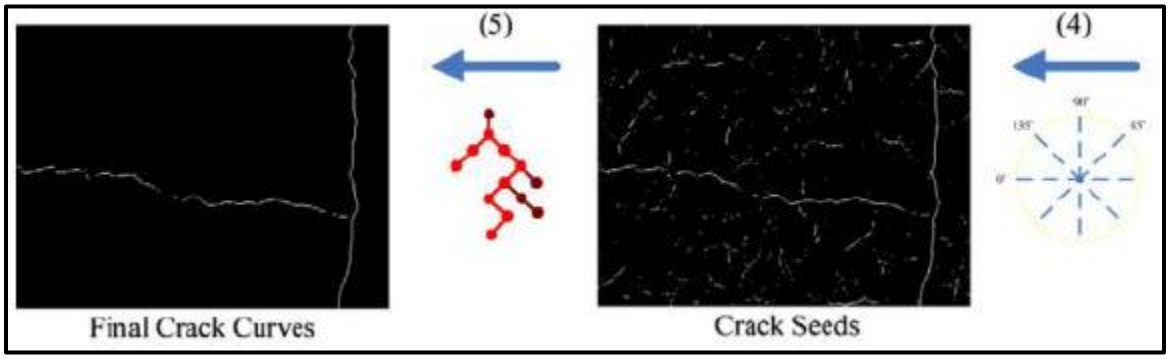

Figure 21: Final crack curve results (Zou *et al.*, 2012)

3.4.2 CrackNet

Zhang *et al.* (2018) developed a fully automated crack detection software called CrackNet, using a deep-learning approach. The software uses three-dimensional data from a digital highway data vehicle (DHDV); the vehicle can be seen in Figure 22. The DHDV in Figure 22 is fitted with two 3D line laser sensors on the back. The sensors calculate 3D data using triangulation principles. The main advantage of using line laser sensors is that the laser provides consistent illumination of the pavement surface regardless of the lighting conditions (Zhang *et al.*, 2018).

Figure 22:The Waylink DHDV used for CrackNet data acquisition (Zhang *et al.*, 2018)

The image library used to train the deep-learning algorithm consisted of 3000 3D images and pavement surface images. The images were collected at different driving speeds ranging between 35 km/h to 100 km/h over five years. Images included different pavement textures, warm mix asphalt (WMA) and hot mix asphalt (HMA). The software uses the 1-millimetre three-dimensional data and the corresponding ground truth images to determine pavement surface cracks (Zhang *et al.*, 2018).

The 3D images had a fixed image size of 4096 x 2048; this resulted in 70 billion floating points in each image layer. The high amount floating point are nearly impossible to processing in a realistic time, even with a high-end desktop computer with a high-performance dedicated graphics processing unit (GPU). To reduce the floating points, each image is downscaled to an image size of 1024x 512 using a minimum-pooling technique.

The minimum-pooling technique outputs the minimum elevation value of a 4x4 block pixels of the original 3D image to produce the downscaled image. This enables the software to identify fine or hairline cracks in the pavement surface more accurately. The software can detect more than 89% of the cracks in the pavement surface. The typical output of the software can be seen in Figure 23 (Zhang *et al.*, 2018).

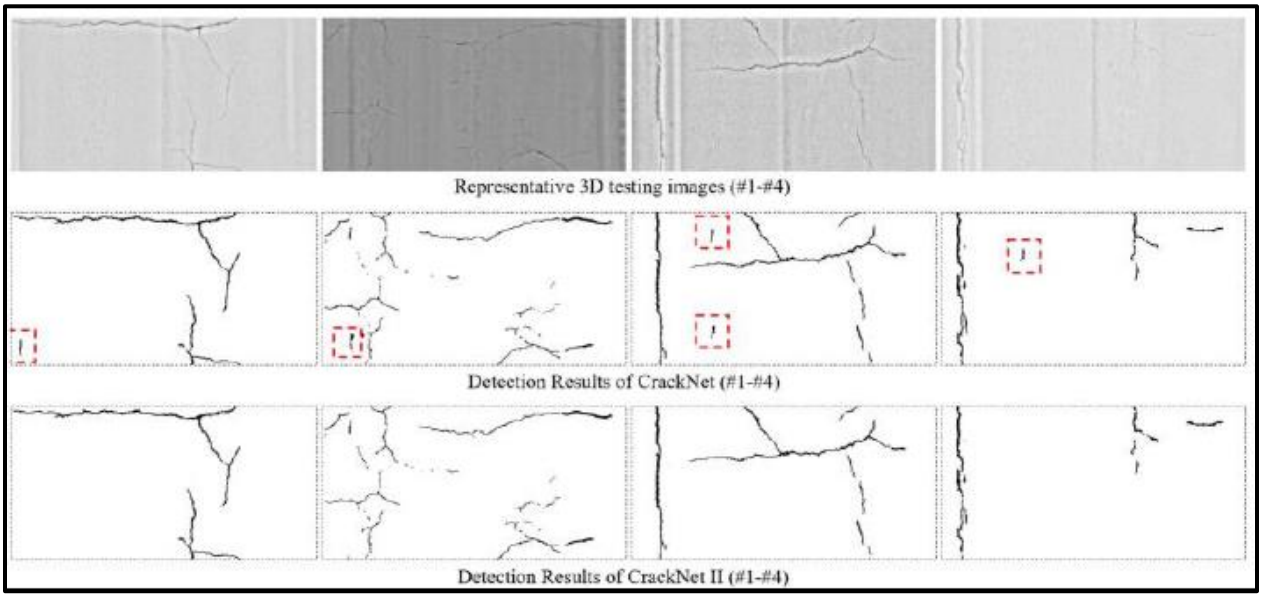

Figure 23: Typical CrackNet software output (Zhang *et al.*, 2018)

3.5 Lessons Learned from Literature

Two different pavement types have different cracking patterns. Rigid pavement types are prone to environmental cracking which include shrinkage cracks; this is typical of a concrete slab. Flexible pavements have cracks caused by continuous deflection over a period.

The inspection life cycle of a pavement surface includes two inspections. The network analysis is used to identify problem areas in the road network and the formal inspection evaluates the problem areas through a time-consuming walk-through evaluation. This thesis will focus on network-level analysis.

Alternative inspections provide non-destructive methods to evaluate pavement surface through remote sensing. Non-destructive methods include UAV's fitted with different sensors and imaging devices and ground-based vehicles fitted with multiple technologies which include:

- Light Detection and Ranging (LIDAR)
- Microsoft Kinect
- Ground Penetrating Radar (GPR)
- Digital camera
- Accelerometer

Vibration-based sensors can reduce data reliability due to the sensors limited ability to measure only high energy events. Vibration-based sensors are limited to capturing data in the wheel path only and will not provide data for the entire lane width.

Different UAV types are used for different scenarios and data capturing. The multi-rotor UAV will be best suited for pavement surface inspections due to the ability to operate in limited spaces, autonomous operation, multiple operating speeds and easy operation.

Previous studies about the use of digital imaging for pavement surface inspections recorded data with an accuracy of 82.5%. The study by Shatnawi (2018) recommends research in image acquisition.

Previous studies about the use of LIDAR devices for pavement surface inspections achieved an accuracy of 95.86%. Current pavement inspection platforms fitted with LIDAR devices include expensive purpose build vehicle not suitable for network-level analysis. The use of low-cost LIDAR devices for pavement surface inspections remains an area of investigation.

Thermal devices are used in Finland to identify moisture ingress in pavement layers. The images published in the report by Heijsman (2014) include a cracked pavement surface where the cracks are easily identifiable from the thermal image. Limited research has been done using thermal devices for pavement inspections.

Various distress identification software exists; this software is predominantly for digital images and LIDAR data. Machine learning software for various industries and applications are being developed with new software being available for pavement surface evaluations with digital images. The software is expensive, and some software will be required to evaluate the different technologies and platforms.

Chapter 4: Image Processing Program Development

Currently available image processing software for defect detection focuses on the identification of cracks and surface defects in pavements. The software available for commercial use are expensive and cannot be used to evaluate the technology types and inspection platforms in this thesis; therefore, an image processing program was developed.

The computer program was developed to process images and videos of pavement surfaces using image thresholding methods. The developed program is aimed to aid the user in evaluating the collected data for image quality, defect detection and video processing. The program is needed to determine suitable travel speeds based on the image quality, creating images from videos to evaluate the use of video for data collection, and to evaluate the use of image thresholding for defect detection.

The program will not be used in real-world pavement surface evaluations to identify distress mechanisms; therefore, the accuracy and ability to identify distress mechanisms will not be evaluated. The program is developed to determine suitable travel speeds based on image quality, creating images from videos to evaluate the use of video for data collection.

The program is developed using the Java API development platform, video processing libraries and image processing libraries to develop a graphical user interface (GUI) able to process video and image files. The code of the Image Processing Program can be seen in Appendix C.

4.1 Program Structure

The structure of the image processing program can be seen in Figure 24. The program consists of a Graphical User Interface (GUI), an image class and a video class.

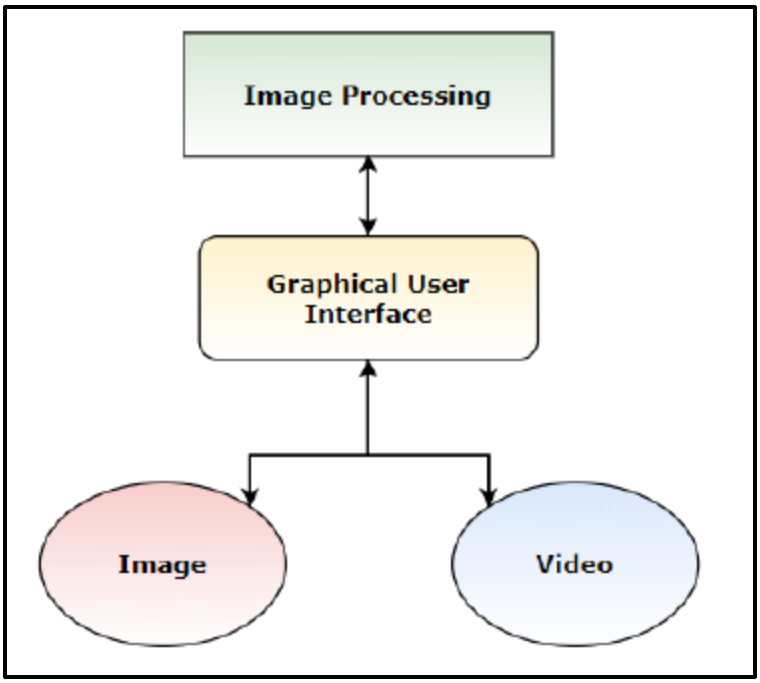

Figure 24: Image Processing Program Structure

4.1.1 Graphical User Interface (GUI)

The image processing program will use a Graphical User Interface (GUI) to communicate with the user. The GUI uses a JFrame extension to create the User Interface (UI) panel. The GUI implements action listeners to communicate with the user and perform predefined actions or calculations. The GUI uses an Image class to process image files and a Video class to process video files. Both the Video and Image classes communicate with the GUI through a background process to perform the analysis of the pavement surface.

The GUI consists of 9 buttons, a text output area and the general window frame commands including the exit, minimize and maximize buttons. Each of the buttons on the GUI performs a specific task to process the image or video file. The buttons implement action listeners to accept the user input when a button is clicked. The text output area communicates with the user with specific line commands to inform the user of the progress or current operation of the program. The GUI window can be seen in Figure 25.

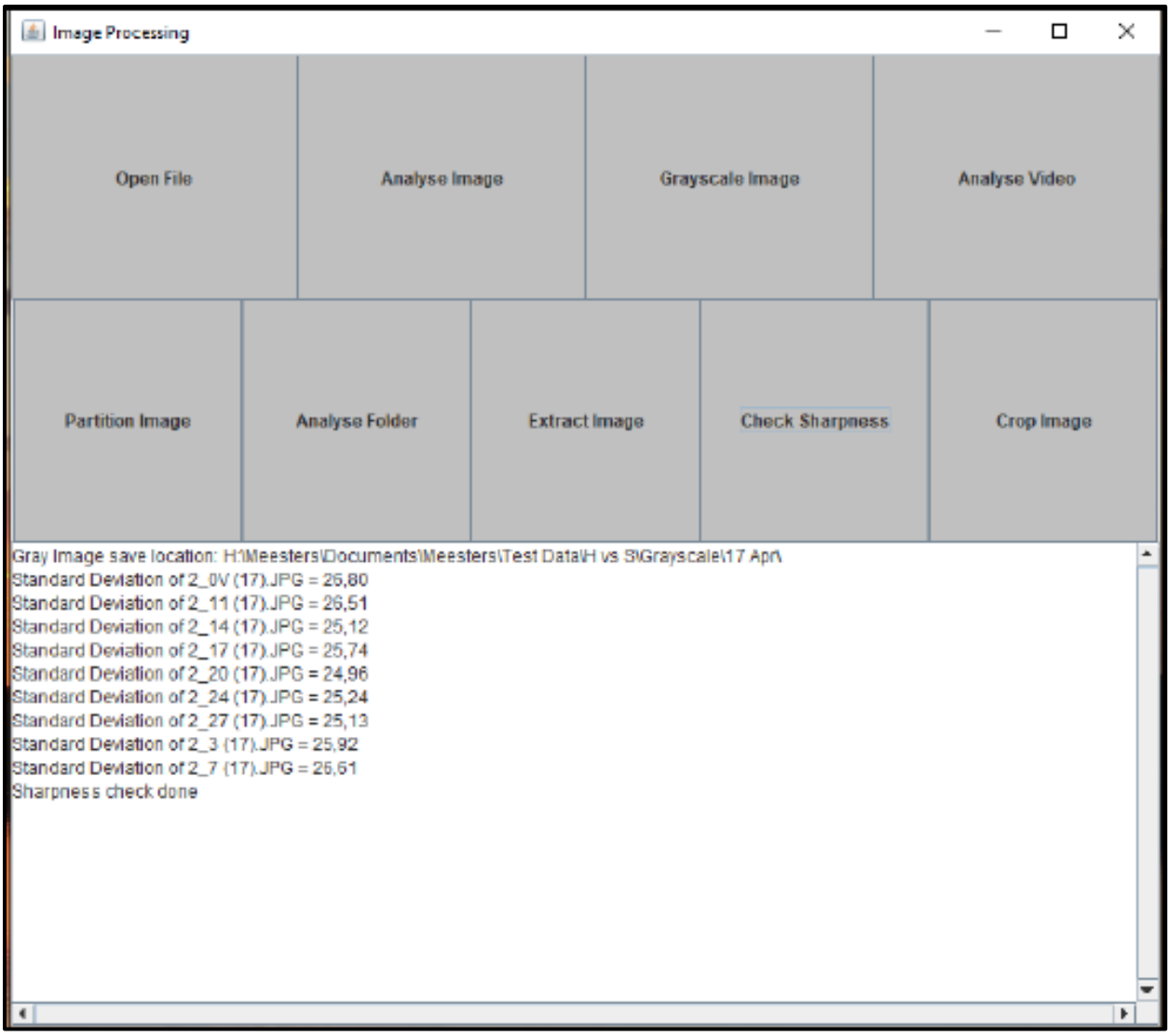

Figure 25: Graphical User Interface (GUI)

The program obtains the image file, image folder or video file using an open dialogue box. When a button is clicked by the user an open dialogue box (Figure 26) appears on the GUI, this allows the user to select the specific file or folder the program must access to perform the selected actions. If an image will be the result of the actions the user-specified a save location for the image file is required by the program.

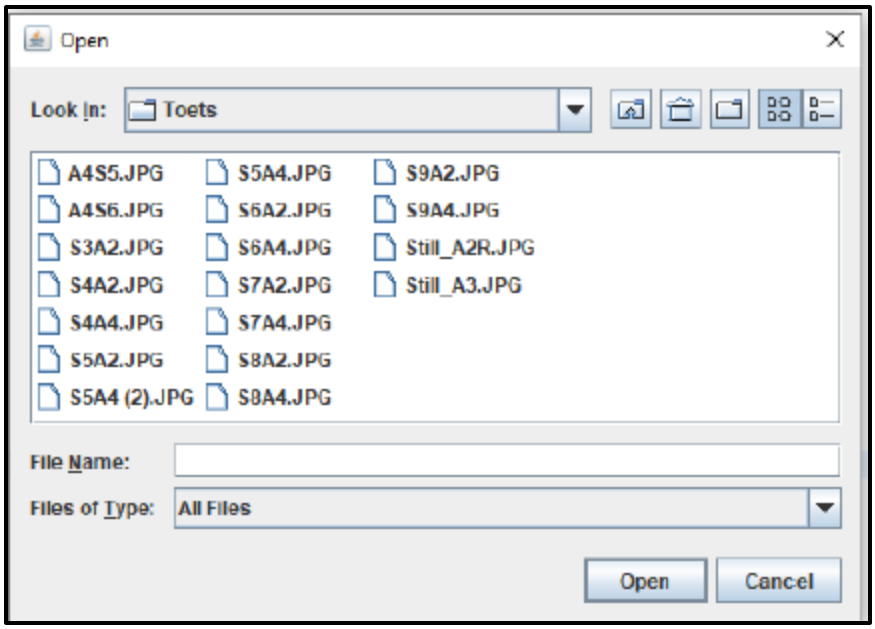

Figure 26: Open dialogue box

The user can specify the image file save location through the save dialogue box (Figure 27) that will appear on the GUI if a save location is required. In some cases, will the user be asked to select multiple save locations for different steps in the program. This allows the user to access the different type of images required for the analysis.

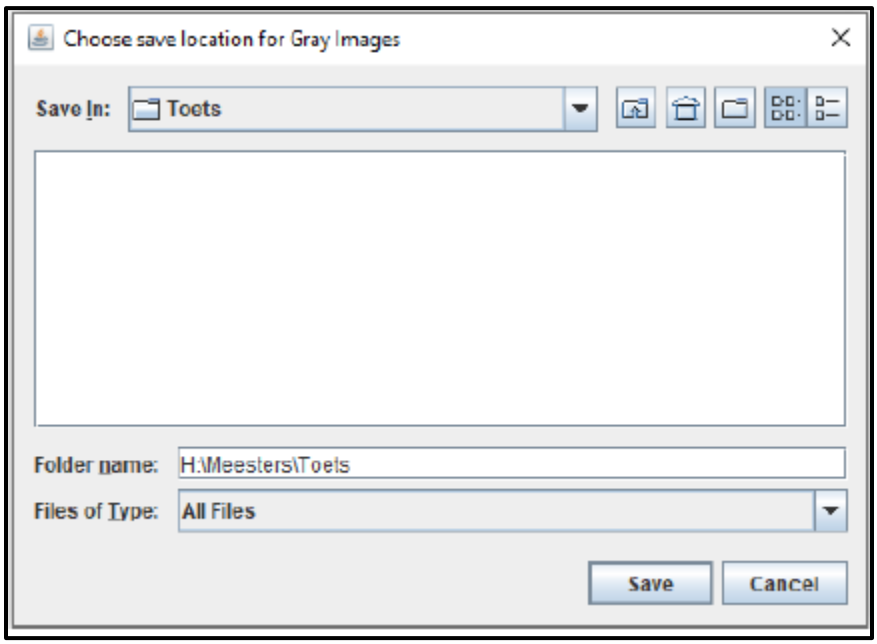

Figure 27: Save dialogue box

4.1.2 Image class

The Image class is used by the GUI to process image files. The image class include methods to paint the image file, read the image file, calculate the average image intensity, highlight the defects on the pavement surface, convert the RGB image to a grayscale image and calculate the image sharpness. The paint method allows the GUI to paint the image that was created by the program. The paint method opens the created image and the image will be displayed on a JFrame over the GUI. The image reader allows the GUI to read the image file and perform image thresholding calculations on the image.

The GUI convert the selected RGB image to a grayscale image by converting the red, green and blue pixel values by using the following:

- red = (**int**) (c.getRed() * 0.299)
- green = (**int**) (c.getGreen() * 0.587)
- blue = (**int**) (c.getBlue() * 0.114)

The three RGB colours should be combined to create a grayscale image. The combination follows:

```
newColor = new Color(red + green + blue,red + green + blue, red + green + blue)
```

The average intensity of the image is calculated using Equation 2.

Equation 2: Average Image Intensity

$$Average\ Image\ Intensity = \frac{\sum_{Image\ Height\ \times Image\ Width} Pixel\ Intensity}{Image\ Width\ \times Image\ height}$$

The pavement surface defects can be identified by comparing the intensity of each pixel in the image to the average intensity of the image. The average intensity of the image determines the upper and lower boundary. The pixels which are not within the upper or lower boundary of the average are highlighted. The highlighted pixels are part of a pavement surface defect. The highlighted output can be seen in Figure 28.

The sharpness of the image is used to determine the quality of the image. This method is used to determine the maximum travel speed to capture high-quality images. The sharpness is calculated using the standard deviation equation in Equation 4.

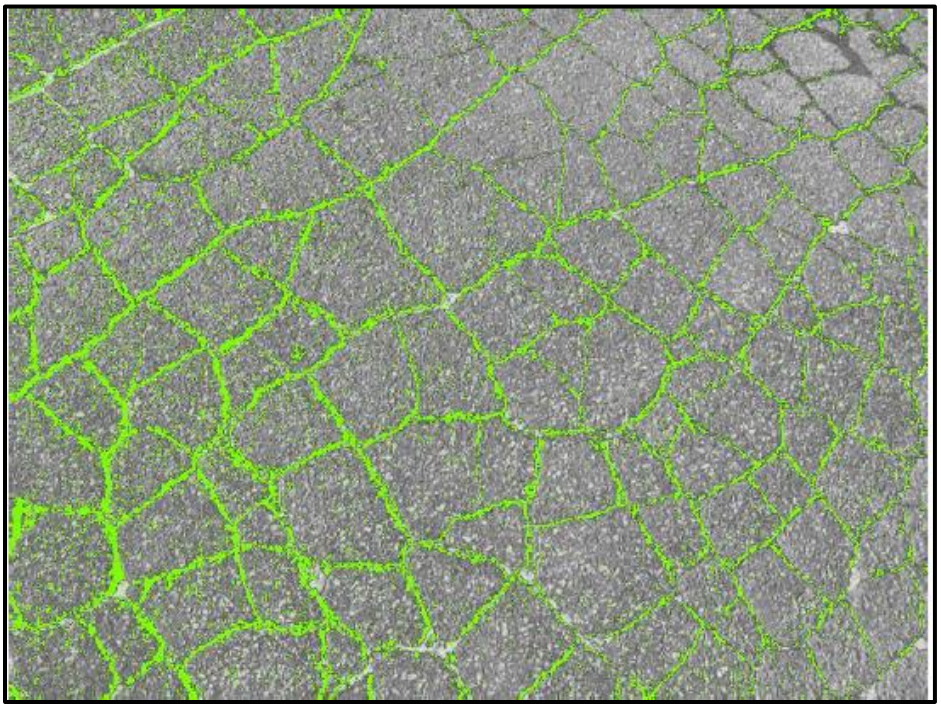

Figure 28: Image Processing Output of an example image

4.1.3 Video class

The Video class is used by the GUI to extract images from the video file. Video processing libraries are not part of the Java API platform; therefore, open-source libraries were imported into the project to process the video files. The imported libraries include Jcodec and Xuggler; each of these libraries consists of different smaller libraries to perform video processing. The Xuggler library was used to obtain metadata of the video. The library includes methods to obtain the duration and frame rate of the video file.

The Jcodec library includes methods to process the video and create images from the video. The Jcodec method used in the program extracts an image at the specified time. The image grabbed at the specified time is a Picture type file which requires changing the file type to a buffered image to be able to implement the methods in the Image class and perform the image file processing.

The image processing program will be used in Chapter 5 and Chapter 6 to determine suitable travel speeds based on the image quality, creating images from videos to evaluate the use of video for data collection, and to evaluate the use of image thresholding for defect detection.

Chapter 5: Testing of platforms and technology types

Testing of different technological devices and platforms are used to determine the capabilities and specifications of the devices and platforms. The devices are tested on different vehicles and UAV's where possible. Some devices will not fit on UAV's; these devices are tested on vehicles only. The platform testing will start by evaluating a home build UAV and a DJI Mavic Mini.

The home build UAV can be fitted with a GoPro Hero 3 or Hero 8 Black. The tests include both the digital cameras at different settings, heights and flying speeds. The home build UAV can fly autonomous missions loaded to the flight controller. Two flight plan software programs will be evaluated to determine the most suitable software for this application. The DJI Mavic mini is factory fitted with a 2.7K digital camera from DJI. The Mavic Mini tests will include all three UAV settings at different heights and flying speeds.

The vehicle testing will include two vehicles fitted with GoPro cameras and a thermal device, the first an Audi A4 and the second a Toyota Hilux. The device can be fitted at the height of 1.3 meters above the surface on the Audi and 2 meters above the surface on the Hilux. The tests included both video and images captured to determine which will be best suited.

The vehicle can be fitted with additional lighting sources to enhance the surrounding conditions for the digital camera. The additional lighting system consisted of the following hardware:

- 80W LED Floodlight
- 1000W Inverter
- Multiplug
- Lead
- Cable Ties
- Two poles

The poles and cable ties are used to attach the floodlight to the vehicle, the lead and multiplug connect the inverter and floodlight respectively and the inverter is used to power the 220V LED floodlight from the 12V car battery.

5.1 UAV Testing

5.1.1 Home-Built UAV Specifications

Two different types of UAV's were used in the preliminary testing phase. The first UAV is a home-build UAV using a standard 450-millimetre quadcopter drone frame, four brushless motors, a flight controller, GPS, and battery. The UAV can be fitted with a standard GoPro digital camera.

The home-build UAV fitted with the GoPro Hero 8 digital camera possesses a flight time of 13 to 18 minutes depending on the flying conditions. The home-built UAV can be seen in Figure 29.

Figure 29: Home-Built UAV

The specifications of the home-built UAV can be seen in Table 14.

Table 14: Home-Built UAV specifications

Item	Description
Frame	F450 Quadcopter Frame with landing gear
Motor	Emax MT2216
Propeller	1045
ESC	BL-Heli 30A
Flight controller	Pixhawk
GPS	U-Blox
Battery	Onbo 5200 mah
Camera	Fitted with GoPro Hero 8 Black

The first set of tests with the home-built UAV was done using the GoPro Hero 3 camera set to 1080p, 60 frames per second, and a wide camera angle. The tests were done by flying the UAV manually at an average height of 6 meters above the pavement surface at an average speed of 7 meters per second. With the wide viewing angle of the GoPro Hero 8 and the high-flying height, most of the image contains the road reserve and wider areas.

The wide lens of the GoPro Hero 8 resulted in some image distortion on the outer parts of the images. The wide lens results in a rounded image with an unrealistic representation of the object being captured. The rounded effect on the image is known as the fish-eye effect. In Figure 30, the difference between the wide lens image and the linear lens image is visible. The linear lens provides a realistic representation of the object. The linear lens is achieved with image processing within the GoPro Hero 8 camera.

Figure 30: GoPro Hero 8 wide lens vs Linear lens image

The GoPro Hero 8 was not tilted to a parallel angle with the pavement surface resulting in an image that contains large parts of the pavement surface ahead of the device instead of the parts directly underneath the device. The GoPro Hero 8 lens captured a fisheye view of the pavement surface. This fisheye effect results in a rounded image instead of a linear image. The rounded parts of the image are difficult to analyze due to the fisheye effect that creates an unrealistic image of the pavement surface. The test specification can be seen in Table 15.

The manual flying of the UAV proved to be inadequate for pavement surface analysis due to inconsistent travel speeds and height above the pavement surface. Few road sections are completely flat, resulting in a constant adjustment to the flying height of the UAV.

Table 15: First UAV test

Variable	Value
Average Height	6 meters above the surface
Average Speed	7 m/s
Camera Settings	1080p @ 60 fps at a wide angle

The first set of tests indicated that the flying height would depend on the camera viewing angle and the road width, due to the flying height of 6 meters above the pavement surface that included the road reserve and other areas alongside the pavement surface. The average moving speed of 7m/s is not adequate with a frame rate of 60 fps and an automatic shutter speed of the lens but may be adequate with a faster frame rate and shutter speed. The camera must be parallel to the pavement surface to avoid capturing the pavement surface ahead of the device. An automated flight plan will be required to ensure a constant flying speed and height above the pavement surface.

5.1.2 Flight Plan Software

The flight controller and GPS of the home-built UAV can be programmed to autonomously fly the UAV on a predefined route by using flight plan software. Different flight controlling software is available. Two free flight controlling software is Qground control and Mission Planner computer software. Both the flight controlling software programs are compatible with the flight controller of the home-build UAV. The autonomous flying capabilities of the UAV have been tested with Qground control and Mission planner to compare the software uses.

The first flight plan software to be tested is the Qground control software. The predefined route was set-up to test the autonomous flying ability of the UAV and the height of the UAV relative to the ground surface. Qground control enables the user to set the predefined travel speed of the UAV. This allows the user to capture data at constant moving speeds. The Qground Control mission setup interface and autonomous flight test setup can be seen in Figure 31

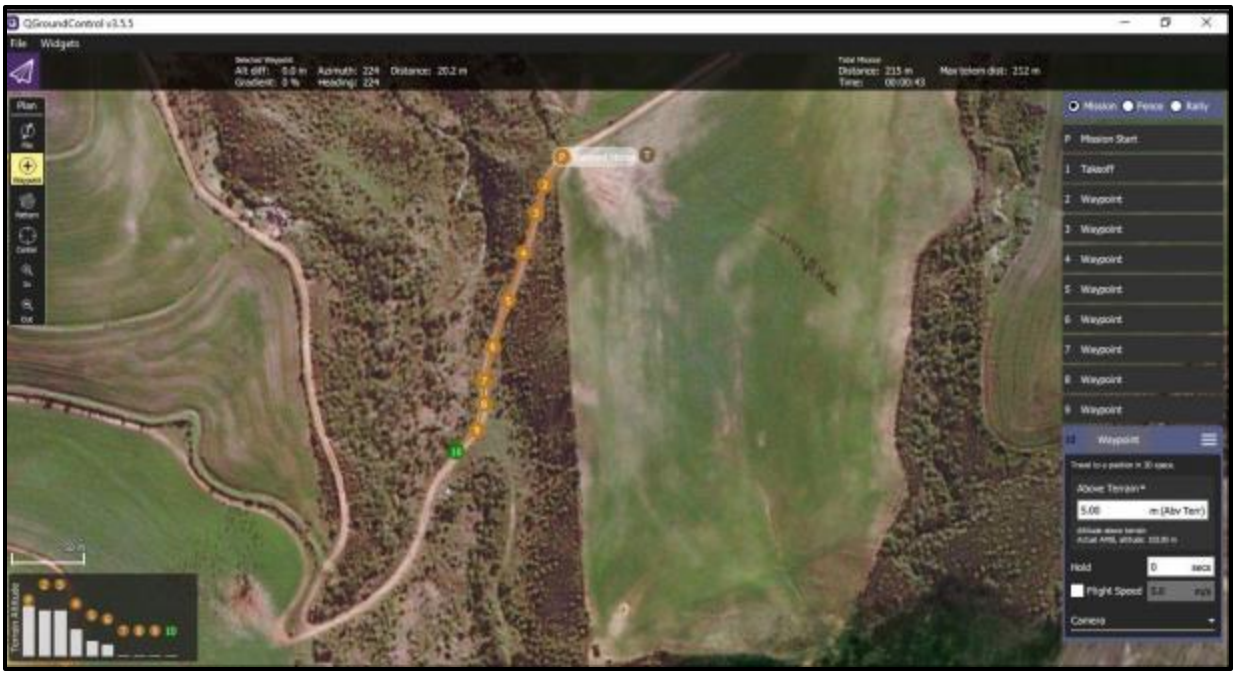

Figure 31: Autonomous flight test setup

The waypoint settings window for Qground control can be seen in Figure 32. The waypoint settings are used to specify the height of the UAV relative to the terrain or relative to the home point altitude.

Figure 32: Waypoint window in QGround control

The UAV uses ground surface data from Google Earth to determine the specific height above the ground surface. The data is captured at the specific coordinates of the waypoints entered by the

user. The waypoint coordinates and altitude are stored on the flight controller and can be enabled using the autonomous flying function on the receiver and transmitter.

The test specifications for autonomous flying can be seen in Table 16.

Table 16: Autonomous UAV test

Variable	Value
Average Height	5 meters above the ground surface
Average Speed	5 m/s
Camera Settings	-

The autonomous flight profile from Google Earth can be seen in Figure 33. The flight path and elevation model of the UAV is indicated as the green and yellow lines. The flight tested the ability of the software to determine the flight path over a steep drop in terrain elevation.

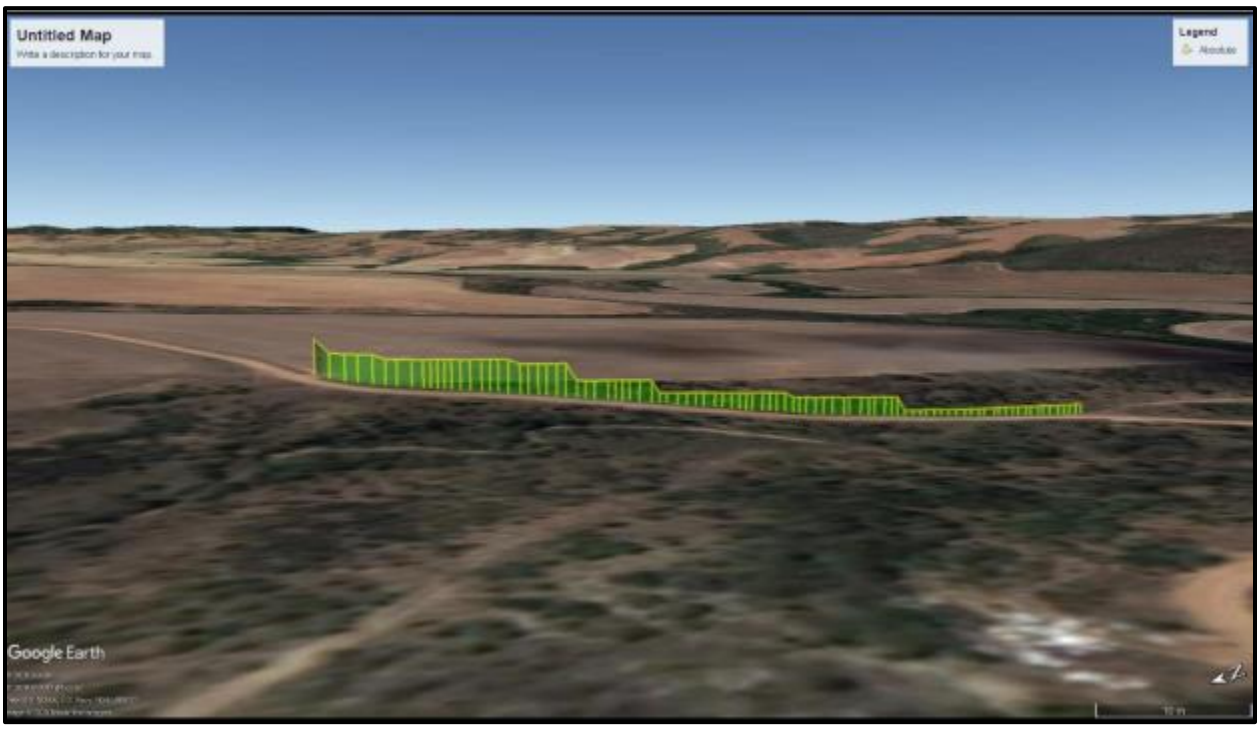

Figure 33: QGround Control flight profile

Comparing the UAV elevation model and the ground elevation model in Figure 34 indicates that the Qground Control software is not able to follow the changes in the terrain continuously. The UAV only adjust the altitude at the specified waypoint.

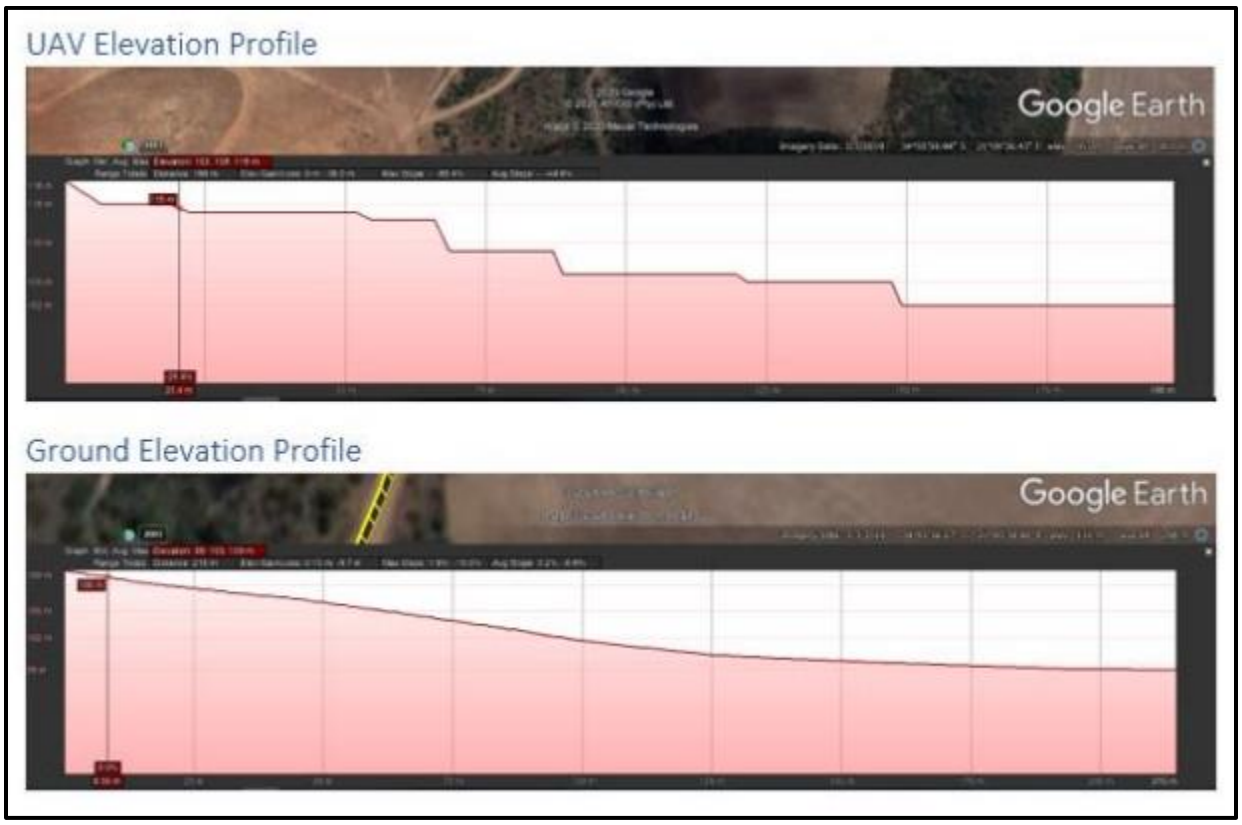

Figure 34: QGround Control Autonomous flight elevation model

The second flight plan software to be tested is the Mission Planner software. The predefined route was set-up on the same location as the previous flight test. Mission Planner enables the user to set the predefined travel speed of the UAV through a speed change waypoint. This allows the user to capture data at constant moving speeds.

The Mission Planner flight plan setup interface and autonomous flight test setup can be seen in Figure 35.

Figure 35: Mission Planner flight plan interface

The waypoint settings window for the Mission Planner can be seen in Figure 36. The waypoint settings allow the user to change the waypoint altitude relative to the terrain, the home location or absolute altitude. The moving speed of the UAV must be set through a change mission speed command. The UAV will continue to travel at the indicated speed until a new change speed command is set. Mission Planner allows the flight path to be smoothed through a spline path command.

Figure 36: Mission Planner waypoint settings window

Comparing the UAV elevation model and the ground elevation model in Figure 37 indicates that the Mission Planner flight plan software can follow the changes in the terrain continuously. The UAV adjusts the elevation between waypoints to ensure a smooth descent along with the slope change.

Figure 37: Mission Planner Autonomous flight elevation model

The second set of tests indicated that the autonomous flying abilities of the UAV are necessary to ensure a constant travelling speed and height above the ground surface. The home-build UAV and Mission Planner software proved to be adequate for autonomous flying. The waypoint levels were

accurately obtained from Google Earth and proved to be an adequate method to specify the flying height. It is recommended to insert as many waypoints as possible to ensure an accurate and continuous flying profile above the pavement surface.

5.1.3 DJI Mavic Mini Test

The third set of tests involved the use of a DJI Mavic Mini UAV. The UAV is an entry-level off the shelf UAV fitted with a DJI 2.7K digital camera. The UAV has a tiltable gimbal and video transmission up to four kilometres. The UAV has three different modes: Positioning mode, with a maximum travel speed of 8 m/s; Sport mode, with a maximum travel speed of 13 m/s; and Cinesmooth mode, with a maximum travel speed of 4 m/s. The DJI Mavic mini can be seen in Figure 38.

Figure 38: DJI Mavic Mini

The digital camera settings used for the test can be seen in Table 17 (Corrigan, 2020). The test was completed using all three modes of the UAV at different flying heights.

Table 17: DJI Mavic mini camera specifications (Corrigan, 2020)

Item	Description
Pixels	12 MP
Video bitrate	40 Mbps
Maximum Video Resolution	2720 x 1530 @ 25 fps or 30 fps
Minimum Video Resolution	1920 x 1080 @ 25/30/50/60 fps
Horizontal Field of view	83 degrees
Vertical Field of view	43.2 degrees

The best flying height above the pavement surface depends on the road width. The test flights were completed on a single carriageway with a width of 6 meters. The maximum height above the pavement surface for this road width is 4 meters. The UAV captured parts of the side of the roadway when the height becomes more than 4 meters. This can cause problems when traffic is encountered due to the maximum permissible height of vehicles in South Africa of 4.3 meters (Department: Transport, 2009).

The time of day and travel direction can influence the results of the UAV system. During the tests, the road section was traversed to ensure adequate testing. The tests were performed around 11h 00, which mean that the position of the sun was more to the east. This resulted in the constant capture of the UAV's shadow in the video image when travelling in a western direction. The shadowed image can be seen in Figure 39. The shadow can obstruct important pavement surface information and can lead to the misanalysis of the pavement surface.

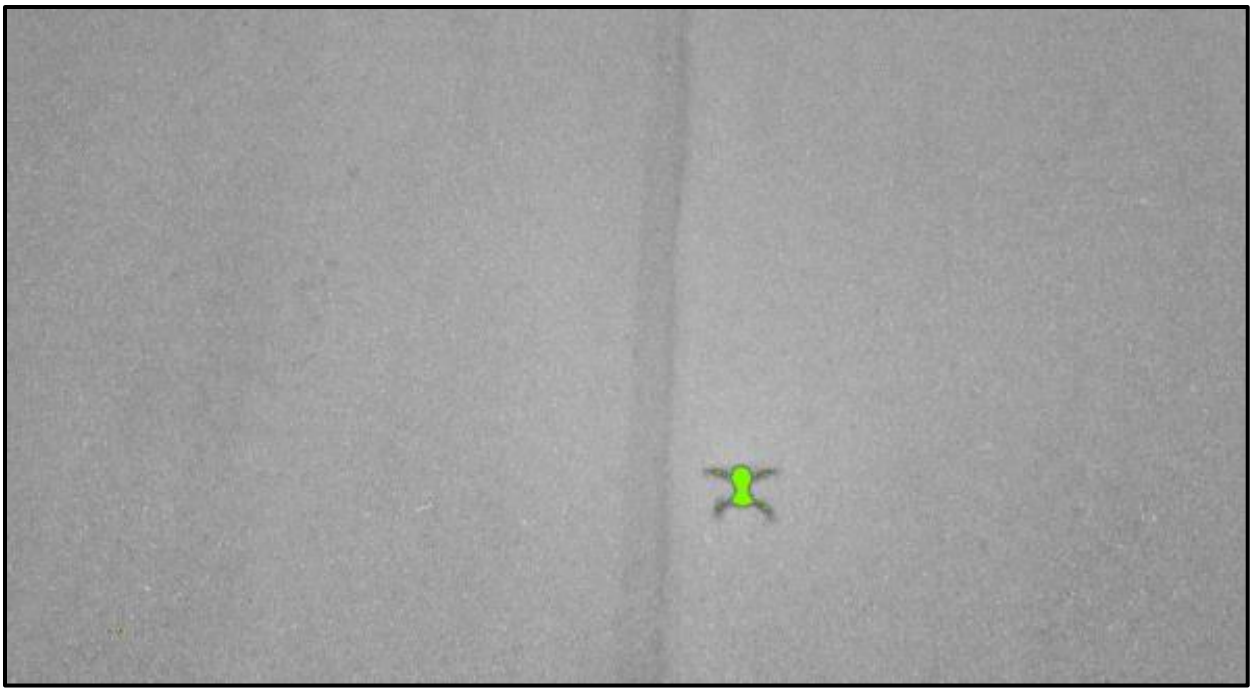

Figure 39: The shadow influence in the UAV video

5.1.4 Lessons Learned from UAV tests

Testing of UAV's and different digital cameras provided import information to consider before data capturing using a UAV can commence. The important considerations include:

- The camera should be tilted parallel to the pavement surface
- The flying height will depend on the camera viewing angle and road width
- Autonomous flying is required to ensure a constant height above the pavement surface and travelling speed
- The travelling speed will depend on the video quality and frame rate of the camera
- The flying direction should be towards the sun to avoid unwanted shadows of the UAV in the video

5.2 Vehicle Testing

Two different ground-based vehicles were used during the testing of the vehicles. The first vehicle was an Audi A4 (lower vehicle) and the second vehicle a Toyota Hilux (higher vehicle).

5.2.1 Lower Vehicle Testing

The first set of tests involved the lower vehicle (Audi A4) fitted with the GoPro Hero 8. The device was fitted to the back of the vehicle with a GoPro suction mount. The device recorded to the back of the vehicle; the mounting position can be seen in Figure 40.

The GoPro Hero 8 device needed to be tilted slightly upward from a 90-degree angle to avoid the rear bumper of the car being captured in the video frame. The device was mounted at the height of 1.3 meters above the pavement surface and recording 2.4 meters of the road surface.

Figure 40: Lower vehicle device mount

The tests required the vehicle to travel at speeds of 20 km/h (5.56 m/s) and 30km/h (8.33 m/s) respectively. Both the set of tests yielded useable video material with the GoPro Hero 8 set to 1080p and a frame rate of 25 fps. The tests were repeated with the GoPro Hero 8 set to 4K, a frame rate of 30 fps and a linear lens. The better video resolution resulted in an improved crack pattern identification due to the higher number of pixels in each video frame. The higher video frame rate

resulted in a higher travelling speed before the video quality started to deteriorate. The linear lens proved to eliminate the fisheye effect of the GoPro Hero3.

The tests with the lower vehicle highlighted two distinct difficulties; the first difficulty proved to be the tilted camera angle. The tilted camera resulted in a video frame that included a large part of the pavement surface a distance away from the device. The road defects were difficult to identify due to the camera not recording the defects from above. This resulted in a less distinctive difference between the defect intensity and the road surface. The second difficulty proved to be the lighting conditions at the back of the vehicle. The vehicle's shadow was recorded in some parts of the video, which may lead to missing some important surface defects.

5.2.2 Higher Vehicle Testing

The tests with the higher vehicle (Toyota Hilux) were aimed to address the difficulties from the lower vehicle. The Hilux was fitted with the GoPro Hero 8 set to 4K, a frame rate of 30 fps and a linear lens. The device was fitted to the vehicle's roof rack with a monopod to serve as a gantry system. The monopod extended to one meter past the back of the vehicle to avoid the back bumper being included in the video. The gantry system provided the opportunity to tilt the GoPro device parallel to the pavement surface tilted camera results. The gantry system can be seen in Figure 41.

Figure 41: High vehicle fitting

The tests required the vehicle to travel at speeds of 20 km/h (5.56 m/s) and 30km/h (8.33 m/s) respectively. Both sets of tests yielded useable video material with the GoPro Hero 8 set to 4K, a frame rate of 30 fps and a linear lens. The parallel video image improved the difficulty of identifying the defects due to the 90-degree angle of the device. The difficulty of the lighting conditions and shadows remained. This could be fixed by providing alternative illumination at the back of the vehicle to eliminate unwanted shadows.

Figure 42: Additional Lighting Test setup

Figure 42 shows the setup on the higher vehicle to test the digital camera with additional lighting added to the system. The setup included a 1000-Watt inverter connected to the vehicle's deep cycle battery system through a Brad Harris type connection. The light used in the setup was an 80W, 6000 lumens LED floodlight mounted next to the digital camera.

The additional lighting added to the system made no noticeable improvement in shadowed areas during the daytime. The system was used to determine if data capturing with a digital camera will be a viable option during the night-time (Figure 43). The system worked to some extent, with the centre of the image well-lit but the outer edges were too dark to identify distress mechanisms. The camera shutter speed limited the image quality with blurry images at 3 km/h; this can be seen in

Figure 43. Adding more additional lights to the system may eliminate the dark edges of the images. Still, a low-cost camera will not be able to capture moving images during night-time.

Figure 43: Night-time test with a digital camera

5.2.3 Lessons Learned from vehicle tests

Testing of different digital cameras fitted to vehicles provided important information to consider before data capturing using a vehicle can commence. The important considerations include:

- The camera should be tilted parallel to the pavement surface
- The higher vehicle will provide the best platform for data capturing
- The travelling speed will depend on the video quality and frame rate of the camera
- Alternative illumination should be provided at the back of the vehicle to eliminate unwanted shadows
- Three or more lights should be used to eliminate shadowed edges

5.3 Data collection speed limit testing

The data collection speed limit for each device can be determined by calculating the severity of pixel blur at a specific speed. A digital image becomes blurred when a pixel's size in the direction of travel exceeds one. The equation used to determine an image's theoretical pixel size will be validated using a GoPro Hero 8. The validation process involves capturing images at two meters above the pavement surface at different moving speeds and calculating the standard deviation between the pixel intensities.

5.3.1 Pixel Size Calculation

Equation 3 is used to calculate the pixel size given the exposure time, moving speed, the number of pixels in the direction of travel and the camera field of view (Smart Vision Lights, no date). An individual pixel can be regarded as blurred when the pixel's size exceeds one.

Equation 3: Image blur (Smart Vision Lights, no date)

$$Pixel\ Size = (Moving\ speed\ \times Exposure\ Time) \times (\frac{No.of\ pixels}{Field\ of\ view})$$

Where:

$FOV = height\ above\ surface\ \times \tan(\emptyset)$, where $\emptyset$ is the camera view angle.

$$No.of\ pixels = Amount\ of\ pixels\ in\ the\ traveling\ direction$$

5.3.1 Determining the Allowable Standard Deviation between pixels

The maximum allowable standard deviation percentage is determined by capturing a zero-speed image and moving images of a white object at various speeds. The standard deviation of the moving images is compared to the standard deviation of the zero-speed image to determine the maximum allowable standard deviation percentage when excessive image blur occurs. All the captured images are converted to grayscale images, and the standard deviation between pixels is calculated for each image using the image processing program developed in Chapter 4. This process was repeated in increments of 1m/s, starting at 1 m/s up to 8 m/s

The standard deviation between pixels of a specific image represents the contrast between pixels. A lower standard deviation, therefore, indicates image blur due to no clear difference between the pixels. The higher the standard deviation and contrast, the clearer the difference between pixels and less blurry an image becomes. The test images are similar to Figure 44. The image in Figure 44 was captured at the height of two meters above the pavement surface at a speed of four meters per second using a GoPro Hero 8.

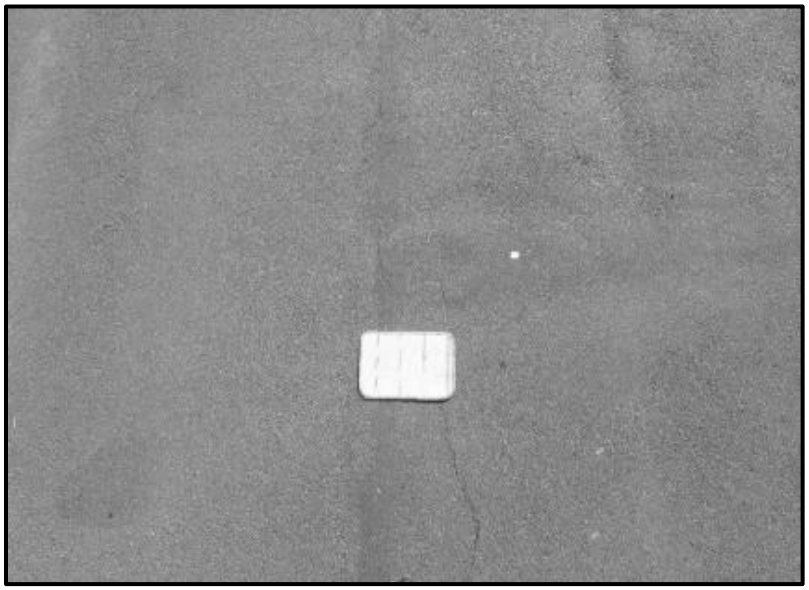

Figure 44: Blur Test image at 2 meters and 4 m/s using a GoPro Hero 8

The standard deviation between the pixel intensities was calculated for each image according to Equation 4. The standard deviation of the moving images was compared to the standard deviation of the zero-speed image. A significantly lower standard deviation indicates excessive pixel blur because of more uniform pixel intensities between pixels. Pixel contrast between the pavement surface and cracks also become less significant when an image is blurry. This can result in inaccurate results from the image processing program.

Equation 4: Standard Deviation (Math Centre, 2003)

$$\sigma = \sqrt{\frac{\sum(x - \mu)^2}{N}}$$

Where: N, is the number of pixels
x, is the intensity of the pixel

μ, is the average intensity of all the pixels
σ, is the standard deviation

Table 18 contains the test results of images and videos taken at two meters above the pavement surface at varying speeds. Table 18 indicates an increasing standard deviation percentage when the travel speed increase. This indicates less pixel sharpness and more image blur at increased speeds due to more uniform pixel colours.

Table 18: Standard Deviation Percentage results from Blur Tests using a GoPro Hero 8

		Standard Deviation Percentage (%)		
		Shutter Speed		
Image Name	**Speed (m/s)**	**Auto (1/2500)**	**1/11755**	**Video**
A2Zero		0.0%	0.0%	0.0%
A2S1	1	1.9%	3.3%	20.6%
A2S2	2	4.1%	0.7%	19.8%
A2S3	3	14.2%	1.1%	24.3%
A2S4	4	19.3%	6.3%	36.4%
A2S5	5	24.8%	4.0%	38.8%
A2S6	6	25.5%	6.9%	37.7%
A2S7	7	28.5%	5.8%	41.6%
A2S8	8	36.9%	6.2%	

The maximum allowable standard deviation of a moving image compared to the standard deviation of a zero-speed image can be determined by comparing the difference between the theoretical travel speed (Equation 3) and tested travel speed for a blurred image. The difference between the theoretical speed and tested speed is used to determine the point of minimum difference between the theoretical travel speed (Equation 3) and tested travel speed (Table 18) when an image becomes blurred. This point will be accepted as the maximum allowable standard deviation of a moving image compared to the standard deviation of the zero speed image.

Figure 45 shows the graphical representation of the difference between the theoretical speed (Equation 3) and tested speed (Table 18) when an image becomes blurred. The minimum difference between the speeds can be found at a 10% standard deviation difference between the moving image and the zero-speed image.

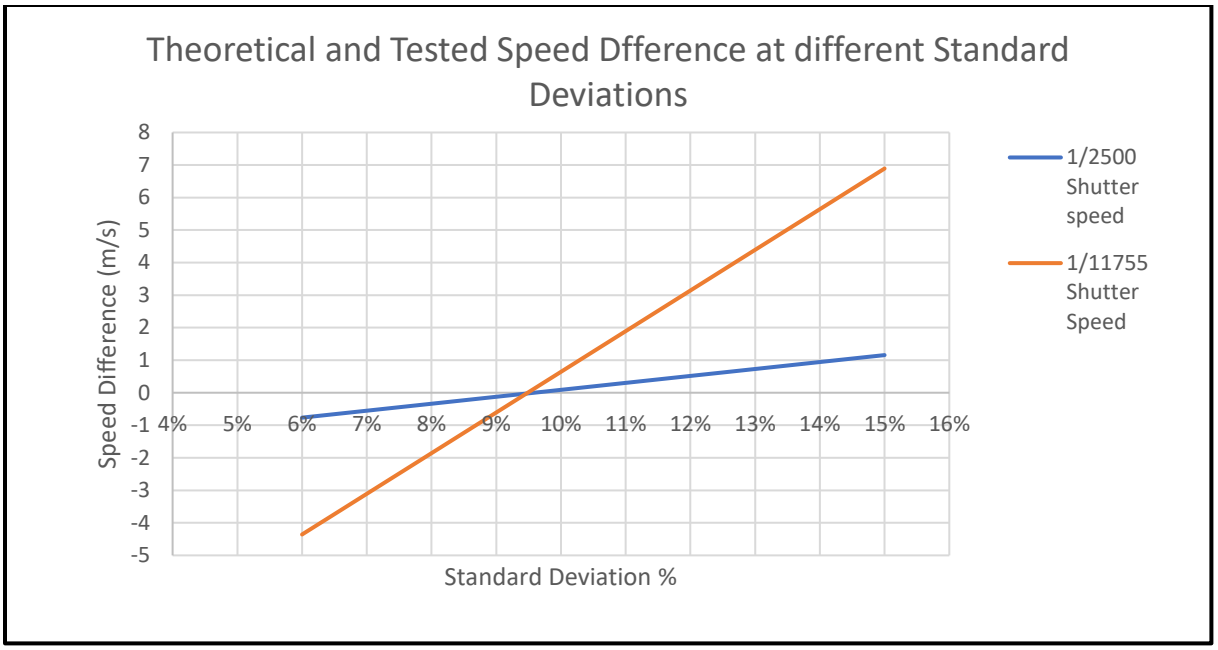

Figure 45: Theoretical and Tested speed difference at different Standard Deviations

It is determined that images with a standard deviation within 10% of the standard deviation of the zero-speed image will have the adequate quality to identify distresses in the pavement surface. The data in Table 18 is used in Figure 46 to graphically represent the standard deviation compared to the zero speed image. The 10% standard deviation (SD) limit is indicated in orange. Figure 46 indicates excessive image blur at a travel speed of 2.6 m/s for a 2m altitude and 1/2500 shutter speed.

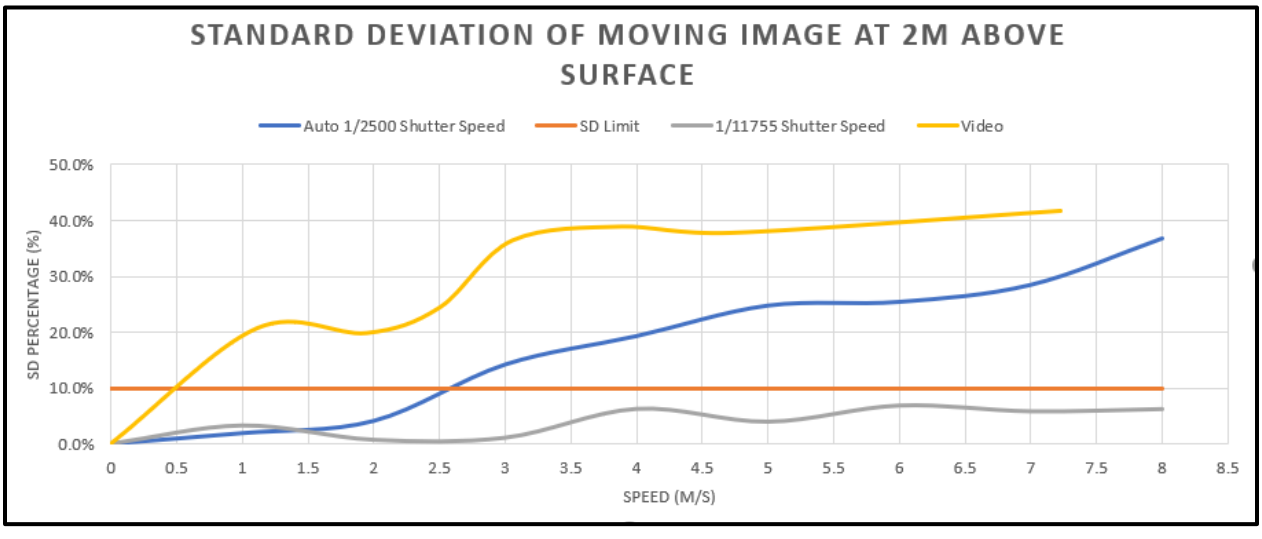

Figure 46: Image Sharpness at 2m above the surface with different shutter speeds

5.3.3 Verification of the Pixel Size Equation

Equation 3 was verified by comparing the results of Equation 3 to the results of the manual tests in Chapter 5.3.2. Calculations using

Equation 3 indicated that the GoPro Hero 8 image at 4K resolution would blur at 2.36 m/s travelling speed for an altitude of 2 meters above the pavement surface with a shutter speed of 1/2500 seconds. The test data using the GoPro Hero 8 with an image resolution of 4K indicated excessive image blur would occur at 2.45 m/s travelling speed for an altitude of 2 meters above the pavement surface.

Equation 3 with a shutter speed of 1/11755 seconds, the GoPro Hero 8 at 4K resolution and a height of 2 meters above the surface indicated excessive image blur at 11.08 m/s and the test data at 11.73 m/s. Table 19 contains a summary of the results.

Table 19: Calculated and tested image blur summary

Shutter Speed	Maximum Travel Speed (m/s)		Accuracy
	Formula	Tested	
1/2500	2,36	2,45	96,3%
1/11755	11,08	11,73	94,5%

Test data in Table 19 confirms that the formula used in Equation 3 will yield a 95% accurate answer for travelling speeds at different variable values. It can be seen that Equation 3 will yield more conservative results for the data capturing speeds. Equation 3 will be adequate to determine the required or limit speed of data capturing when the device's exposure time, the field of view and number of pixels in the image is known.

5.4 Crack Width Testing

Pavement surface cracks can be categorised in three categories; the first category is faint cracks where the crack width is equal to 1 millimetre. The second category is distinct cracks where the crack width is equal to 3 millimetres with some secondary defects in the form of spalling. The third category is cracks larger than 3 millimetres with significant secondary defects or open cracks larger than 5 millimetres with no secondary defects (TMH 9, 2016).

Figure 47 shows the results of different crack widths using a digital camera. The pictures on the left side of Figure 47 are the 1mm, 3mm and 5mm crack width measurements, while the pictures

on the right side are the same cracks at the height of 1.5 meters above the pavement surface. The digital camera was able to detect distinct cracks of 3mm and significant cracks of 5mm. Fine cracks of 1mm are not visible on the digital images.

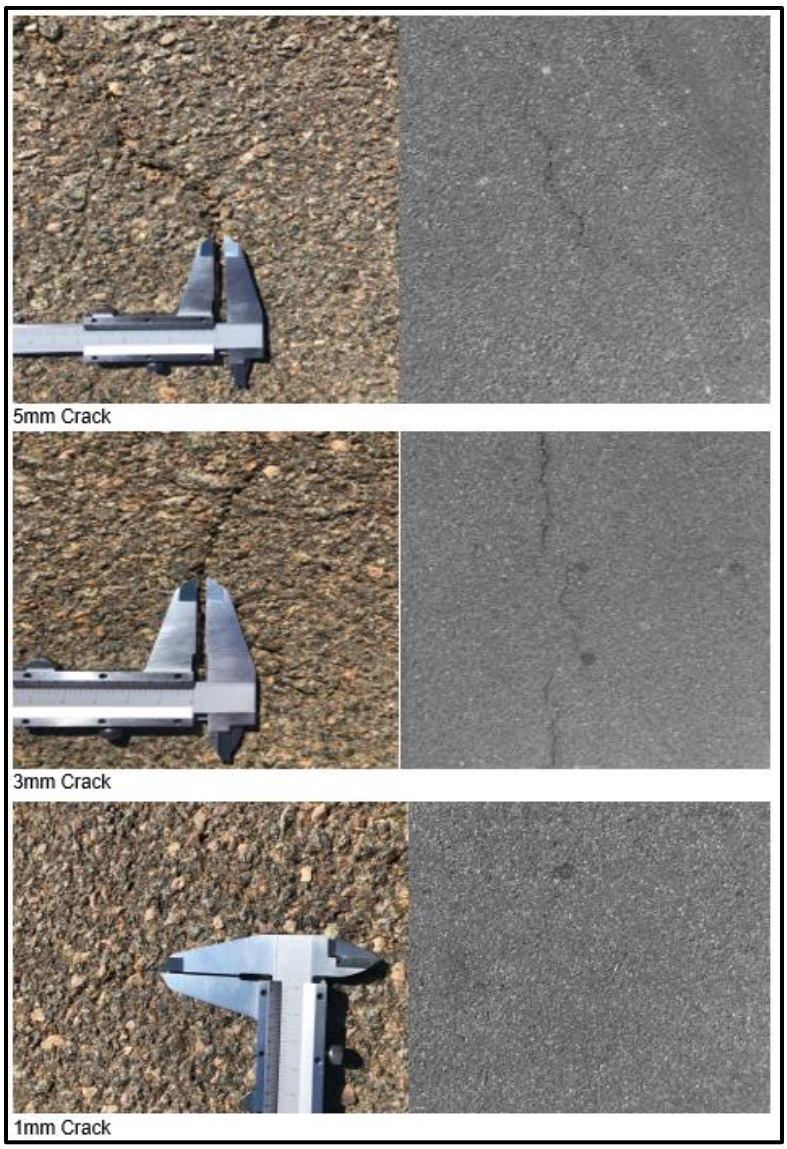

Figure 47: Crack Widths at 1.5 meters above the surface using a Digital camera

5.5 Thermal Device Testing

The thermal device used was a Major Tech MT 2005 with a thermal sensor of 80 x 80 pixels (Figure 48). The device is a multimeter with a thermal camera and is normally used for electrical inspections.

Figure 48: Major Tech MT2005 thermal multimeter

The device was used to test the use of thermal cameras in pavement surface inspections. The tests investigated the ability to capture cracks and potholes in the road surface, measure crack widths that can be captured and test the influence of lighting conditions on the camera.

The thermal device has colour pallets which indicate hot and cold spots with different colours. Figure 49 shows three different pallets where black is hot, red is hot, and orange is hot respectively. Figure 49 indicates that the crack will be hotter than the surrounding pavement surface.

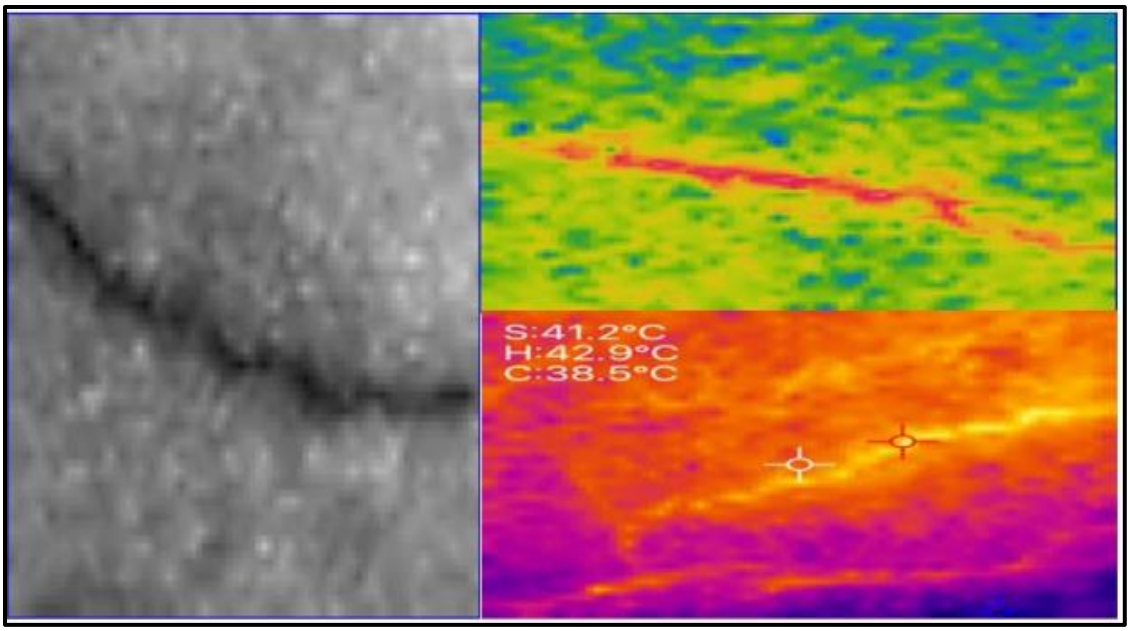

Figure 49: Typical colour pallets of thermal images

The colour pallet where black is hot indicated a more distinct difference between the crack and the surrounding pavement surface. This colour pallet was used for all the thermal testing images. Figure 50 shows the ability of the thermal device to highlight multiple cracks.

Figure 50: Multiple cracks with the thermal device at 1.5 meters above the surface

The image distortion in Figure 50 is due to the limited number of pixels of the thermal sensor. The distortion becomes a concern when the image is viewed on a larger screen than the thermal device. Thermal devices with a higher pixel count thermal sensor should be able to improve the image distortion and provide sharper thermal images.

Figure 51 contains two images of a pothole; the normal RGB image was captured using a digital camera and can be used as a reference for the thermal image of the same pothole. The thermal device can capture the pothole; however, the thermal image lacks sharpness to identify the edges of the pothole.

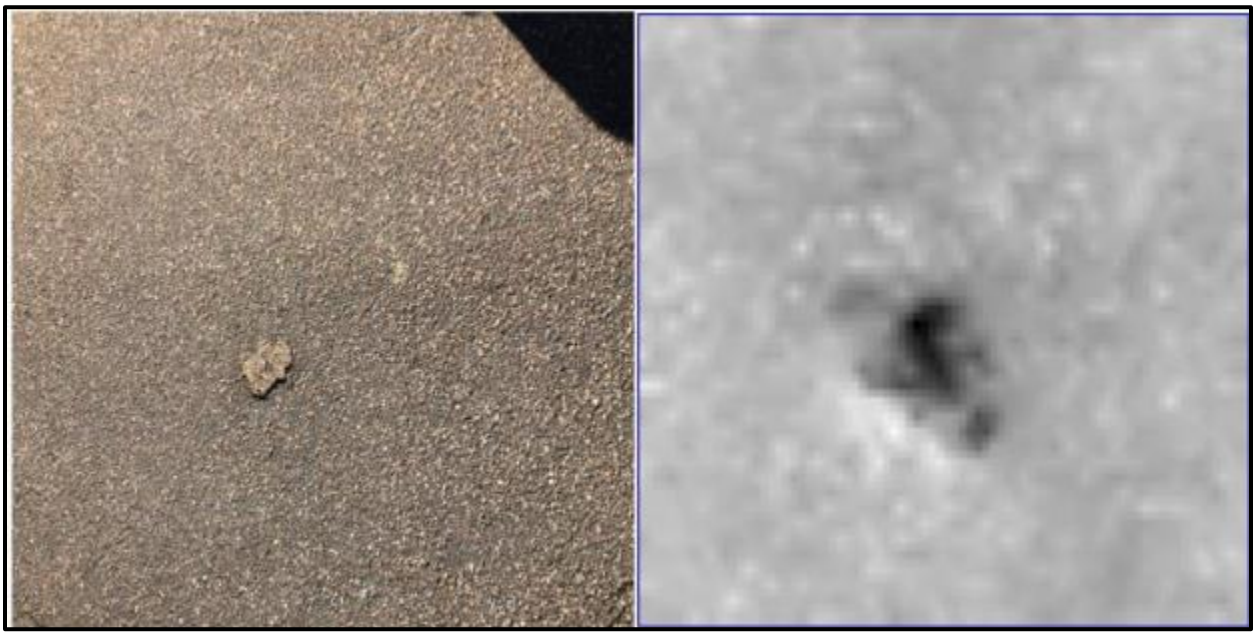

Figure 51: Pothole with a thermal device at 1.5 meters above the surface

Figure 52 shows the tests to determine if the thermal device can detect cracks with different widths. The thermal device was able to detect fine cracks of 1mm, distinct cracks of 3mm and significant cracks of 5mm at the height of 1,5 metres above the surface. The 5mm cracks are more distinct compared to the 3mm and 1mm cracks. The visibility of the fine cracks will improve with a higher resolution thermal sensor.

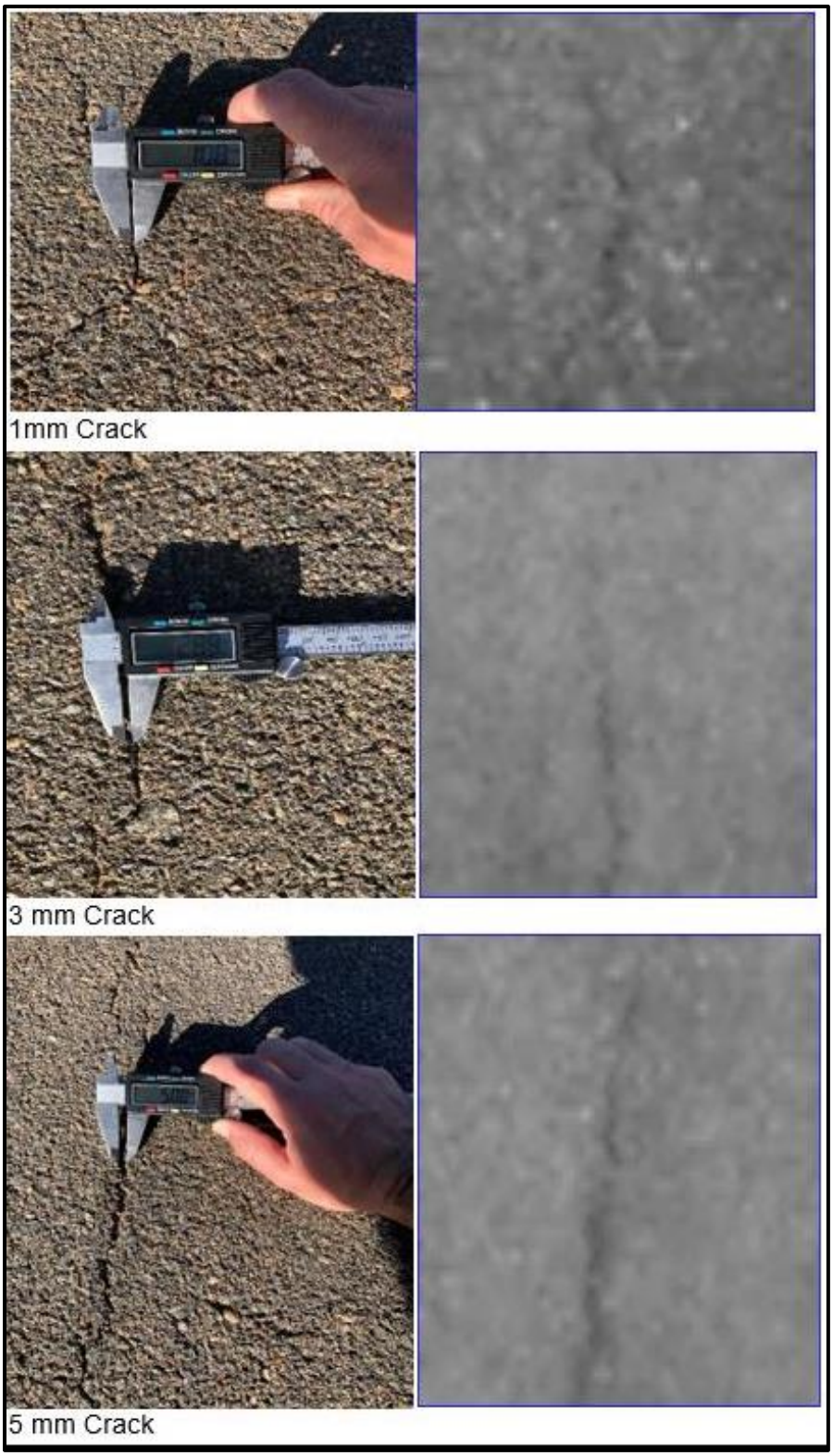

Figure 52: Crack widths using the thermal camera at 1.5 meters above the surface

The thermal device can capture images regardless of the surrounding lighting conditions. Figure 53 indicate this ability by comparing the thermal image of a crack to the digital image taken at the same time. Image processing software may find it difficult to identify cracks in shaded areas from a digital image, while the identification from a thermal image may be much easier. The thermal device can produce the same image quality during complete darkness. This can allow the collection of pavement surface data during night hours

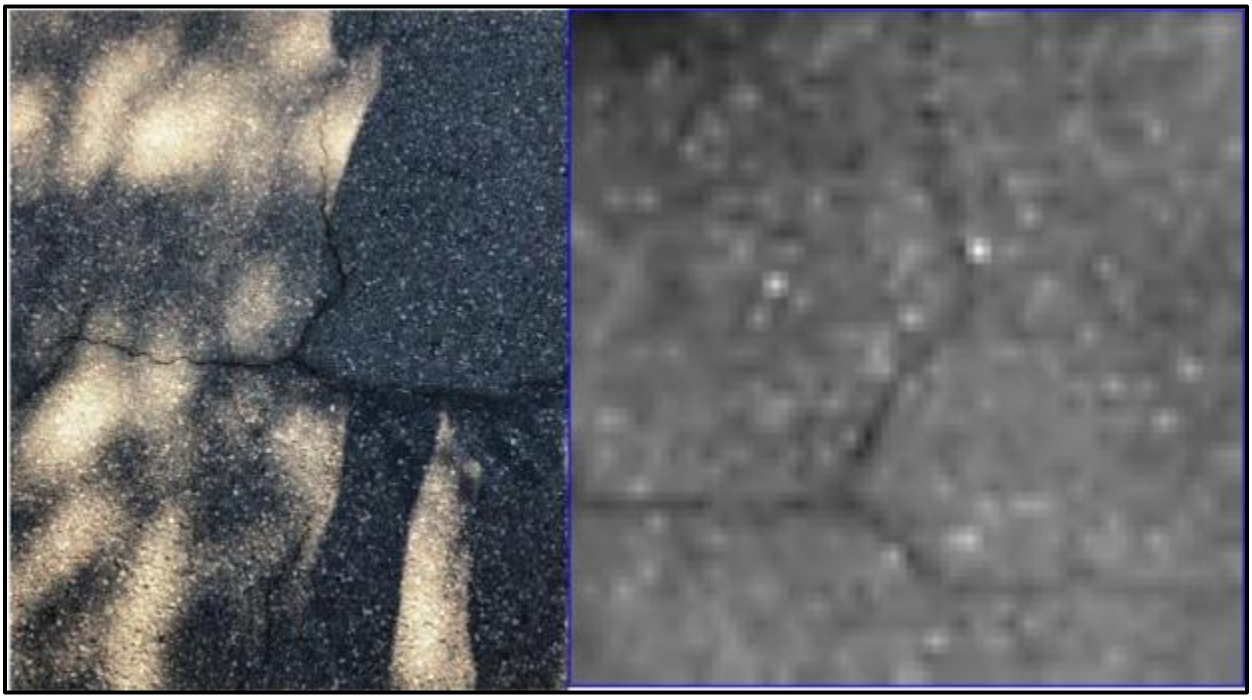

Figure 53: Shaded images with a thermal camera

5.5.1 Lessons learned using the thermal device

Testing the thermal device provided import information to consider before data capturing using a thermal device can commence. The important considerations include:

- The thermal device requires a thermal sensor with a higher pixel count than 80 x 80
- The colour pallet where black indicates the hot areas work best for identifying cracks
- The travelling speed will depend on the imaging speed
- Lighting conditions do not affect the thermal device performance

Chapter 6: Time, Cost and Quality Evaluation

This chapter will evaluate the use of digital cameras, thermal cameras and LIDAR devices for pavement surface inspections in terms of their time, cost and quality requirements.

6.1 Time Evaluations

The time evaluation compares the different technologies and platforms in terms of their data collection speed. The time evaluation will only include data capturing time and not data processing time. The data processing time is computer dependant and no significant difference in processing time have been identified between the technology types. Therefore, will data processing time be omitted during the evaluations.

The time evaluation will be based on the data collection speed limit calculations where the speed is either limited by the device or maximum travel speed of the platform. According to the TMH 9 manual should the assessor drive on the shoulder of the road at a maximum speed of 20 km/h during the tradition inspection method (TMH 9, 2016).

The time each platform requires for data collection will depend on different sensors for different technologies and the height above the pavement surface. A constant height of 2 meters above the pavement surface will be used to perform a comparison between the different devices

The time it takes for a digital camera to capture an image is determined by the shutter speed of the camera. The data collection time is limited by the shutter speed of the camera and the minimum time-lapse speed of the camera. The time-lapse speed can decrease by using additional microcontrollers to control the camera. The currently recommended microcontroller to control the GoPro Hero 8 includes the Arduino UNO, ESP 8266 and the Raspberry Pi (Dean, 2017).

Figure 54 is a graphical representation to proof Equation 5. The left side of Figure 54 represents the platform and the distance (D1) the platform travel in I seconds at a speed of v m/s. The right side represent the field of view of the camera and the distance (D2) the camera capture in a single image at a height (H). Distance D1 must be equal to D2 when determining the camera limit speed and height.

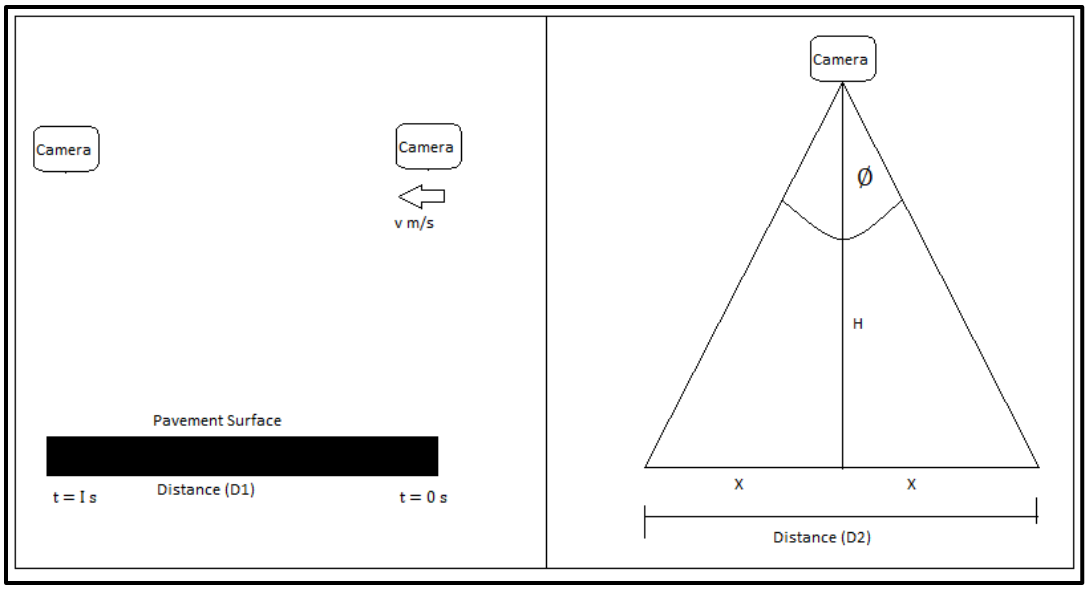

Figure 54: Equation 5 graphical illustration

Equation 5: Camera limit

$$D_1 = v \times I \times (1 - O)$$
$$x = H \times \tan(\emptyset)$$
$$D_2 = 2 \times x$$

D_1must be equal to D_2

$$v \times I \times (1 - O) = 2 \times H \times \tan(\emptyset)$$

Therefore:

$$H = \frac{v \times I \times (1 - O)}{2 \times \tan(\emptyset)}$$

Where: D_1 is the distance travelled by the platform
D_2 is the distance covered by the camera in a single image
v is the travel speed of the platform in m/s
I is the minimum image interval in seconds
$\emptyset$ is the device field of view divided by two
O is the image overlap percentage
H is the height above the pavement surface

The recommended maximum travel speed and altitude at different image resolutions using different devices and shutter speeds can be seen in Figure 55. Figure 55 indicates the maximum travel speed is directly proportional to the height above the pavement surface. The lower the image resolution, the higher the travel speed at a specific altitude can be. This is due to the larger image pixel size in lower resolution images.

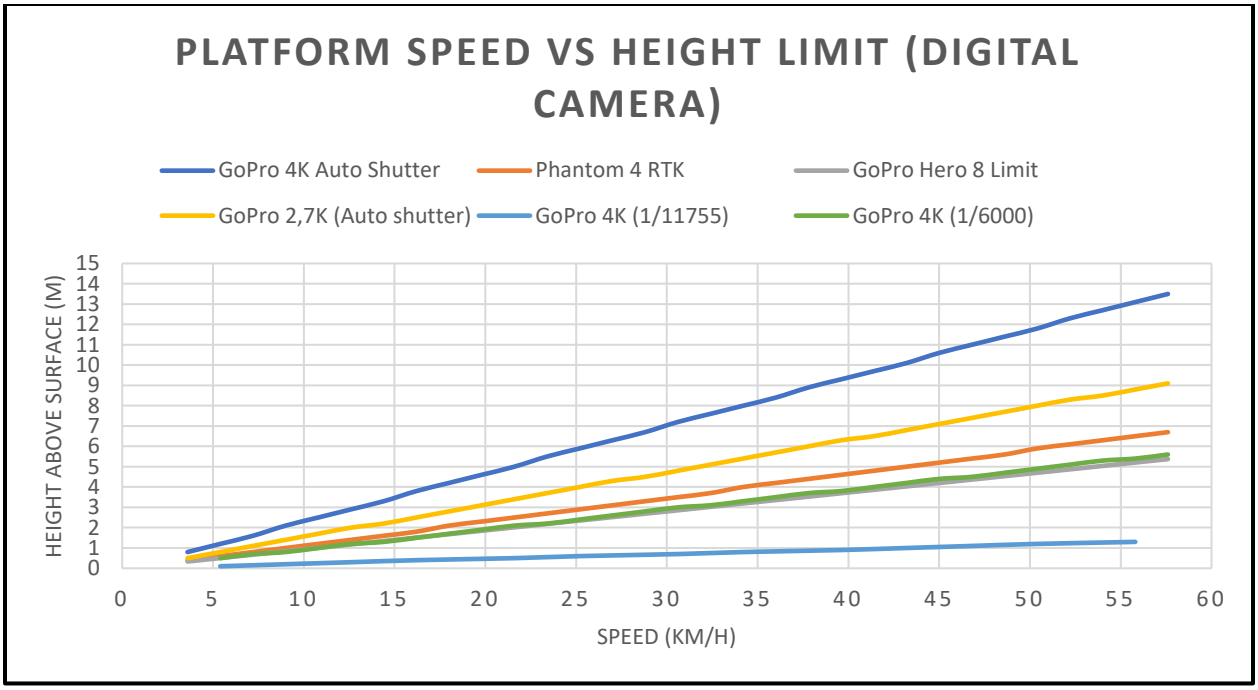

Figure 55: Digital camera Limit Graph

The GoPro Hero 8 limit line (grey) in Figure 55 indicates the minimum time-lapse speed of the GoPro Hero 8 camera of 0.5 seconds. The limit line is calculated using Equation 5 with the minimum image interval of 0.5 seconds and an image overlap percentage of 5%.

All images captured at values below the GoPro Hero 8 Limit line will not overlap or miss some part of the pavement surface due to the camera not being able to capture images in that close succession. The recommended GoPro Hero 8 settings are 4K image quality with a shutter speed of 1/6000 seconds. This will allow moderate data collection speed at a relatively low height above the surface. **At 2 meters above the surface data collection can occur at 20 km/h, this equal 3 minutes per kilometre**.

The time it takes for a thermal camera to capture an image is determined by the frame rate of the sensor and not the shutter speed like normal digital cameras. The frame rate is longer than the shutter speeds of digital cameras (Pix4D, 2018). Typical frame rates of thermal devices are 9 Hz, 30 Hz and 60 Hz. The frame rate of the device indicates the number of images created per second. A 9 Hz camera creates nine images per second; this results in a minimum image interval of 0.11 seconds (FLIR, no date).

Figure 56 indicates the device limit for different thermal devices at different frame rates and field of views. The thermal camera limit is calculated using Equation 5, with a 5% image overlap. Devices with a lower frame rate require higher altitudes at a specific height compared to the devices with a higher frame rate. The 9 Hz, FLIR Vue pro, require three times the height of the same device with a 30 Hz frame rate. The Seek ShotPro have a wider field of view than the FLIR Vue Pro resulting in the FLIR Vue Pro requiring a higher altitude to capture data at the same travel speed.

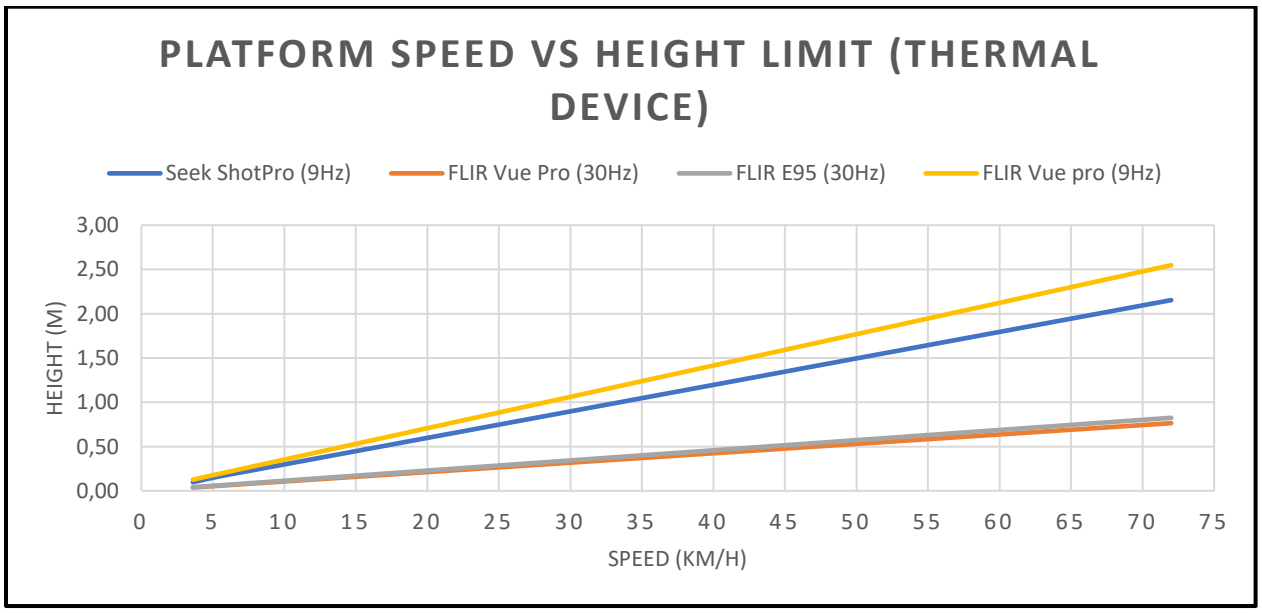

Figure 56: Thermal Camera Limit Graph

The Seek ShotPro at the height of 2m above the pavement surface will allow data collection at 63 km/h; this equals 57 seconds per kilometre. **The FLIR Vue Pro (9Hz) at the height of 2m above the pavement surface will allow data collection at 51 km/h, this equal 1 minute and 10 seconds per kilometre.**

The data collection speed of LIDAR devices is not limited by the height or sensor speed due to the laser beam emitting at the speed of light. Data collection speed of 2D LIDAR devices depend on the rotating speed of the LIDAR sensor, the typical rotating speed of a device is 10Hz (Zhang and Singh, 2017; Autonomous Vehicle Sensors Conference, 2018). This means that the sensor is rotating ten times per second.

Laser profilers currently in use for pavement surface scanning can scan at speeds up to 28 000 profiles per second with a profile spacing of 1 mm to 5 mm (Pavemetrics, no date). The high-speed scanning devices allow the platform to collect data at speeds between 25 km/h and 100 km/h regardless of the scanner's height above the surface.

6.2 Cost Evaluations

The cost of each platform fitted with different technology types include the initial cost and operating cost. The initial cost will include all costs required for the system to be fully functional, and the operating cost will be the cost per kilometre of the system. The operating cost will depend on the maximum travel speed of each platform and device determined in Chapter 6.1.

The cost model of each technology type fitted to different platforms entails variable values for certain parameters. The Monte Carlo analysis method is used to develop comparable cost results between the types and platforms. The Monte Carlo method is used to quantify values for each parameter with variable cost values through a probabilistic approach.

Each parameter with a variable cost can be modelled with a probability distribution function to obtain a specific cost for the parameter. To obtain the value for the parameter, the probability distribution of the parameter value is used to plot the cumulative probability distribution of the parameter. One random probability between zero and one is used to determine the parameter value at this probability.

To obtain the specific value for the parameter, the process is iterated for 150 random probabilities to determine the frequency distribution of the outcome. The final value for the parameter is equal to the value with the highest frequency.

Some of the parameters have fixed cost values, but the cost can be influenced by the exchange rate between the South African Rand and US Dollar. The development for each distribution model can be seen in Appendix A. Table 20 includes the parameters with a range of variable values and the distribution through which the values can be modelled.

The operating cost of each platform is based on a single carriageway road section. The final operating cost will be a cost per section kilometre. The UAV and traditional inspection platform can evaluate both lanes during a single drive-through while the vehicle platform must travel both

lanes during an evaluation. The operator costs obtained from Salary Expert, Payscale, Indeed and Best Jobs databases appear somewhat low.

Table 20: Parameters with variable cost

Parameter	**Range of Values**	**Source**	**Distribution Model**
DJI Phantom 4 Pro RTK	$6 500.00	DJI Store	Exchange Rate
DJI Phantom 4 Pro additional battery	$185.00	DJI Store	Exchange Rate
DJI Matrice 210 RTK	$13 995.00	Cnet	Exchange Rate
DJI Matrice 210 additional battery	$450.00	DJI Store	Exchange Rate
Electricity for battery charges	R0.46 – R3.18	Eskom	Electricity cost
Vehicle running cost	R1.54 – R1.77	AA	Fuel Price
Thermal Camera	$650.00 - $3649.00	FLIR	Exchange Rate
Digital Camera	$400.00	Amazon	Exchange Rate
LIDAR Device	$599.00 - $1499.00	DJI Store, RS Components	Exchange Rate
UAV Operator	R84.38 – R167.00 per Hour	Salary Expert, Payscale, Indeed	UAV Operator Rate
Vehicle Driver	R54.05 – R111.80	Salary Expert, Payscale, Indeed	Driver Rate
Pavement Engineer	R188.75 – R347.40	Payscale, Indeed, Best Jobs	Pavement Engineer Rate

6.2.1 Vehicle Cost

The vehicle used in the calculations is a Volkswagen Transporter 2.0 TDI DSG fitted with a tow bar and device mount. The Volkswagen Transporter is used by companies specializing in road surface inspections due to the automatic transmission, cruise control and space available to install computers and monitoring devices. The devices used in the calculations is the GoPro Hero 8 Black, Seek ShotPro, Livox Mid-100 and Baumer OM70 point laser.

I. Vehicle Initial Cost

The initial cost for the Vehicle platform includes the fixed vehicle cost and the variable device cost. The initial cost of the vehicle platform can be calculated using Equation 6.

Equation 6: Vehicle Initial Cost

$$C_i = V + Mount + D \times E$$

Where:

C_i is the initial cost

V is the fixed vehicle cost

D is the device cost in US dollar

$Mount$ is the total cost of mounting the device; this includes the tow bar, device mount and floodlight where required.

E is the variable Rand/Dollar exchange rate

The initial cost is dependent on the variable exchange rate between the South African rand and the US dollar. Therefore, can the initial vehicle cost be modelled according to the exchange rate probability distribution in Appendix A.

The frequency of the cost occurring within the specific increment range, and each increment range's probability is determined for the 150 iterations. The initial cost outcome probability distribution is used to determine the most probable value for the initial cost of the vehicle platform. The initial cost is calculated using Equation 6 with the parameter values according to Table 21.

Table 21: Vehicle Initial Cost

Vehicle Inspection				
Initial Cost				
Item	**GoPro Hero 8 Black**	**Seek Thermal Seekshot Pro**	**Livox Mid-100**	**Baumer OM70**
Volkswagen Transporter 2.0TDI DSG	R544 300,00	R544 300,00	R544 300,00	R544 300,00
Transporter Tow bar	R7 868,00	R7 868,00	R7 868,00	R7 868,00
Device	R5 854,00	R19 025,50	R21 937,87	R670 000,00
Holux GPS Data Logger	R4 750,00	R4 750,00	R4 750,00	R4 750,00
Device Mount	R5 000,00	R5 000,00	R5 000,00	R5 000,00
50W 12V LED Floodlight	R990,00	R0,00	R0,00	R0,00
Initial Cost	**R568 762,00**	**R580 943,50**	**R583 855,87**	**R1 231 918,00**

The exchange rate used during the calculations is determined using the Monte Carlo analysis and the exchange rate distribution model in Appendix A. The exchange rate used is R14.64.

The GoPro Hero 8 camera is the only device which requires additional light sources due to the sensitivity of the device to changing or variable light. Two thermal devices are required when mounted at the height of two meters above the pavement surface to capture the lane width of 3.7m (SANRAL, 2009). The Baumer OM70 point laser device requires multiple devices mounted on the device mount to capture data over the lane width of 3.7m. The cost of one Baumer OM70 laser is R33 500, and the system requires 20 lasers at a spacing of 185 millimetres between the lasers.

The initial cost outcome probability distribution for the digital camera can be seen in Figure 57. Figure 57 indicates the most probable initial cost of the vehicle with a digital camera will be R568 762.00; the detailed Monte Carlo analysis data can be seen in Appendix B. This process is repeated for all the different devices.

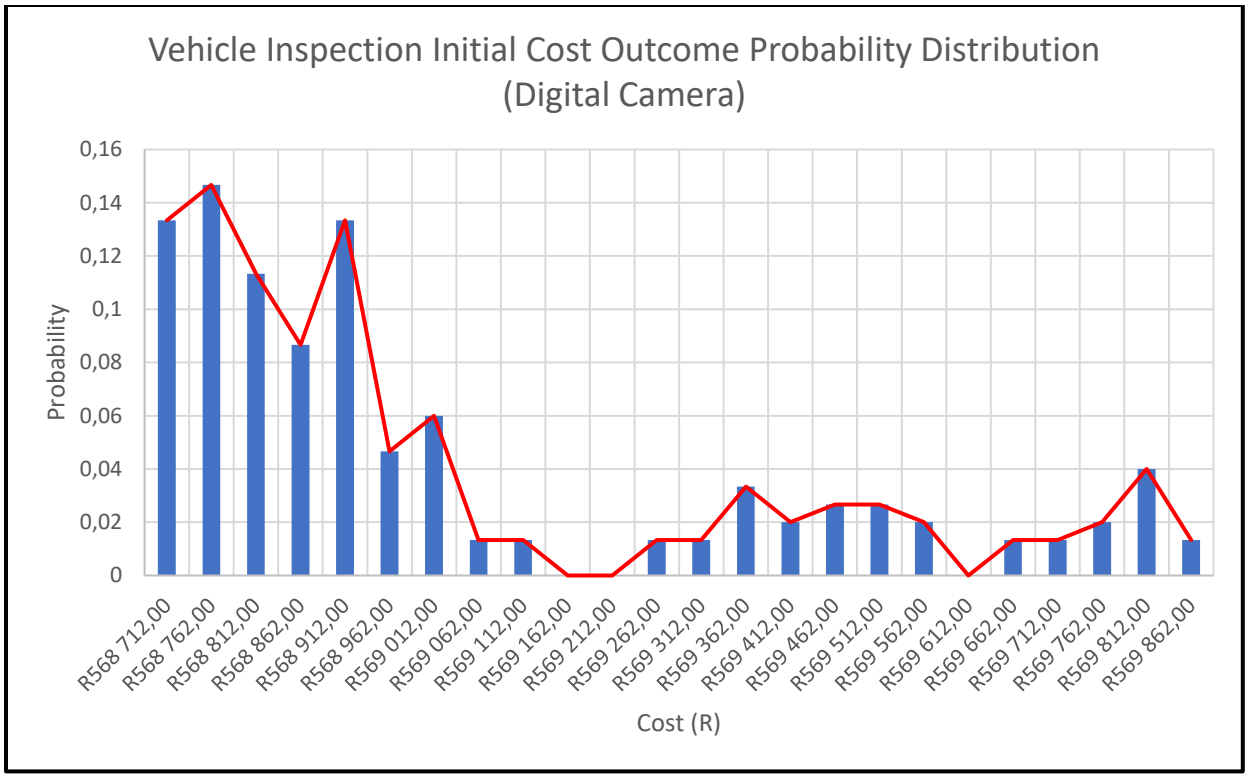

Figure 57: Vehicle initial cost outcome probability distribution

II. Vehicle Operating Cost

The operating cost for the vehicle platform includes the variable operator cost and vehicle running cost. The Operator cost can be modelled through the operator distribution (Appendix A) and the vehicle running cost can be modelled through the fuel price distribution in Appendix A. The operating cost of the vehicle platform can be calculated using Equation 7.

Equation 7: Vehicle Operating Cost

$$C_o = \frac{Op}{S} + Rc$$

Where:

C_o is the operating cost
Op is the operator cost
S is the data collection speed
Rc is the running vehicle cost

The parameters of the vehicle operating cost with the different devices can be seen in Table 22. The only changing variable is the travel speed of data collection resulting in the different operating costs. The operating cost is calculated with devices mounted at two meters above the pavement surface where possible. The Baumer OM70 devices should be mounted at 0.5 meters above the surface.

Table 22: Vehicle Operating cost parameters

Vehicle Inspection				
Operating Cost				
Item	**GoPro Hero 8 Black**	**Seek Thermal Seekshot Pro**	**Livox Mid-100**	**Baumer OM70**
Average Running Cost (R/Km)	R1.53	R1.53	R1.53	R1.53
Operator (R/hr)	R78.26	R78.26	R78.26	R78.26
Travel speed (km/h)	20	68	48	80
Total (R/Section Km)	**R10.88**	**R5.35**	**R6.31**	**R5.01**

Table 22 shows the operating cost outcome probability distribution of the vehicle platform fitted with the GoPro Hero 8 Black after 150 random probability iterations for each of the variable costs. The vehicle operating cost is multiplied by two to achieve a cost per section kilometre. Figure 58 indicates the most probable operating cost will be R10.88; the detailed Monte Carlo analysis data can be seen in Appendix B. The process is repeated for all the different devices.

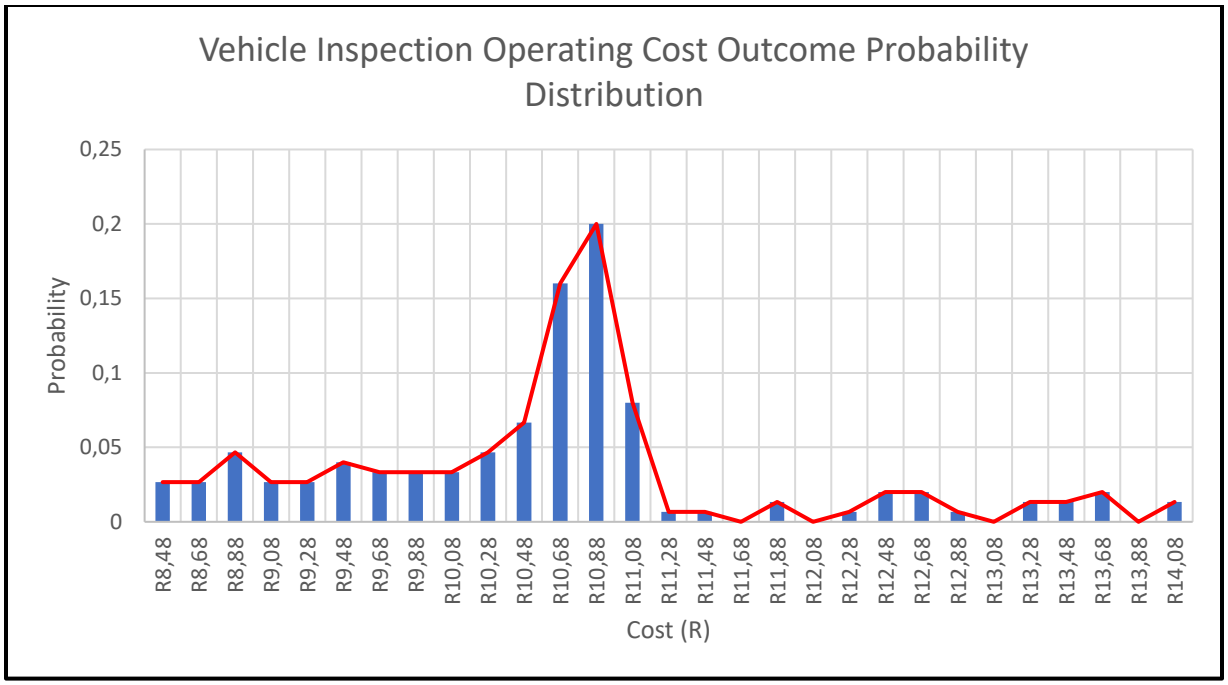

Figure 58: Vehicle Operating Cost Outcome Probability Distribution

6.2.2 UAV Cost

I. UAV Initial Cost

The initial cost of the UAV platform fitted with a data collecting device includes the fixed vehicle cost and the variable costs of the UAV and additional batteries. The vehicle is required to transport the operator and UAV to the specific road sections. The vehicle used in the cost calculation is the Volkswagen Caddy 2.0 TDI DSG. The UAV used in the calculations is a DJI Phantom 4 Pro V2 RTK and a DJI Matrice 210 RTK, both with additional batteries. The Matrice 210 can be fitted with a digital camera, thermal device or a LIDAR device, while the Phantom 4 Pro could not be fitted with a LIDAR device. The initial cost of the UAV platform can be calculated using Equation 8.

Equation 8: UAV Initial Cost

$$C_i = (UAV + Bat \times N_{Bat}) \times E + V$$

Where: C_i is the initial cost

UAV is the UAV cost in US dollar

Bat is the battery cost in US dollar

N_{Bat} is the number of additional batteries

E is the variable Rand/Dollar exchange rate

V is the fixed vehicle cost

The UAV and battery costs are dependent on the variable exchange rate between the South African Rand and the US Dollar. Therefore, can the UAV initial cost be modelled according to the exchange rate probability distribution in Appendix A.

The frequency of the cost occurring within the specific increment range and each increment range's probability of is determined for the 150 iterations. The initial cost outcome probability distribution is used to determine the most probable value for the initial cost of the UAV platform fitted with a digital camera. The initial cost is calculated using Equation 8, with all the parameter values according to Table 23. The Phantom 4 RTK is factory fitted with a premium quality 4K digital camera.

Table 23: UAV initial cost parameters

UAV Inspection			
Initial Cost			
Item	**DJI Phantom 4 RTK**	**Matrice 210 Flir Vue Pro**	**Matrice 210 Livox Mid-40**
UAV	R94 470,66	R203 402,60	R203 402,60
Additional Batteries	R8 066,34	R19 620,83	R19 620,83
Device	R0,00	R53 034,37	R8 705,83
Volkswagen Caddy 2.0 TDI DSG	R466 800,00	R466 800,00	R466 800,00
Total	**R569 337,00**	**R742 857,80**	**R698 529,26**

The exchange rate used during the calculations is determined using the Monte Carlo analysis and the exchange rate distribution model in Appendix A. The exchange rate used is R14.53.

The initial cost of the UAV is the initial cost with the highest probability of occurring. The initial cost outcome probability distribution for the DJI Phantom 4 RTK can be seen in Figure 59. Figure 59 indicates the most probable initial cost of the UAV fitted with a digital camera will be R569 337.00; the detailed Monte Carlo analysis data can be seen in Appendix B. The process is repeated for all the different devices.

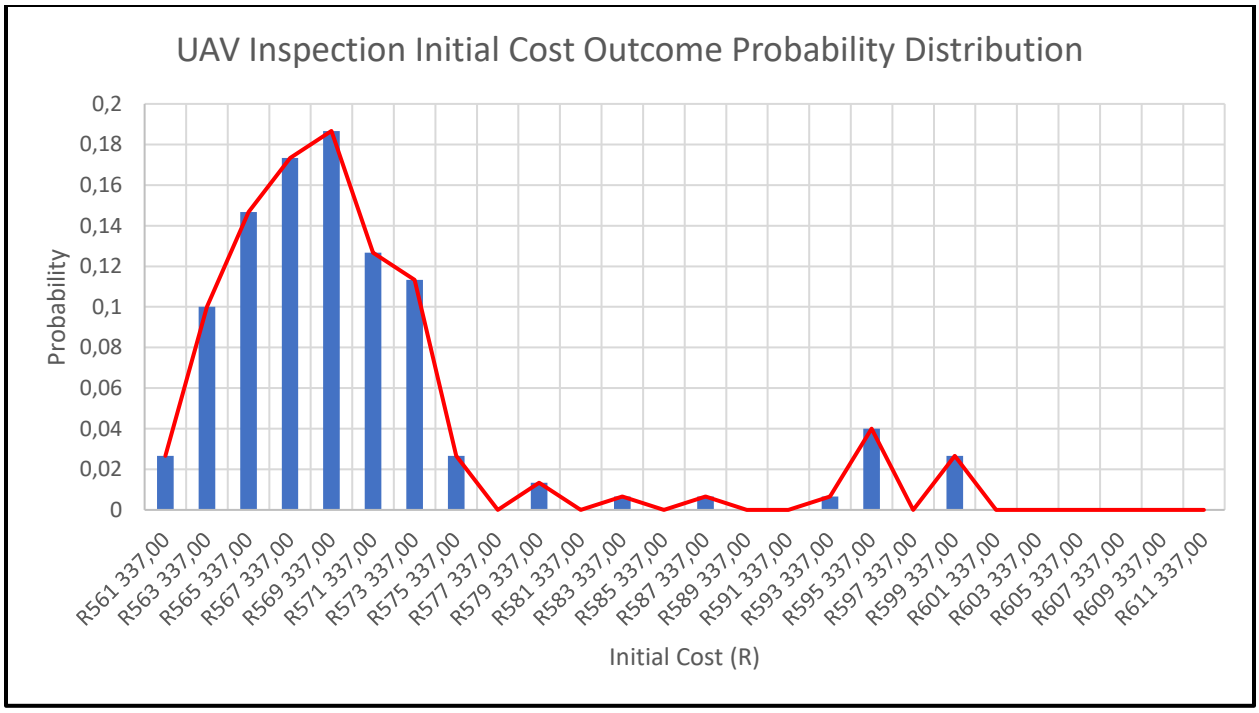

Figure 59: UAV with digital camera Initial Cost Outcome Probability Distribution

II. UAV Operating Cost

The operating cost of the UAV platform includes the variable operator cost, vehicle running cost, and cost per battery charge. The Operator cost can be modelled through the operator distribution (Appendix A), the battery charge cost can be modelled through the power distribution (Appendix A) and the vehicle running cost can be modelled through the fuel price distribution in Appendix A. The operating cost of the UAV platform can be calculated using Equation 9.

Equation 9: UAV Operating Cost

$$C_o = \frac{Op}{S} + Rc + Cc$$

Where:

C_o *is the operating cost*

Op *is the operator cost*

S *is the data collection speed*

Rc *is the running vehicle cost*

Cc *is the battery charge cost*

The parameters of the UAV operating cost with the different devices can be seen in Table 24. **The vehicle is required to travel in one direction only due to the ability of the UAV to capture both lanes of the road section simultaneously**. This reduces the operating cost significantly compared to the vehicle platform.

Table 24: UAV operating cost parameters

UAV Inspection			
Operating Cost			
Item	**DJI Phantom 4 RTK**	**Matrice 210 Flir Vue Pro**	**Matrice 210 Livox Mid-40**
Operator (R/hr)	R111.92	R111.92	R111.92
Cost per Battery Charge	R0.86	R0.86	R0.86
Vehicle Running Cost (R/Km)	R1.53	R1.53	R1.53
Data Collection Speed (km/h)	33.60	80.00	48.00
Total (R/ Section Km)	**R4.88**	**R2.94**	**R3.88**

Figure 60 shows the operating cost outcome probability distribution of the UAV platform fitted with a digital camera after 150 random probability iterations for each of the variable costs. Figure 60 indicates the most probable operating cost will be R4.88; the detailed Monte Carlo analysis data can be seen in Appendix B. The process is repeated for all the different devices.

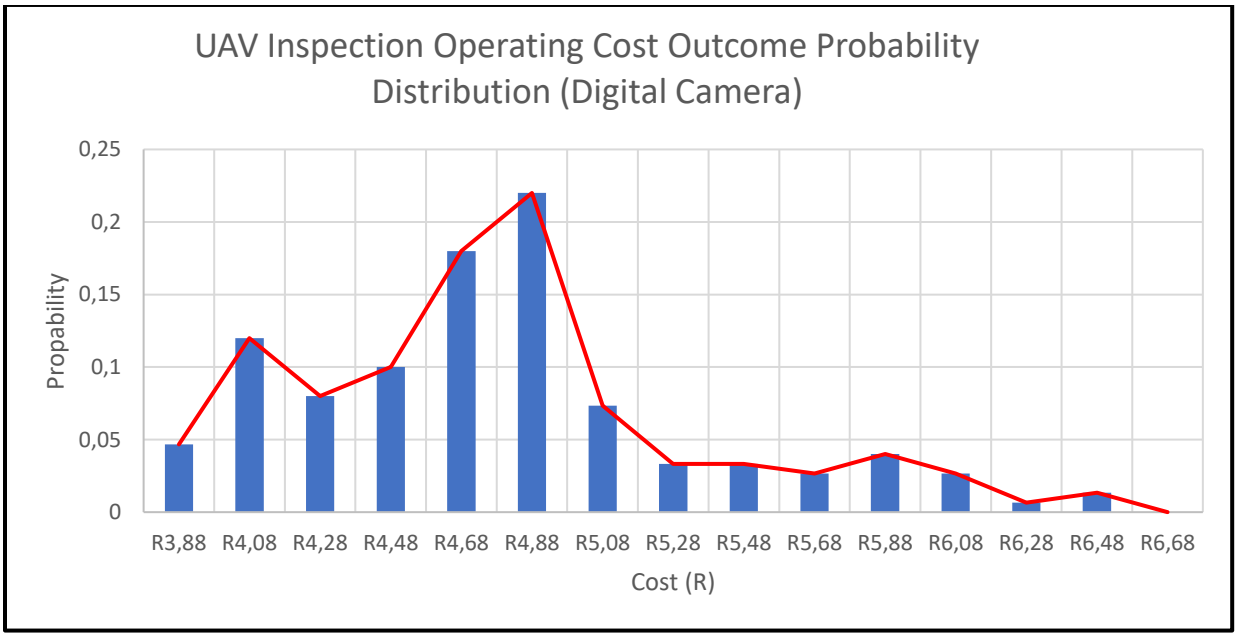

Figure 60: UAV with digital camera Operating Cost Outcome Probability Distribution

6.2.3 Traditional Inspection Cost

The traditional inspection method requires a trained assessor to drive a road section at 20 km/h and visually identify road surface defects. To perform a pavement surface evaluation, the only initial cost is the vehicle cost. The vehicle used in the cost calculation is the Volkswagen Caddy 2.0 TDI DSG. Table 25 include the different variables contributing to the cost of the traditional inspection method.

The operating cost for the traditional inspection platform includes the fixed vehicle cost, the variable operator cost and vehicle running cost. The operating cost can be modelled through the operator distribution (Appendix A), and the vehicle running cost can be modelled through the fuel price distribution in Appendix A. The operating cost of the traditional inspection platform can be calculated using Equation 7 and the variables in Table 25.

Table 25: Traditional Inspection Costs

Traditional Inspection		
Initial Cost		
Item	**Price/#**	**Total**
Volkswagen Caddy 2.0 TDI DSG	R466 800.00	R 466 800.00
Initial Cost		**R 466 800.00**
Operation Cost		
Average Running Cost (R/Km)	R 1.53	R 1.53
Operator (R/hr)	R 266.76	R 266.76
Travel speed (km/h)	20.00	
Total (R/Section Km)		**R 14.86**

Figure 61 shows the operating cost outcome probability distribution of the traditional inspection platform after 150 random probability iterations for each of the variable costs. Figure 61 indicates the most probable operating cost will be R14.86; the detailed Monte Carlo analysis data can be seen in Appendix B. The higher operating cost compared to the other platforms are due to the speed of the inspection and the expensive operator hourly rate.

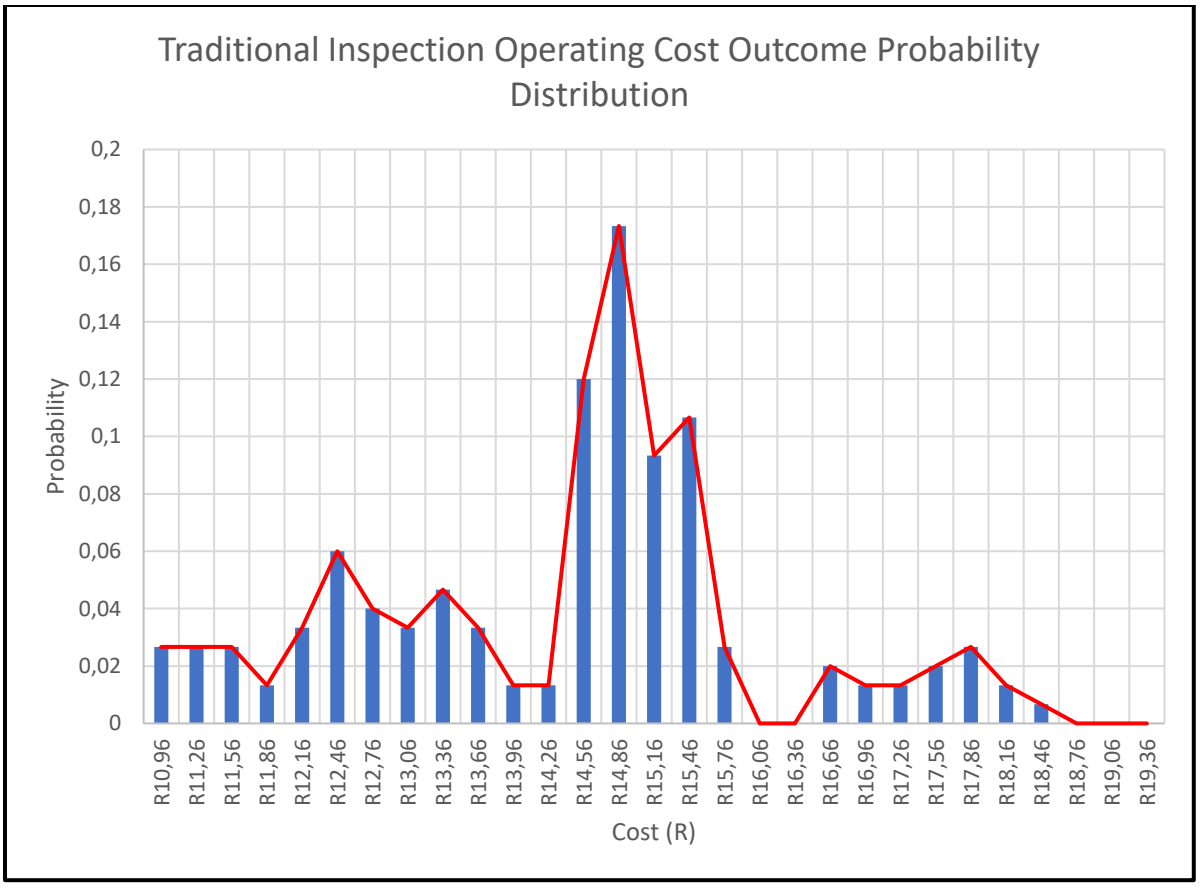

Figure 61: Traditional Inspection method Operating Cost Outcome Probability Distribution

6.3 Quality Evaluations

The quality of the different platforms and technologies are now evaluated according to their ability to identify different distress mechanisms present on pavement surfaces correctly. The TRH 22 manual contains a list of the different distress mechanisms which should be identified during a regular pavement surface evaluation; the list can be seen in Table 26 (Committee of State Road Authorities, 2018).

The weight of the distress in Table 26 is used to sort the distress mechanisms according to their relative importance based on the distress weight assigned according to the TRH 22 manual. Potholes/failures are therefore regarded as the most important and textures or voids as the least important distresses to identify.

Table 26: Weight of Distress from TRH 22 (Committee of State Road Authorities, 2018)

Distress	Weight (Wn)	Distress	Weight (Wn)
Potholes/Failures	15,0	Longitudinal Crack (Medium)	4,5
Crocodile Crack	10,0	Undulation/Settlement	4,0
Pumping	10,0	Longitudinal Crack (Large)	4,0
Rutting	8,0	Aggregate loss (active)	4,0
Patching	8,0	Edge Breaking	3,5
Block Crack (Narrow)	8,0	Unpaved Shoulder	3,5
Surface Failure	6,5	Surface Drainage	3,0
Block Crack (Medium)	6,0	Skid Resistance	3,0
Riding Quality	5,5	Bleeding	3,0
Block Crack (Large)	5,0	Dry/Brittle	3,0
Surface Crack	5,0	Aggregate loss (Non- active)	2,0
Transverse Cracking	4,5	Voids	0,0
Longitudinal Crack (Narrow)	4,5	Texture	0,0

If a technology type can correctly identify a specific distress from Table 26, then the weight of the distress will be added to the technologies' total score. The quality score of the technology is then calculated as the percentage of distress mechanisms correctly identified according to Equation 10.

Equation 10: Quality Score Evaluation

$$Quality\ Score\ (\%) = \frac{(\sum Weight)_{Technology}}{(\sum Weight)_{Total}}$$

The road section available for testing and evaluation did not cover all the different distress mechanisms in Table 26. Narrow, medium and large cracks were tested in Chapter 5 to determine the technology's ability to identify the different crack widths. If a specific crack width were successfully identified during testing, it is assumed that all types of distresses with the same width can be identified.

Table 27 indicates the ability of the different technologies to identify different distress mechanisms on a pavement surface. The traditional inspection method is assumed to identify 100% of the weighted distress mechanisms correctly. The LIDAR, Thermal device and digital camera are compared to the traditional inspection method by calculating the percentage of the various distress mechanisms that each of the technologies can identify.

Table 27: Weighted Quality Score Evaluation per distress mechanism

Distress	Weight (Wn)	Traditional	Digital Camera	Thermal	LIDAR
Potholes/Failures	15.0	15.0	15	15	15
Crocodile Crack	10.0	10.0	10	10	0
Pumping	10.0	10.0	10	10	0
Rutting	8.0	8.0	0	0	8
Patching	8.0	8.0	8	8	0
Block Crack (Narrow)	8.0	8.0	0	8	0
Surface Failure	6.5	6.5	6.5	6.5	6.5
Block Crack (Medium)	6.0	6.0	6	6	0
Riding Quality	5.5	5.5	0	0	5.5
Block Crack (Large)	5.0	5.0	5	5	5
Surface Crack	5.0	5.0	5	5	0
Transverse Cracking	4.5	4.5	4.5	4.5	0
Longitudinal Crack (Narrow)	4.5	4.5	0	4.5	0
Longitudinal Crack (Medium)	4.5	4.5	4.5	4.5	0
Undulation/Settlement	4.0	4.0	0	0	4
Longitudinal Crack (Large)	4.0	4.0	4	4	4
Aggregate loss (active)	4.0	4.0	0	0	0
Edge Breaking	3.5	3.5	3.5	3.5	3.5
Unpaved Shoulder	3.5	3.5	3.5	0	0
Surface Drainage	3.0	3.0	3	0	0
Skid Resistance	3.0	3.0	0	0	0
Bleeding	3.0	3.0	3	3	0
Dry/Brittle	3.0	3.0	0	0	0
Aggregate loss (Non- active)	2.0	2.0	0	0	0
Voids	0.0	0.0	0	0	0
Texture	0.0	0.0	0	0	0
Total	**133.5**	**133.5**	**91.5**	**97.5**	**51.5**
Percentage		**100.00%**	**68.54%**	**73.03%**	**38.58%**

The ability of the digital camera to correctly identify the different distress mechanisms depend on the surrounding lighting conditions and the image processing software. At 20 km/h the camera was not able to capture narrow cracks, but medium and wide cracks were captured successfully. Pumping was successfully identified in cases where pumping was present. The digital camera is unable to identify rutting and undulation due to the inability to measure distance. The digital

camera can thus only identify 68.54% of the weighted distress mechanisms when the lighting conditions are suitable.

The thermal device was able to capture narrow, medium and wide cracks; therefore, all the different cracks can be identified using a thermal device. The thermal device used during testing lacked image quality, and a higher resolution thermal device is recommended. Patching may be identified using a thermal device if there is a distinct temperature difference between the patch and road surface. A thermal device is unable to identify rutting and undulation due to the inability to measure distance. The thermal device can identify 73.03% of the weighted distress mechanisms, regardless of the lighting conditions.

Low-cost LIDAR devices typically have an accuracy of 20mm; this will allow the device to capture only wide cracks. The device will identify rutting and undulation only in severe circumstances due to the accuracy issue with cost-effective LIDAR devices. Edge breaking can be identified if the horizontal field of view of the device is wide enough. The cost-effective LIDAR device can thus identify 38.58% of the weighted distress mechanisms regardless of the lighting conditions.

The 73.03% weighted of distress mechanisms captured by the thermal device is the highest percentage of distress mechanisms captured by low-cost technologies. Typically, will this not be sufficient for pavement surface evaluations due to the inability to capture all the distress mechanisms. A combination of different technologies could, however, improve the system.

Chapter 7: Discussion of Evaluation Results

This chapter discusses the vehicle and UAV platforms fitted with different technologies. The discussion will include general remarks of each platform, advantages and disadvantages. Each of the technologies should be able to meet the following requirements to be appropriate for a network-level analysis of pavement surfaces:

- Capture high-quality, clear road surface data at speeds exceeding 20 km/h
- Identify faint (1 millimetre), distinct (3 millimetres) and open (5 millimetres) cracks at moving speeds
- Identify rutting and undulation
- Easy to operate while the platform is moving
- Mountable on a vehicle or UAV

7.1 Vehicle Platform Discussion

The vehicle platform is currently used by the industry to survey and evaluate pavement surfaces. Vehicles can be fitted with one or more devices that can capture high-quality, clear road surface data at speeds exceeding 20 km/h. A vehicle fitted with a high accuracy LIDAR system will have the lowest operating cost at R5.01 per section kilometre due to the faster scanning rate. The low-cost alternative technologies have a more expensive operating cost of R5.35 per section kilometre. The initial cost of the high accuracy LIDAR system is R1 231 918.00 compared to a much lower initial cost of the low-cost alternative of R580 943.50. The high initial cost of the high accuracy system does not decrease the operating cost significantly.

The main concern with the cost-effective technologies is the inability to capture all the distress mechanisms with a single device. Combining different technologies will improve the percentage of distress mechanisms captured, as can be seen in Table 28. Table 28 was developed by adding the distress weights in Table 27 together for the different technology combinations. If more than one technology can identify the specific distress mechanism, only one weight is added to the total.

Combining a digital camera with a thermal device will not provide a significant increase in the percentage of distress mechanisms captured. The minimal increase may be the result of both technologies' inability to measure distance. The recommended travel speed for this system will be limited by the time-lapse speed of the digital camera, which is 20 km/h. This system will require additional lighting to keep the surrounding conditions as constant as possible.

A combination of a thermal and LIDAR device will produce a significant increase in the percentage of distress mechanisms captured. This system combines the distance measuring ability of the LIDAR with the imaging capability of the thermal device. This system will require no additional lighting due to both technologies that are not affected by lighting conditions. The LIDAR systems' scanning speed will limit the recommended travel speed for this system at 48 km/h.

Combining all three the technologies will not produce a significant increase in the percentage of distress mechanisms captured over the thermal and LIDAR system. This system will increase the overall cost of the system without a significant gain in the percentage of distress mechanisms captured. The recommended travel speed for this system will be limited by the time-lapse speed of the digital camera at 20 km/h, resulting in an increased operating cost.

Table 28: Combination of Technologies Weighted Quality Evaluation

Distress	Weight (Wn)	Digital + LIDAR	Digital + Thermal	Thermal + LIDAR	ALL
Potholes/Failures	15	15	15	15	15
Crocodile Crack	10	10	10	10	10
Pumping	10	10	10	10	10
Rutting	8	8	0	8	8
Patching	8	8	8	8	8
Block Crack (Narrow)	8	0	8	8	8
Surface Failure	6.5	6.5	6.5	6.5	6.5
Block Crack (Medium)	6	6	6	6	6
Riding Quality	5.5	5.5	0	5.5	5.5
Block Crack (Large)	5	5	5	5	5
Surface Crack	5	5	5	5	5
Transverse Cracking	4.5	4.5	4.5	4.5	4.5
Longitudinal Crack (Narrow)	4.5	0	4.5	4.5	4.5
Longitudinal Crack (Medium)	4.5	4.5	4.5	4.5	4.5
Undulation/Settlement	4	4	0	4	4
Longitudinal Crack (Large)	4	4	4	4	4
Aggregate loss (active)	4	0	0	0	0
Edge Breaking	3.5	3.5	3.5	3.5	3.5
Unpaved Shoulder	3.5	3.5	3.5	0	3.5
Surface Drainage	3	3	3	0	3
Skid Resistance	3	0	0	0	0
Bleeding	3	3	3	3	3
Dry/Brittle	3	0	0	0	0
Aggregate loss (Non-active)	2	0	0	0	0
Voids	0	0	0	0	0
Texture	0	0	0	0	0
Total	**133.5**	**109.0**	**104.0**	**115.0**	**121.5**
Percentage		**81.65%**	**77.90%**	**86.14%**	**91.01 %**

The vehicle platform has several advantages and disadvantages which must be highlighted. The advantages and disadvantages can be seen in Table 29. The vehicle platform will be most suited to mount low-cost technologies for pavement surface evaluations. The platform is easy to operate, can move with traffic and can be fitted with multiple devices to ensure a comprehensive evaluation of the pavement surface.

Table 29: Vehicle platform advantages and disadvantages

Advantages	Disadvantages
Ability to mount more than one device	Height limit for device mount
Move with traffic	Driver operated
Easy operation	Operator safety at risk
Lowest operating cost	

7.2 UAV Platform Discussion

The UAV platform is used in many industries to collect data in a fast and effective way. The UAV possesses the ability to collect data at higher distances above the pavement surface than vehicle platforms. This ability can allow the UAV to collect data at faster travelling speeds. This can be seen in Figure 55 and Figure 56.

The UAV should collect data at heights above the maximum allowable vehicle height in South Africa of 4.3m to avoid traffic interference (van der Merwe and Edwards, 2018). Minimum bridge heights in South Africa range from 4.5 meters for older bridges and 5.5 meters for modern bridges; this will be exactly in the operating height of the UAV (Nordengen, Steynberg and Sallie, 2002). This will require pre-route surveillance to identify possible obstacles in the flight path; obstacles include:

- Bridges
- Overhanging tree branches
- Streetlights
- Overhead power lines
- Gantries

The pre-route surveillance and mission set up to fly the UAV autonomously can result in a time-consuming process to set up the flight route for the UAV. The mission setup requires waypoint entries at every directional, altitude or speed change resulting in a time-consuming task. However, after the mission is set up, the mission can be saved for future use.

The UAV will capture data above the pavement surface and traffic streams. Parts of the pavement surface data will be obstructed if a vehicle is captured instead of the pavement surface. This may require the capturing of data for a given road section twice to ensure the entire pavement surface was captured.

Each UAV is designed for a maximum payload which includes the UAV's battery. This limits the battery capacity of UAV's, which will limit the flight time per battery and device weight. The average UAV flight time will be around 25 minutes where after a new battery has to be inserted and the mission must resume. The UAV will not be able to capture data with a thermal and LIDAR device simultaneously. This may require repetitive missions to ensure all the distress mechanisms are captured.

Current UAV technology doesn't allow remote operation of UAVs for inspections. A vehicle is required in conjunction with the UAV to drive to the starting point of each road section. The vehicle will follow the UAV, which will increase the operating cost significantly.

Industry applications are predominantly large-scale work where 20-50mm accuracy of distance measurements are accepted. Pavement surface evaluations require millimetre accuracy when data is captured. UAV's fitted with RTK technology have the best level positioning at 10mm accuracy. Combining the RTK UAV with a LIDAR sensor with an accuracy of 10-20mm will result in an accuracy error of 30mm. The UAV fitted with a LIDAR sensor is not suitable for precision measurements such as pavement surface evaluations.

The UAV platform has advantages and disadvantages that must be highlighted. The advantages and disadvantages can be seen in Table 30.

Table 30: UAV Platform Advantages and Disadvantages

Advantages	**Disadvantages**
Height is not limited	Limited flight time
Faster travel speed	Vehicle is required
Autonomous flying	Limited payload to one device
Increased operator safety	Vehicle obstructions
	Pre-flight surveillance of the route required

The UAV platforms used in previous studies achieved high crack detection results but have not been tested for rutting or undulation where precise distance measurements are required. Previous research does not highlight the current limitations of UAV systems. Improvements to current limitations may result in the use of UAVs for pavement surface evaluations.

Chapter 8: Conclusions and Recommendations

This chapter provides conclusions regarding the thesis and recommendations regarding the use of low-cost technology for pavement inspections and future research.

8.1 Conclusions

Provincial governments in South Africa perform manual pavement visual inspections on an annual basis resulting in high inspection costs. Expensive alternative inspection methods are successfully used for network analysis inspections by private companies. A need to evaluate the use of low-cost technologies for pavement inspections have been identified to test their viability as alternatives to current practices.

The focus of this thesis was to evaluate the use of low-cost technology types for pavement surface evaluations in terms of time, cost and quality. The technologies included low-cost devices of a digital camera, thermal camera and LIDAR device. An image processing program was developed to aid the user in evaluating the different technology types.

The image processing program developed uses image thresholding methods to identify possible defects in the road surface. The developed program was used to evaluate the different technology types successfully and to determine:

- suitable travel speeds based on the image quality
- creating images from videos to evaluate the use of video for data collection
- evaluate the use of image thresholding for defect detection

Various technologies were evaluated through two platforms; the first is a vehicle platform where the devices are mounted to the vehicle and the second platform is a UAV where the technology is mounted to the UAV. Platform testing was done to determine the limitations and requirements for each platform. The platform testing included the following tests:

- A home-built UAV and DJI Mavic Mini
- A lower vehicle (Audi A4) and a higher vehicle (Toyota Hilux)
- Data collection speed limits
- Crack widths
- Thermal device
- Additional light sources

The time evaluation was used to determine the allowable data collection speed of the different technologies and platforms. The sensors of different technologies limit the travel speed of the platforms. The platform speed versus height limit graphs developed in the thesis was used for each technology in the cost calculations. The platform speed versus height limit graphs should be used to determine a suitable data collection speed using a specific device. **The UAV and vehicle platforms fitted with low-cost technologies can increase the surface evaluation speed significantly compared to the traditional inspection methods**.

The cost evaluation followed a Monte Carlo analysis to determine the most probable outcome of the initial and operating cost based on different distribution models. The operating costs were calculated based on a single carriageway road section. The UAV and traditional inspection method require one-way travel to evaluate the whole section, while the vehicle platform requires travel in each lane of the section. **The UAV platform fitted with a thermal camera will have the lowest operating cost (R2.94 per section km), while the vehicle platform fitted with a digital camera will have the highest operating cost (R10.88 per section km)**. A higher cost device can reduce the operating cost due to the increased scanning speed, but this will increase the initial cost significantly.

The quality evaluation of the different technology types was assessed through the ability of the technologies to identify different distress mechanisms according to the TRH 22 manual. The ability of a technology type to capture different types of cracks depended on the successful identification of different crack widths during testing. **A thermal device can identify all the different crack widths and major distress mechanisms regardless of the surrounding lighting conditions**. A thermal device and digital camera cannot identify rutting and undulations due to the inability to measure distance. A LIDAR device can identify rutting and undulations, but a limited number of other distress mechanisms can be identified.

A combination of technologies will increase the number of distress mechanisms that can be identified significantly. **A combination of all the technologies will be able to identify all the important distress mechanisms. In contrast, a thermal and LIDAR device can identify the same distress mechanisms except for the unpaved shoulder and surface drainage**. A digital camera and LIDAR device are limited to medium and large cracks due to the inability of the technologies to capture narrow cracks.

The ground-based vehicle platform requires travelling of each lane in the road section, which increases the operating cost significantly, but key advantages have been identified during testing. T**he main advantages are the ability of the ground-based vehicle platform to move with the traffic stream and the ability to mount a combination of technology types to the platform**. The height of the devices is limited on the ground-based vehicle platform, and the operator is more at-risk during data collection. The vehicle platform fitted with a digital camera has the lowest initial cost (R568 762.00) and the highest operating cost.

The UAV platform can reduce operating cost significantly but requires pre-route surveillance and mission setup to determine waypoints and altitude changes. The main objective of the pre-route surveillance will be to identify obstacles in the flight path. **The UAV platform can increase inspection safety due to the autonomous operation of the UAV**. The UAV platform tests identified key problems with current platforms and technology types. The main problems are the limited flight time of current UAV systems and traffic streams that cover parts of the pavement surface when the UAV capture data. The UAV platform fitted with a thermal device has a higher initial cost (R742 857.80) and the lowest operating cost.

Ultimately will the ground-based vehicle platform be the most suited to mount low-cost technologies for pavement surface evaluations. The mounting of multiple low-cost technology types and moving with the traffic stream are crucial advantages. The platform is easy to operate, can move with traffic and can be fitted with multiple devices to ensure a comprehensive evaluation of the pavement surface. Future improvements of the UAV platform are required for a UAV to be considered for pavement surface evaluations.

8.2 Recommendations for Future Work

The low-cost technology devices provided were used in the thesis to develop height and speed limit graphs for different devices and technologies. Continuous advancements in technological devices can improve the use of low-cost technologies for pavement evaluations. **The development of updated limit graphs for new low-cost devices would be recommended.**

The operator rates obtained from Salary Expert, Payscale, Indeed and Best Jobs databases appear to be lower than current industry rates. Additional research would, however, be needed to confirm the current/actual costs used in the road survey industry.

The development of a pavement evaluation system using a combination of thermal and LIDAR devices would contribute to the use of low-cost technology devices for pavement surface evaluation systems. The development can include software capable of evaluating both technologies simultaneously. The combination of thermal and LIDAR devices should be used to capture each distress mechanisms to obtain a more accurate representation of the ability to identify each distress mechanism.

The ability of low-cost technology to identify different distress mechanisms can be improved by the software used to process the collected data. Image thresholding principles were able to identify cracks and defects with some success from digital and thermal images. Machine learning software specially developed to identify distress mechanisms in pavement surfaces would be recommended to improve the ability of low-cost technology for pavement surface evaluations.

The sensor speed of the different technology devices limits the data capturing speed of each device. **Developing a device that can increase the data capturing speed by increasing the shutter speed or time-lapse speed of a specific device can improve the data collection speed significantly**.

The main drawback of the UAV platform is the limited flight time with a single battery. **Developing a solar-powered UAV with a flight time of 5 or more hours can increase the use of UAVs for pavement surface evaluations**. The solar-powered UAV must be able to carry at least one thermal device. A combination of a LIDAR and thermal device would be recommended to reduce altitude variations of the UAV. The use of a solar-powered UAV may allow remote UAV operations where the UAV and pavement inspections can be controlled from an office instead of driving in a vehicle behind the UAV. Remote UAV operations will decrease the operation cost of the UAV platform significantly.

A combination of a vehicle platform and UAV platform can be researched to utilize the vehicle travelling behind the UAV and allow multiple technology devices to capture data. It would be recommended that the vehicle will be fitted with a LIDAR device and the UAV with a thermal device. This would allow low-cost short distance LIDAR to be fitted to the vehicle and a high-quality thermal device to be fitted to the UAV. This would require longer flight time of the UAV, and a solar-powered UAV can be a good solution.

The UAV platform can be tethered to the vehicle with a long power cable to increase the flight time of the UAV; this will increase the device height and travel speed compared to the vehicle platform. The vehicle can be fitted with a battery bank to provide enough power to the UAV. This system requires research to determine the suitability and amount of battery power required for the UAV.

Chapter 9: References

3D Systems Inc. (no date) *3D scanners - A guide to 3D scanner technology*. Available at: http://www.rapidform.com/3d-scanners (Accessed: 30 August 2019).

AA (2020) *Fuel Pricing*. Available at: https://www.aa.co.za/fuel-pricing (Accessed: 26 March 2020).

Abbie (2018) *What Type of Drone Is More Common – Fixed Wing or Rotary*. Available at: https://www.outstandingdrone.com/fixed-wing-rotary-drones/ (Accessed: 22 February 2019).

Abulude, O. F., Akinyinka, A. and Adeyemi, A. (2015) 'Global Positioning System and It ' S Wide', *Continental J. Information Techonology*, 9(October), pp. 22–32. doi: 10.5707/cjit.2015.9.1.22.32.

Adlinge, S. S. and Gupta, A. K. (2013) 'Pavement Deterioration and its Causes', *IOSR Journal of Mechanical & Civil Engineering*, pp. 2278–1684. Available at: http://www.iosrjournals.org/iosr-jmce/papers/sicete(civil)-volume6/60.pdf.

Andrejašicˇ, M. (2008) 'MEMS ACCELEROMETERS', *Electronics and Power*, 11(11), p. 385. doi: 10.1049/ep.1965.0296.

Autonomous Vehicle Sensors Conference (2018) 'What Matters in LIDAR?', in. Available at: https://www.autonomoustechconf.com/sites/autosensorsconf/files/assets/6D LiDAR Face-Off Ouster_Mardirosian.pdf.

Baumer (2009) 'Om70-p0600.hh0500.vi', pp. 1–2. Available at: https://www.baumer.com/us/en/product-overview/distance-measurement/laser-distance-sensors-/high-performance/large-measuring-distances-up-to-1500-mm/om70-p0600-hh0500-vi/p/36901.

Bhattacharjee, A. (2015) *Rigid Pavement Response*. C.I.E.M. Available at: https://www.slideshare.net/AnkitSarkar9/rigid-pavement-distress?from_action=save.

Cao, L. *et al.* (2019) 'Comparison of UAV LiDAR and digital aerial photogrammetry point clouds for estimating forest structural attributes in subtropical planted forests', *Forests*, 10(2), pp. 1–26. doi: 10.3390/f10020145.

Carter, J. *et al.* (2018) 'Performance and expenditure review', (February).

Chapman, A. (2016) 'Types of Drones: Multi-Rotor vs Fixed-Wing vs Single Rotor vs Hybrid VTOL'. Available at: https://www.auav.com.au/articles/drone-types/.

Christenssoon, P. (2006) *Pixel definition*. Available at: https://techterms.com/definition/pixel (Accessed: 22 May 2019).

Colorado Department of Transportation (2015) 'Survey Manual - Chapter 4: Aerial Surveys', p. 40. Available at: https://www.codot.gov/business/manuals/survey/chapter-4/chapter4.pdf.

Committee of State Road Authorities (2018) 'TRH 22 Pavement Management Systems'.

Corrigan, F. (2020) *DJI Mavic Mini review*. Available at: https://www.dronezon.com/drone-reviews/dji-mavic-mini-review-of-features-specs-and-faqs/ (Accessed: 20 January 2020).

Davis Instruments (no date) 'Thermal Imaging Technical Resource', in. Available at: https://pim-resources.coleparmer.com/data-sheet/thermalimagingtechresource.pdf.

Dean, E. (2017) *How to interface your GoPro to a microcontroller*. Available at: https://cam-do.com/blogs/camdo-blog/how-to-interface-your-gopro-to-a-microcontroller-arduino-esp8266-etc-using-blink (Accessed: 12 June 2020).

Department: National Treasury of South Africa (2014) 'Roads and transport', (1999), pp. 117–132. Available at: http://www.treasury.gov.za/publications/igfr/2006/prov/08. Chapter 7 - Roads and Transport.pdf.

Department: Transport (2009) *Dimensional and Mass Limitations and Other Requirements for*. Available at: https://www.nra.co.za/content/TRH11-8thEdition2009.pdf.

Department: Transport (2018) *Overview: South Africa's road network*. Available at: http://www.transport.gov.za/roads (Accessed: 20 May 2019).

DJI (no date) *OSMO*. Available at: https://www.dji.com/osmo/info (Accessed: 14 April 2020).

DJI Store (2020a) *Livox Mid-100*. Available at: https://store.dji.com/product/livox-mid?vid=48981 (Accessed: 29 June 2020).

DJI Store (2020b) *Livox Mid-40*. Available at: https://store.dji.com/product/livox-mid?vid=48991 (Accessed: 29 June 2020).

Doug Deals (2020) *Quanergy M8*.

DPReview (2016) *4K: Fujifilm X-T2 offers 24MP*. Available at: https://www.dpreview.com/news/8595291296/now-with-4k-fujifilm-x-t2-offers-24mp-improved-af-and-video-specs (Accessed: 14 April 2020).

Drone Deploy (2017) *Choosing the Right Mapping Drone for Your Business Part I: Multi-Rotor vs. Fixed Wing Aircraft*. Available at: https://blog.dronedeploy.com/choosing-the-right-mapping-drone-for-your-business-part-i-multi-rotor-vs-fixed-wing-aircraft-6ec2d02eff48 (Accessed: 22 July 2019).

Du, J. C. and Teng, H. C. (2007) '3D laser scanning and GPS technology for landslide earthwork volume estimation', *Automation in Construction*, 16(5), pp. 657–663. doi: 10.1016/j.autcon.2006.11.002.

Dynatest (2020) *ROAD SURFACE PROFILER (RSP) MK-III*. Available at: https://www.dynatest.com/road-surface-profiler-rsp-mk-iii (Accessed: 29 June 2020).

EMS USA (2016) 'Types of 3D Scanners and 3D Scanning Technologies'. Available at: www.ems-usa.com.

Eriksson, J. *et al.* (2008) 'The Pothole Patrol: Using a Mobile Sensor Network for Road Surface Monitoring', pp. 515–525. Available at: http://nms.csail.mit.edu/papers/p2-mobisys-2008.pdf.

Eskom (Pty) Ltd. (2017) 'Tariffs & Charges 2017/2018', (June).

FLIR (no date) *Difference between 9 Hz and 60 Hz cameras*. Available at: https://flir.custhelp.com/app/answers/detail/a_id/913/~/difference-between-9-hz-and-60-hz-cameras/session/L2F2LzEvdGltZS8xNTkzNTAwMDM2L2dlbi8xNTkzNTAwMDM2L3NpZC9mVTZBcmhyQU96S0ZQMTh6aVBqZXZvX00xWUVhRzBtVm5MQVlIZ1RlaWF1X3UzY1QxeTR6YiU3RWNoQ2tMMlRxakJtRGMlN (Accessed: 12 June 2020).

FLIR Systems (2015) *Cooled vs uncooled thermal imaging: discover the difference*. Available at: https://www.labonline.com.au/content/analytical-instrumentation/article/cooled-vs-uncooled-thermal-imaging-discover-the-difference-1139382997 (Accessed: 20 April 2020).

Fowler, M. (1962) 'The Speed of Light', *IRE Transactions on Instrumentation*, I–11(3–4), pp.

138–148. doi: 10.1109/IRE-I.1962.5006618.

Gavilán, M. *et al.* (2011) 'Adaptive road crack detection system by pavement classification', *Sensors*, 11(10), pp. 9628–9657. doi: 10.3390/s111009628.

Go Thermal (2020a) *FLIR TG267*. Available at: https://www.gothermal.co.za/collections/industrial/products/tg267 (Accessed: 20 April 2020).

Go Thermal (2020b) *FLIR THERMAL INDUSTRIAL INSPECTION CAMERAS*. Available at: https://www.gothermal.co.za/collections/industrial#T-SERIES (Accessed: 20 April 2020).

Go UAV (2020) *DRONE CAMERAS*. Available at: https://gouav.co.za/collections/uav-cameras?gclid=Cj0KCQjwhZr1BRCLARIsALjRVQP_KPcnRvmdjcyN7ywvUmXJJoQ9JZLFoHKZ0Ap_boQXK_EZ8CI5MggaAnkNEALw_wcB (Accessed: 20 April 2020).

Heijsman, R. (2014) *Thermal Imaging Cameras Help Determine Road Conditions in Finland*. Available at: https://www.maintworld.com/Applications/Thermal-Imaging-Cameras-Help-Determine-Road-Conditions-in-Finland.

'Hero 8 Black Manual' (no date).

Herrick, S. (2017) *THE 3 MAIN CATEGORIES OF DRONES AND THEIR ADVANTAGES AND DISADVANTAGES*. Available at: https://botlink.com/blog/the-3-main-categories-of-drones-and-their-advantages-and-disadvantages (Accessed: 1 August 2019).

Hoque, M. Z. (2016) 'Basic Concept of GPS and Its Applications', *IOSR Journal Of Humanities And Social Science (IOSR-JHSS*, 21(3), pp. 31–37. doi: 10.9790/0837-2103023137.

Horts (2020) *RIEGL VUX-1UAV*. Available at: https://horts-solutions.com/hardware/zf-imager-5006h-3d-laser-scanner-2/ (Accessed: 29 June 2020).

ILSI Engineering (2019) *5 WAYS 2018 TECHNOLOGY IS IMPROVING CIVIL ENGINEERING*. Available at: http://www.ilsiengineering.com/industry-news/5-ways-2018-technology-improving-civil-engineering/ (Accessed: 29 August 2019).

Instruments, D. (no date) *Accelerometer Pros and Cons*. Available at: http://www.djbinstruments.com/information/technical-information-hub/accelerometer-pros-and-cons (Accessed: 2 October 2019).

Kannemeyer, L. (2016) 'South African Road Network Condition, Needs and Funding'. Available at: https://sarf.org.za/wp-content/uploads/2016/08/Louw-Kannemeyer.pdf.

Koch, C. and Brilakis, I. (2011) 'Advanced Engineering Informatics Pothole detection in asphalt pavement images', *Advanced Engineering Informatics*. Elsevier Ltd, 25(3), pp. 507–515. doi: 10.1016/j.aei.2011.01.002.

Law Insider (2018) *Definition of Fixed-wing*. Available at: https://www.lawinsider.com/dictionary/fixed-wing (Accessed: 20 May 2019).

Li, Z. *et al.* (2019) 'Identifying asphalt pavement distress using UAV LiDAR point cloud data and random forest classification', *ISPRS International Journal of Geo-Information*, 8(1). doi: 10.3390/ijgi8010039.

LiDAR USA (2020) 'M200 Series Snoopy M8 LiDAR Package', p. 833. Available at: https://www.lidarusa.com/uploads/5/4/1/5/54154851/prelim_m200_210sslidarpkgqm8.pdf.

Livox Lidar (2019) 'Livox Mid Series', pp. 1–28. Available at: www.livoxtech.com/mid-40-and-mid-100www.livoxtech.com/mid-40-and-mid-100https://github.com/Livox-SDK.

Longoria, P. R. G. (2014) 'Accelerometer Concepts and Selection Updated Fall 2014'.

Major Tech (2020) *True RMS Thermal Multimeter*. Available at: https://www.major-tech.com/product/true-rms-thermal-multimeter/ (Accessed: 4 May 2020).

Makro (2020) *Seek Thermal ShotPro Thermal Imaging Camera*. Available at: https://www.makro.co.za/electronics-computers/fitness-trackers-wearables/smart-watches-fitness-trackers/smart-watches-fitness-trackers/seek-thermal-shotpro-thermal-imaging-camera/p/6f6a64c6-4067-469e-8af7-f1440bba7a83?gclid=Cj0KCQjwhZr1BRCLARIsALjRVQOxSid (Accessed: 20 April 2020).

Mani, G. F., Feniosky, P. M. and Savarese, S. (2009) 'D4AR-A 4-dimensional augmented reality model for automating construction progress monitoring data collection, processing and communication', *Electronic Journal of Information Technology in Construction*, 14(June), pp. 129–153.

Martin, B. and Rapp, R. (2017) 'COLLAPSIBLE MULTI-ROTOR UAV', 2(12). Available at:

https://patents.google.com/patent/US9573683B2/en.

Math Centre (2003) 'Variance and standard deviation (grouped data)', *Creative Commons*, p. 2. Available at: http://www.lboro.ac.uk/media/wwwlboroacuk/content/mlsc/downloads/var_stand_deviat_group.pdf.

McAndrew, A. (2005) 'An Introduction to Digital Image Processing with Matlab Notes for SCM2511 Image Processing 1', *Image Rochester NY*, 1(1), pp. 1–13. doi: 10.1109/TBME.2009.2017027.

Medina, R., Gómez-García-Bermejo, J. and Zalama, E. (2017) 'Automated Visual Inspection of Road Surface Cracks', *Proceedings -- The 27th International Symposium on Automation and Robotics in Construction*, (Isarc), pp. 155–164. doi: 10.22260/isarc2010/0017.

Medioni, G. and Lee, M.-S. (2000) 'Tensor Voting : Theory and Applications', *Congrès francophone sur la Reconnaissance des Formes et l'Intelligence Artificielle (RFIA)*, p. 3.

van der Merwe, Q. and Edwards, T. (2018) '1 January 2019 Deadline in Relation to Road Transportation of High Cube Containers'. Available at: https://www.wylie.co.za/articles/south-africa-1-january-2019-deadline-relation-road-transportation-high-cube-containers/.

Mishra, G. (2019) *Types of Pavement – Flexible Pavements and Rigid Pavements*. Available at: https://theconstructor.org/transportation/types-of-pavement-flexible-and-rigid-pavement/9570/ (Accessed: 20 May 2019).

MMF (no date) 'AN1E Application Note', pp. 1–2.

MTAG (2003) 'Common Distresses on Flexible Pavements From… Maintenance Technical Advisory Guide (MTAG)', *Caltrans*. Available at: http://www.dot.ca.gov/hq/maint/MTAG-CommonFlexiblePavementDistresses.pdf.

Nordengen, P. A., Steynberg, R. J. and Sallie, I. (2002) 'ABNORMAL LOADS SUPER ROUTES – A STRATEGIC INVESTMENT FOR PROMOTING SOUTH AFRICA ' S ECONOMIC GROWTH', (July), pp. 15–19. Available at: https://repository.up.ac.za/bitstream/handle/2263/7851/076.pdf;sequence=1.

Oswald-Tranta, B. *et al.* (2017) 'Motion Deblurring of Infrared Images', *Proceedings IRS^2 2017*, pp. 783–787. doi: 10.5162/irs2017/i3.1.

Pavemetrics (no date) 'Laser Crack Measurement System', pp. 1–2.

Peterson, K. A. (2005) 'Introduction to Basic Measures of a Digital Image for Pictorial Collections', (June), pp. 1–8.

Petkova, M. (2017) 'Deploying drones for autonomous detection'.

Pix4D (2018) *Processing thermal images*. Available at: https://support.pix4d.com/hc/en-us/articles/360000173463-Processing-thermal-images (Accessed: 20 April 2020).

Podges, T. M. (2017) 'A decision model for the investment in technology to reduce concrete rework', (December).

Rai, M., Maity, T. and Yadav, R. K. (2018) 'Thermal imaging system and its real-time applications : a survey Thermal imaging system and its real-time applications : a survey', (June).

Rand/ US Dollar Exchange Rate Page (2020). Available at: https://www.southafricanmi.com/rand-dollar-exchange-rate.html (Accessed: 25 March 2020).

RIEGL (2015a) 'Datasheet Riegl VZ-2000'. Available at: http://www.riegl.com/uploads/tx_pxpriegldownloads/DataSheet_VZ-2000_2015-03-24.pdf.

RIEGL (2015b) 'RIEGL VUX-1UAV', pp. 2–5.

Roads Coordinating Body, Committee of Transport Officials; and Road Asset Management Systems Subcommittee (2016) *TMH9: MANUAL FOR VISUAL ASSESSMENT OF ROAD PAVEMENTS PART A: GENERAL*.

Ross, D. and Townshend, M. (2018) 'the Road Maintenance Backlog in South Africa'.

RS Online (2020) *Baumer Laser Distance Sensor Point spot - 600mm*. Available at: https://za.rs-online.com/web/p/photoelectric-sensors/1871818/ (Accessed: 29 June 2020).

RS Pro (2020) *RS PRO RS730 Thermal Imaging Camera*. Available at: https://docs.rs-online.com/1cf6/0900766b8169bb71.pdf (Accessed: 20 April 2020).

SABITA (2018) ‘Roads review 2018’.

SANRAL (2009) ‘DESIGN GUIDELINES FOR SINGLE CARRIAGEWAY NATIONAL ROADS’, (May), pp. 1–13.

SANRAL (2014) *SOUTH AFRICAN Chapter 14*.

SANRAL (2018) ‘Road Network Management - Asset Management’, 1. Available at: http://www.nra.co.za/live/content.php?Session_ID=ef3c3d4f52ab3dc249008e0d0b206d13&Category_ID=41.

SANRAL (2019) *Statistics*. Available at: https://www.nra.co.za/live/content.php?Item_ID=279.

Saravanan, C. (2010) ‘Color image to grayscale image conversion’, *2010 2nd International Conference on Computer Engineering and Applications, ICCEA 2010*. IEEE, 2, pp. 196–199. doi: 10.1109/ICCEA.2010.192.

Schnebele, E. *et al.* (2015) ‘Review of remote sensing methodologies for pavement management and assessment’, *European Transport Research Review*, 7(2). doi: 10.1007/s12544-015-0156-6.

Seek Thermal (2020) *Seek Shot Series*. Available at: https://www.thermal.com/seekshot-series.html (Accessed: 20 April 2020).

Shatnawi, N. (2018) ‘Automatic Pavement Cracks Detection using Image Processing Techniques and Neural Network’, (January). doi: 10.14569/IJACSA.2018.090950.

Smart Vision Lights (no date) ‘Pixel blur’, p. 49445.

Solomon, C. and Breckon, T. (2011) *Fundamentals of Digital Image Processing: A Practical Approach with Examples*. West Sussex: John Wiley & Sons. Available at: https://books.google.co.za/books?hl=en&lr=&id=NoJ15jLdy7YC&oi=fnd&pg=PT9&dq=basic+image+processing+in+matlab&ots=es3qBDJg5y&sig=rJEbyEQFCYDXnDlD7pUM4smY12I#v=onepage&q=basic image processing in matlab&f=false.

Surface and Edge (2018) *How the Laser Scanner Works*. Available at: https://www.surfaceandedge.com/technology/how-the-laser-scanner-works (Accessed: 30 August 2019).

Tahar, K. and Ahmad, A. (2013) 'An Evaluation on Fixed Wing and Multi-Rotor UAV Images using Photogrammetric Image Processing', *International Journal of Computer, Electrical, Automation, Control and Information Engineering*, 7(1), pp. 48–52. Available at: http://www.waset.org/publications/11861.

Technologies, S. R. (no date) 'SRT Mark III Road Surface Profiler'. Available at: https://e42cf819-decc-4983-a720-3eab0a9c0def.filesusr.com/ugd/8e522f_5b402b8af66e41f1845869ff6967a8e3.pdf.

TMH 9 (2016) 'TMH 9 MANUAL FOR VISUAL ASSESSMENT OF ROAD PAVEMENTS PART B: FLEXIBLE PAVEMENTS', (May).

Unibrain (2010) *User Operation Manual*, *Analysis*. Available at: https://www.unibrain.com/wp-content/uploads/2013/01/1394bcameras_manual_v13.pdf.

Vollmer, M. and Möllmann, K. . (2018) *Fundamentals of Infrared Thermal Imaging*.

Western Cape Government (2019) 'Road Asset Management Plan 2019', 1. Available at: http://www.nra.co.za/live/content.php?Session_ID=ef3c3d4f52ab3dc249008e0d0b206d13&Category_ID=41.

Zhang, A. *et al.* (2018) 'Deep Learning-Based Fully Automated Pavement Crack Detection on 3D Asphalt Surfaces with an Improved CrackNet', *Journal of Computing in Civil Engineering*, 32(5), pp. 1–14. doi: 10.1061/(ASCE)CP.1943-5487.0000775.

Zhang, C. (2010) 'Monitoring the condition of unpaved roads with remote sensing and other technology', *Final Report US DOT DTPH56-06-BAA-0002*, pp. 1–53. Available at: http://ntl.bts.gov/lib/42000/42300/42378/FinalReport.pdf%5Cnpapers2://publication/uuid/1A0A7E56-CEEE-4F52-86D3-9F4C226C7117.

Zhang, J. and Singh, S. (2017) 'Low-drift and real-time lidar odometry and mapping', *Autonomous Robots*, 41(2), pp. 401–416. doi: 10.1007/s10514-016-9548-2.

Zhang, L. *et al.* (2016) 'Road crack detection using deep convolutional neural network', *Proceedings - International Conference on Image Processing, ICIP*. IEEE, 2016-Augus, pp. 3708–3712. doi: 10.1109/ICIP.2016.7533052.

Zou, Q. *et al.* (2012) 'CrackTree: Automatic crack detection from pavement images', *Pattern Recognition Letters*. Elsevier B.V., 33(3), pp. 227–238. doi: 10.1016/j.patrec.2011.11.004.

Van Zwieten, C. (2010) 'Monitoring South Africa ' s national road network', *Application technical*, pp. 55–57. Available at: http://www.ee.co.za/wp-content/uploads/legacy/PositionIT 2009/PositionIT 2010/Monitoring South Africa.pdf.

Appendices

Appendix A: Monte Carlo Distribution Models

The Monte Carlo analysis is used to calculate the initial and operating cost for each of the technological platforms. The steps can be repeated to obtain one specific value for each of the parameters with a variable cost. The distribution models are used to model the parameters with variable costs to determine the most probable cost for each of the technological platforms.

I. Exchange Rate Distribution

The exchange rate probability distribution is based on the exchange rate data from 2 January 2019 until 26 May 2020 between the South African Rand and US Dollar, the period of this thesis. The minimum exchange rate is R13.29 while the maximum exchange rate R19,07; this indicates the high fluctuations of the exchange rate (*Rand/ US Dollar Exchange Rate Page*, 2020). The exchange rate probability distribution can be seen in Figure 62. The probability of each exchange rate is calculated by dividing the number of times the specific exchange rate appeared by 1809, which is the total number of entries.

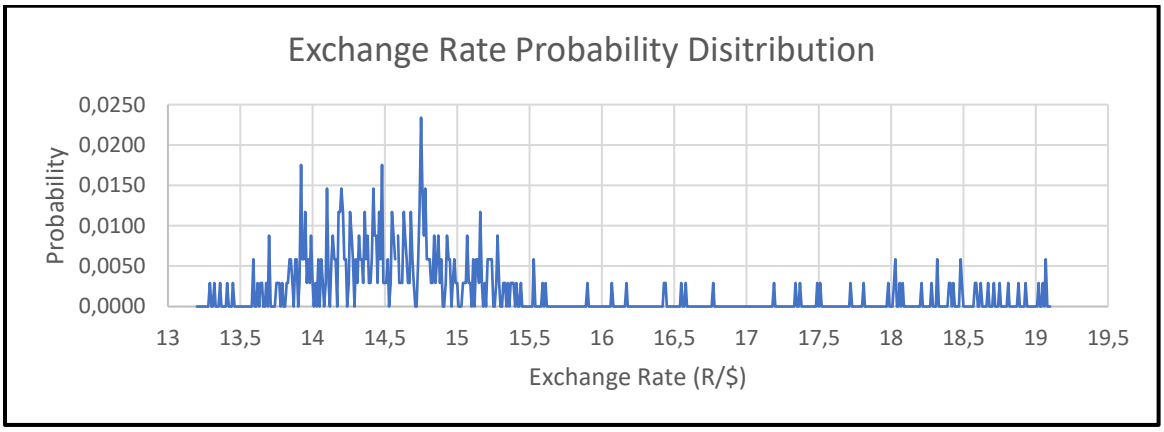

Figure 62: Exchange Rate Probability Distribution

The exchange rate probability distribution was used to develop the exchange rate cumulative distribution graph. The cumulative distribution is required to obtain one answer for each random probability between zero and one. The exchange rate cumulative probability distribution can be seen in Figure 63

The process to determine a realistic exchange rate in the calculation of the cost representing each technological platform was completed with 150 iterations. Each iteration used a random probability between zero and one; each probability is randomly generated using excel functions. The corresponding exchange rate for the random probability was determined using the exchange rate cumulative probability data and the Microsoft Excel VLOOKUP function.

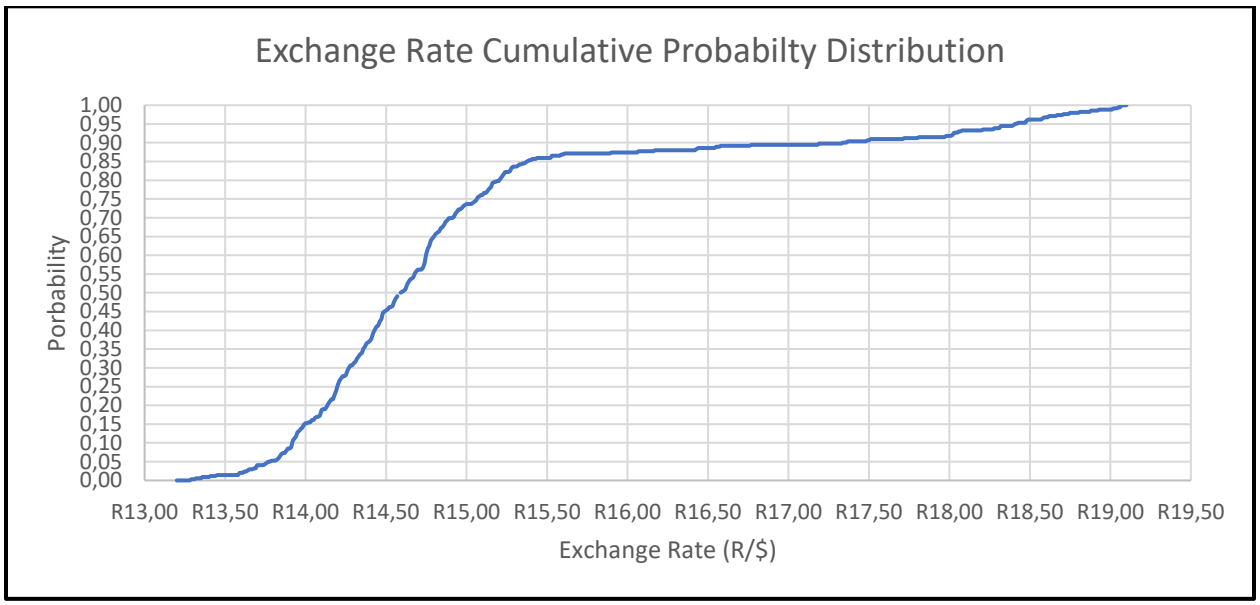

Figure 63: Exchange Rate Cumulative Probability Distribution

II. Operator Distribution

Each platform requires a different operator to collect data. The UAV platform requires the operator to be able to fly the UAV. The moving vehicle platform requires a driver with limited or no knowledge about pavement surface defects; the driver should be able to operate the technological device. The traditional inspection method requires a pavement engineer with experience in pavement surface defects. For each of the operators, a range of hourly rates is available. The hourly rate range of each operator and the source of the rates can be seen in Table 31.

Table 31: Operator Hourly Rate Range

Operator	Hourly Rate	Source
UAV Operator	R84.38 – R167.00	Salary Expert, PayScale, Indeed
Vehicle Driver	R54.05 – R111.80	Salary Explorer, PayScale, Indeed
Pavement Engineer	R188.75 – R347.40	PayScale, Indeed, Best Jobs

The operator distribution for each of the operators followed the same procedure as the exchange rate distribution to develop the probability distribution and cumulative probability distribution for each of the operators. The probability distribution for each operator can be seen in Figure 64.

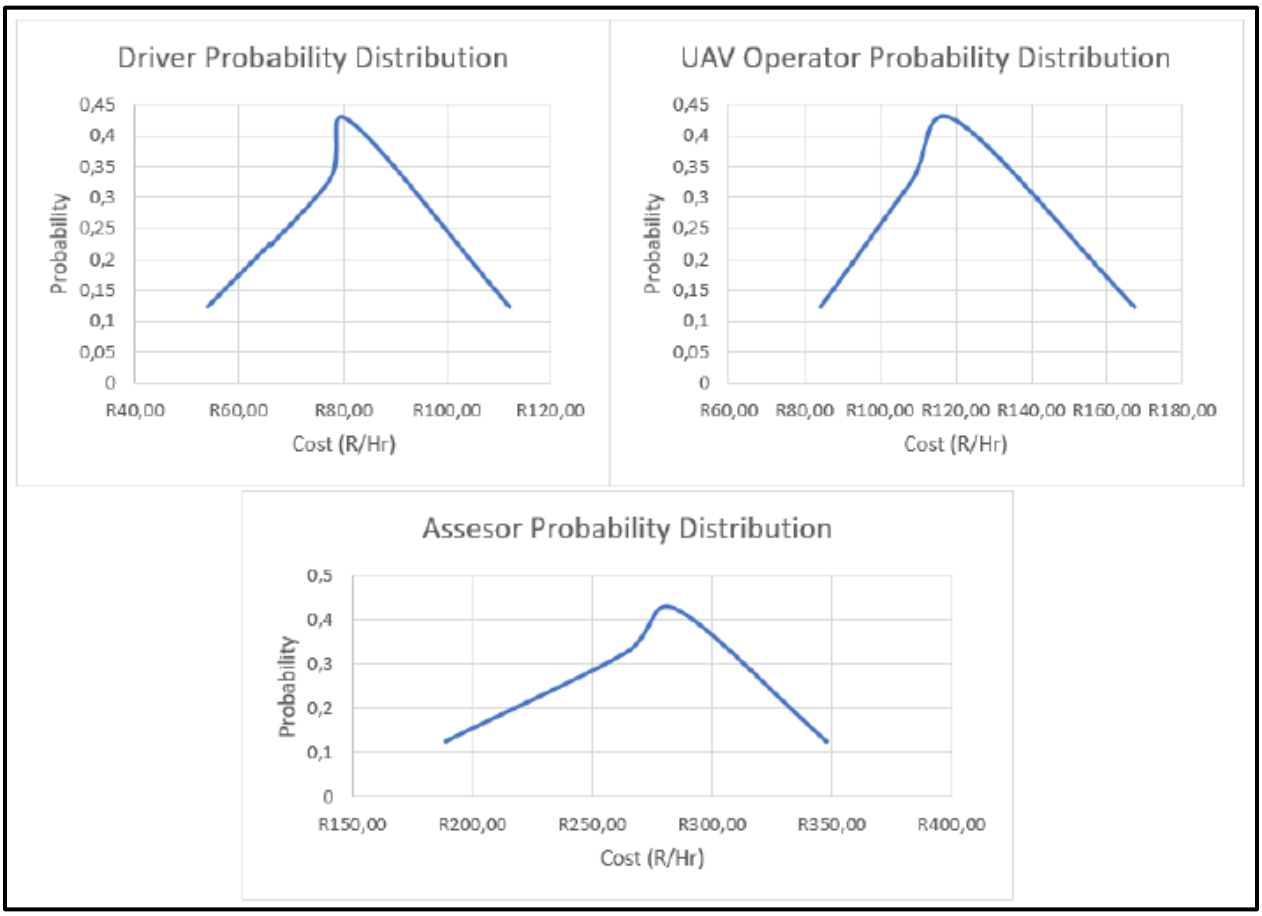

Figure 64: Operator Probability Distributions

III. Vehicle Running Cost

The vehicle running cost is a function of the fuel price, a fuel factor, service and repair cost and the tyre cost. The vehicle running cost equation can be seen in Equation 11.

Equation 11: Vehicle Running Cost (AA Rates for Vehicle Operating Costs, 2008)

$$Running\ Cost = Fp \times FF + S\&R + T$$

Where:

Fp is the fuel price

FF is the fuel factor according to the engine vehicle size

$S\&R$ is the service and repair cost

T is the tyre cost

The service and repair cost in Equation 11 are fixed, known values based on the vehicle engine size. Therefore, will it be possible to model the vehicle running cost using the fuel price probability distribution. The fuel price (Diesel 50PPM) data are for the period between 03 January 2019 and 01 July 2020. The minimum and maximum fuel price within this period were R10.59 and R14.73 respectively, this indicates the variability in the fuel price which requires the Monte Carlo analysis method to determine the vehicle running cost over a time period (AA, 2020).

The vehicle running cost distribution followed the same procedure as the exchange rate distribution to develop the fuel price probability distribution (Figure 65) and the fuel price cumulative probability distribution (Figure 66).

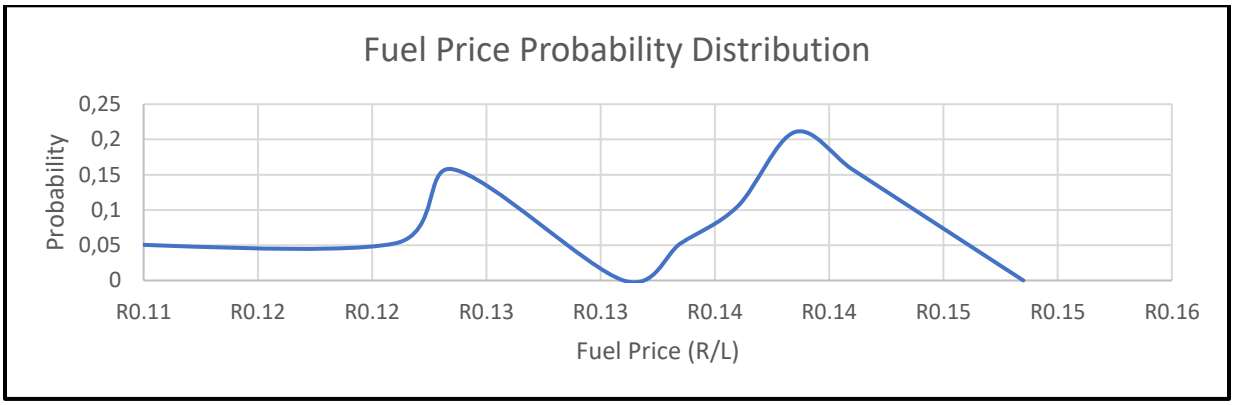

Figure 65: Fuel Price Probability Distribution

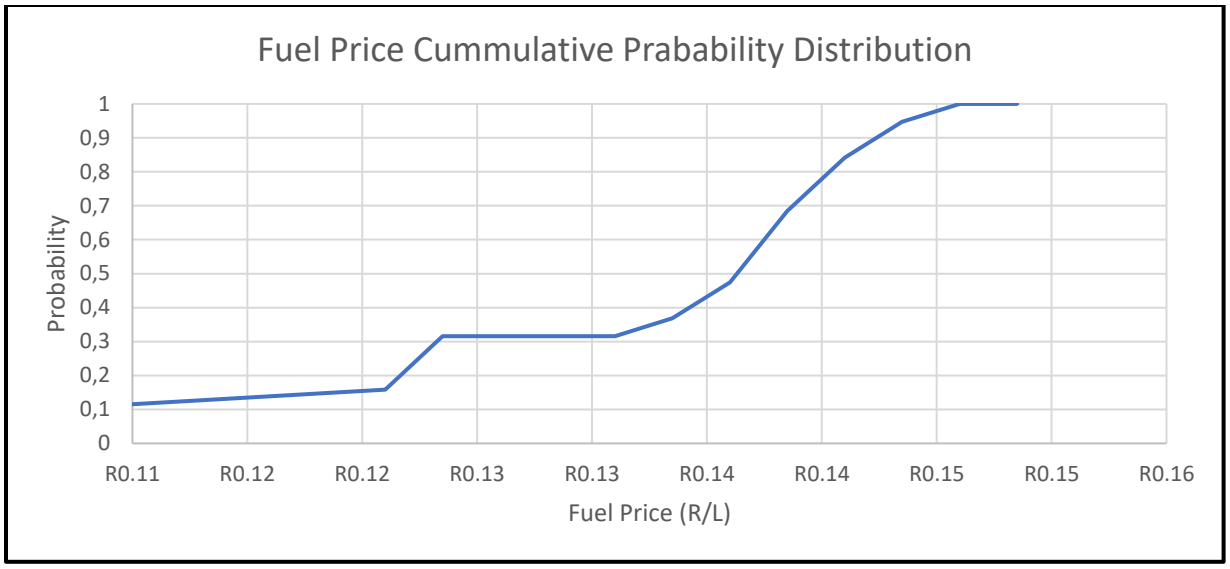

Figure 66: Fuel Price Cumulative Probability Distribution

IV. Power Distribution

The power distribution is used to determine the cost per battery charge of the UAV's batteries. The power distribution followed the same procedure as the exchange rate distribution to develop the power probability distribution (Figure 67) and the power cumulative probability distribution (Figure 68). The high difference of costs in Figure 67 is due to the difference in power costs between high demand and low demand seasons for peak, standard and off-peak hours.

Low Demand seasons are between September and May, while high demand seasons are between June to August. Peak hours are assumed to be 6 hours per day between 10:00 and 16:00; standard hours are 8 hours per day between 06:00 and 10:00, as well as 16:00 and 20:00; and off-peak hours is 10 hours per day between 20:00 and 06:00 (Eskom (Pty) Ltd., 2017).

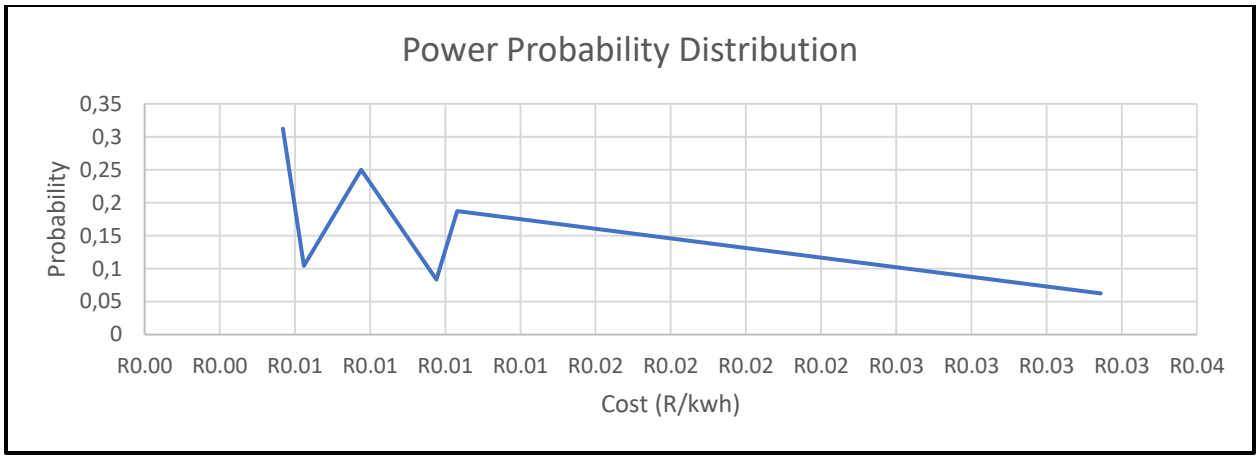

Figure 67: Power Probability Distribution

Figure 68 is used to obtain one cost value for the power consumption of a battery charge. The equation for each section of the distribution is used to calculate a value with the random probability generated by Microsoft Excel.

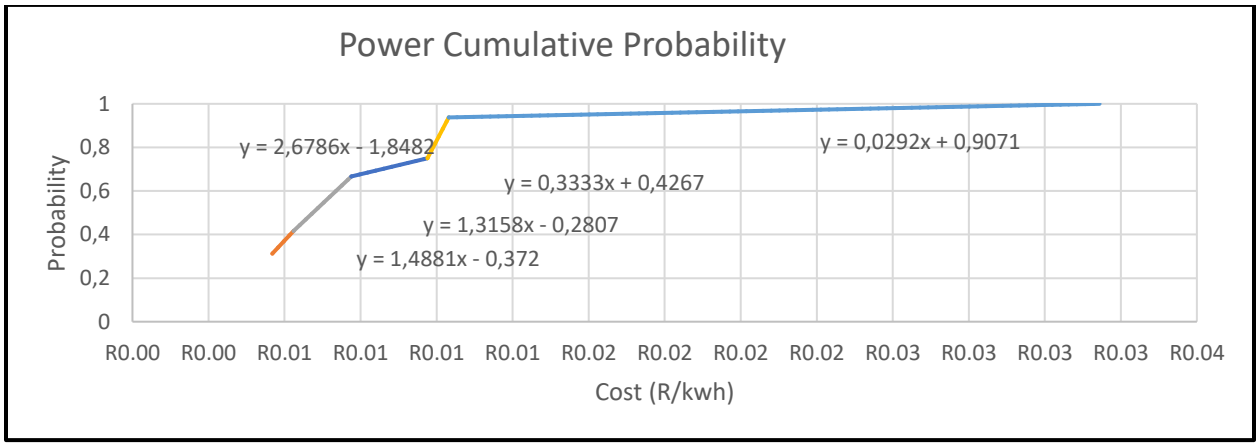

Figure 68: Power Cumulative Probability Distribution

Appendix B: Cost Calculation Data

I. A vehicle with Digital Camera Monte Carlo Analysis Data

Initial Cost				Operating Cost								
				Operator		Fuel Cost				Service and Repair		
Probability	Exchange Rate	Cost	Iteration	Probability	Cost	Probability	Fuel Price	Fuel factor	Cost (C)	Cost (C)	Running Cost (C)	Operating cost/km
0.7028	R14.92	R568 876.00	1	0.517	R77.52	0.59	R13.60	7.21	98.00	55	153.00	R10.81
0.5651	R14.72	R568 796.00	2	0.816	R80.36	0.611	R13.60	7.21	98.00	55	153.00	R11.10
0.8298	R15.27	R569 016.00	3	0.849	R80.67	0.434	R13.35	7.21	96.20	55	151.20	R11.09
0.7391	R15.03	R568 920.00	4	0.25	R62.93	0.383	R13.35	7.21	96.20	55	151.20	R9.32
0.5605	R14.69	R568 784.00	5	0.938	R97.53	0.203	R12.10	7.21	87.19	55	142.19	R12.60
0.7588	R15.08	R568 940.00	6	0.933	R96.28	0.606	R13.60	7.21	98.00	55	153.00	R12.69
0.92	R16.02	R569 316.00	7	0.482	R77.18	0.938	R14.10	7.21	101.60	55	156.60	R10.85
0.7347	R14.99	R568 904.00	8	0.995	R111.78	0.962	R14.35	7.21	103.40	55	158.40	R14.35
0.7993	R15.20	R568 988.00	9	0.842	R80.60	0.112	R10.75	7.21	77.46	55	132.46	R10.71
0.7522	R15.06	R568 932.00	10	0.739	R79.62	0.677	R13.60	7.21	98.00	55	153.00	R11.02
0.8628	R15.52	R569 116.00	11	0.187	R58.49	0.732	R13.85	7.21	99.80	55	154.80	R8.95
0.997	R16.07	R569 336.00	12	0.582	R78.13	0.061	R10.50	7.21	75.66	55	130.66	R10.43
0.5126	R14.62	R568 756.00	13	0.654	R78.82	0.741	R13.85	7.21	99.80	55	154.80	R10.98
0.534	R14.64	R568 764.00	14	0.362	R70.82	0.313	R12.10	7.21	87.19	55	142.19	R9.93
0.6687	R14.83	R568 840.00	15	0.457	R76.95	0.533	R13.60	7.21	98.00	55	153.00	R10.75
0.7466	R15.06	R568 932.00	16	0.232	R61.66	0.762	R13.85	7.21	99.80	55	154.80	R9.26
0.8194	R15.23	R569 000.00	17	0.992	R111.03	0.563	R13.60	7.21	98.00	55	153.00	R14.16
0.8071	R15.21	R568 992.00	18	0.523	R77.57	0.506	R13.60	7.21	98.00	55	153.00	R10.82
0.495	R14.57	R568 736.00	19	0.654	R78.82	0.321	R13.10	7.21	94.40	55	149.40	R10.87
0.8261	R15.27	R569 016.00	20	0.696	R79.22	0.375	R13.35	7.21	96.20	55	151.20	R10.95
0.461	R14.51	R568 712.00	21	0.41	R74.20	0.556	R13.60	7.21	98.00	55	153.00	R10.48
0.5206	R14.63	R568 760.00	22	0.869	R80.86	0.856	R14.10	7.21	101.60	55	156.60	R11.22
0.6942	R14.88	R568 860.00	23	0.52	R77.54	0.212	R12.10	7.21	87.19	55	142.19	R10.60
0.955	R16.19	R569 384.00	24	0.316	R67.58	0.918	R14.10	7.21	101.60	55	156.60	R9.89

0.7963	R15.18	R568 980.00	25	0.808	R80.28	0.495	R13.60	7.21	98.00	55	153.00	R11.09
0.9775	R16.21	R569 392.00	26	0.295	R66.10	0.553	R13.60	7.21	98.00	55	153.00	R9.67
0.9842	R16.22	R569 396.00	27	0.55	R77.83	0.636	R13.60	7.21	98.00	55	153.00	R10.84
0.582	R14.74	R568 804.00	28	0.186	R58.42	0.701	R13.85	7.21	99.80	55	154.80	R8.94
0.682	R14.86	R568 852.00	29	0.426	R75.32	0.411	R13.35	7.21	96.20	55	151.20	R10.56
0.5517	R14.67	R568 776.00	30	0.888	R85.03	0.96	R14.35	7.21	103.40	55	158.40	R11.67
0.6767	R14.85	R568 848.00	31	0.131	R54.55	0.413	R13.35	7.21	96.20	55	151.20	R8.48
0.7576	R15.08	R568 940.00	32	0.615	R78.45	0.356	R13.10	7.21	94.40	55	149.40	R10.83
0.849	R15.37	R569 056.00	33	0.585	R78.16	0.837	R13.85	7.21	99.80	55	154.80	R10.91
0.931	R16.29	R569 424.00	34	0.949	R100.28	0.207	R12.10	7.21	87.19	55	142.19	R12.87
0.7665	R15.12	R568 956.00	35	0.615	R78.45	0.785	R13.85	7.21	99.80	55	154.80	R10.94
0.9454	R16.31	R569 432.00	36	0.927	R94.78	0.513	R13.60	7.21	98.00	55	153.00	R12.54
0.8328	R15.27	R569 016.00	37	0.545	R77.78	0.858	R14.10	7.21	101.60	55	156.60	R10.91
0.9411	R16.33	R569 440.00	38	0.588	R78.19	0.303	R12.10	7.21	87.19	55	142.19	R10.66
0.4698	R14.54	R568 724.00	39	0.682	R79.08	0.342	R13.10	7.21	94.40	55	149.40	R10.90
0.4929	R14.57	R568 736.00	40	0.918	R92.53	0.675	R13.60	7.21	98.00	55	153.00	R12.31
0.8742	R15.89	R569 264.00	41	0.466	R77.03	0.703	R13.85	7.21	99.80	55	154.80	R10.80
0.5603	R14.69	R568 784.00	42	0.356	R70.39	0.965	R14.35	7.21	103.40	55	158.40	R10.21
0.8127	R15.22	R568 996.00	43	0.468	R77.05	0.912	R14.10	7.21	101.60	55	156.60	R10.84
0.9179	R16.39	R569 464.00	44	0.619	R78.48	0.086	R10.50	7.21	75.66	55	130.66	R10.46
0.6709	R14.83	R568 840.00	45	0.408	R74.06	0.414	R13.35	7.21	96.20	55	151.20	R10.43
0.7494	R15.06	R568 932.00	46	0.487	R77.23	0.368	R13.10	7.21	94.40	55	149.40	R10.71
0.607	R14.75	R568 808.00	47	0.678	R79.04	0.678	R13.60	7.21	98.00	55	153.00	R10.96
0.881	R16.42	R569 476.00	48	0.573	R78.05	0.59	R13.60	7.21	98.00	55	153.00	R10.86
0.5652	R14.72	R568 796.00	49	0.627	R78.56	0.371	R13.35	7.21	96.20	55	151.20	R10.88
0.9197	R16.45	R569 488.00	50	0.979	R107.78	0.147	R10.75	7.21	77.46	55	132.46	R13.43
0.5152	R14.62	R568 756.00	51	0.935	R96.78	0.942	R14.10	7.21	101.60	55	156.60	R12.81
0.5156	R14.62	R568 756.00	52	0.633	R78.62	0.709	R13.85	7.21	99.80	55	154.80	R10.96
0.9671	R16.48	R569 500.00	53	0.667	R78.94	0.543	R13.60	7.21	98.00	55	153.00	R10.95
0.7395	R15.03	R568 920.00	54	0.807	R80.27	0.334	R13.10	7.21	94.40	55	149.40	R11.01

0.7418	R15.04	R568 924.00	55	0.243	R62.44	0.715	R13.85	7.21	99.80	55	154.80	R9.34
0.9799	R16.51	R569 512.00	56	0.799	R80.19	0.931	R14.10	7.21	101.60	55	156.60	R11.15
0.8261	R15.27	R569 016.00	57	0.613	R78.43	0.897	R14.10	7.21	101.60	55	156.60	R10.97
0.8929	R16.53	R569 520.00	58	0.355	R70.32	0.793	R13.85	7.21	99.80	55	154.80	R10.13
0.474	R14.54	R568 724.00	59	0.46	R76.97	0.374	R13.35	7.21	96.20	55	151.20	R10.72
0.5642	R14.72	R568 796.00	60	0.69	R79.16	0.779	R13.85	7.21	99.80	55	154.80	R11.01
0.5735	R14.73	R568 800.00	61	0.275	R64.69	0.156	R10.75	7.21	77.46	55	132.46	R9.12
0.9399	R16.57	R569 536.00	62	0.368	R71.24	0.159	R12.10	7.21	87.19	55	142.19	R9.97
0.7504	R15.06	R568 932.00	63	0.354	R70.25	0.252	R12.10	7.21	87.19	55	142.19	R9.87
0.6792	R14.85	R568 848.00	64	0.878	R82.53	0.603	R13.60	7.21	98.00	55	153.00	R11.31
0.5578	R14.68	R568 780.00	65	0.713	R79.38	0.659	R13.60	7.21	98.00	55	153.00	R11.00
0.7343	R14.99	R568 904.00	66	0.659	R78.86	0.28	R12.10	7.21	87.19	55	142.19	R10.73
0.7055	R14.92	R568 876.00	67	0.519	R77.53	0.162	R12.10	7.21	87.19	55	142.19	R10.60
0.7257	R14.97	R568 896.00	68	0.553	R77.86	0.982	R14.35	7.21	103.40	55	158.40	R10.95
0.9745	R16.64	R569 564.00	69	0.158	R56.45	0.588	R13.60	7.21	98.00	55	153.00	R8.71
0.9954	R16.65	R569 568.00	70	0.976	R107.03	0.637	R13.60	7.21	98.00	55	153.00	R13.76
0.667	R14.83	R568 840.00	71	0.946	R99.53	0.842	R13.85	7.21	99.80	55	154.80	R13.05
0.7652	R15.10	R568 948.00	72	0.546	R77.79	0.994	R14.35	7.21	103.40	55	158.40	R10.95
0.5905	R14.74	R568 804.00	73	0.271	R64.41	0.547	R13.60	7.21	98.00	55	153.00	R9.50
0.7145	R14.93	R568 880.00	74	0.238	R62.08	0.995	R14.35	7.21	103.40	55	158.40	R9.38
0.6669	R14.83	R568 840.00	75	0.971	R105.78	0.509	R13.60	7.21	98.00	55	153.00	R13.64
0.5645	R14.72	R568 796.00	76	0.199	R59.34	0.202	R12.10	7.21	87.19	55	142.19	R8.78
0.8313	R15.27	R569 016.00	77	0.759	R79.81	0.079	R10.50	7.21	75.66	55	130.66	R10.59
0.9881	R16.73	R569 600.00	78	0.309	R67.08	0.711	R13.85	7.21	99.80	55	154.80	R9.80
0.7372	R15.03	R568 920.00	79	0.296	R66.17	0.571	R13.60	7.21	98.00	55	153.00	R9.68
0.6616	R14.82	R568 836.00	80	0.213	R60.32	0.115	R10.75	7.21	77.46	55	132.46	R8.68
0.8789	R16.16	R569 372.00	81	0.709	R79.34	0.781	R13.85	7.21	99.80	55	154.80	R11.03
0.7285	R14.97	R568 896.00	82	0.668	R78.95	0.832	R13.85	7.21	99.80	55	154.80	R10.99
0.7275	R14.97	R568 896.00	83	0.948	R100.03	0.072	R10.50	7.21	75.66	55	130.66	R12.62
0.5065	R14.61	R568 752.00	84	0.975	R106.78	0.145	R10.75	7.21	77.46	55	132.46	R13.33

0.7553	R15.07	R568 936.00	85	0.562	R77.94	0.125	R10.75	7.21	77.46	55	132.46	R10.44
0.5074	R14.61	R568 752.00	86	0.581	R78.12	0.609	R13.60	7.21	98.00	55	153.00	R10.87
0.6724	R14.83	R568 840.00	87	0.813	R80.33	0.521	R13.60	7.21	98.00	55	153.00	R11.09
0.8543	R15.40	R569 068.00	88	0.185	R58.35	0.806	R13.85	7.21	99.80	55	154.80	R8.93
0.5535	R14.68	R568 780.00	89	0.262	R63.77	0.951	R14.35	7.21	103.40	55	158.40	R9.55
0.7707	R15.12	R568 956.00	90	0.719	R79.43	0.676	R13.60	7.21	98.00	55	153.00	R11.00
0.4621	R14.53	R568 720.00	91	0.303	R66.66	0.395	R13.35	7.21	96.20	55	151.20	R9.69
0.7396	R15.03	R568 920.00	92	0.392	R72.93	0.182	R12.10	7.21	87.19	55	142.19	R10.14
0.5031	R14.60	R568 748.00	93	0.176	R57.72	0.685	R13.85	7.21	99.80	55	154.80	R8.87
0.9985	R16.89	R569 664.00	94	0.897	R87.28	0.965	R14.35	7.21	103.40	55	158.40	R11.90
0.6974	R14.88	R568 860.00	95	0.255	R63.28	0.25	R12.10	7.21	87.19	55	142.19	R9.17
0.5072	R14.61	R568 752.00	96	0.576	R78.08	0.719	R13.85	7.21	99.80	55	154.80	R10.90
0.4689	R14.54	R568 724.00	97	0.206	R59.83	0.384	R13.35	7.21	96.20	55	151.20	R9.01
0.5184	R14.62	R568 756.00	98	0.28	R65.04	0.873	R14.10	7.21	101.60	55	156.60	R9.64
0.5842	R14.74	R568 804.00	99	0.52	R77.54	0.151	R10.75	7.21	77.46	55	132.46	R10.40
0.5969	R14.74	R568 804.00	100	0.844	R80.62	0.769	R13.85	7.21	99.80	55	154.80	R11.16
0.4982	R14.57	R568 736.00	101	0.388	R72.65	0.742	R13.85	7.21	99.80	55	154.80	R10.36
0.7329	R14.98	R568 900.00	102	0.898	R87.53	0.977	R14.35	7.21	103.40	55	158.40	R11.92
0.6928	R14.87	R568 856.00	103	0.511	R77.46	0.424	R13.35	7.21	96.20	55	151.20	R10.77
0.7628	R15.10	R568 948.00	104	0.152	R56.03	0.363	R13.10	7.21	94.40	55	149.40	R8.59
0.9808	R17.00	R569 708.00	105	0.644	R78.72	0.545	R13.60	7.21	98.00	55	153.00	R10.93
0.5936	R14.74	R568 804.00	106	0.352	R70.11	0.87	R14.10	7.21	101.60	55	156.60	R10.14
0.4784	R14.55	R568 728.00	107	0.973	R106.28	0.597	R13.60	7.21	98.00	55	153.00	R13.69
0.6781	R14.85	R568 848.00	108	0.983	R108.78	0.305	R12.10	7.21	87.19	55	142.19	R13.72
0.7835	R15.15	R568 968.00	109	0.304	R66.73	0.081	R10.50	7.21	75.66	55	130.66	R9.29
0.8351	R15.28	R569 020.00	110	0.423	R75.11	0.822	R13.85	7.21	99.80	55	154.80	R10.61
0.6747	R14.84	R568 844.00	111	0.263	R63.85	0.175	R12.10	7.21	87.19	55	142.19	R9.23
0.6418	R14.78	R568 820.00	112	0.964	R104.03	0.818	R13.85	7.21	99.80	55	154.80	R13.50
0.9597	R17.08	R569 740.00	113	0.863	R80.80	0.97	R14.35	7.21	103.40	55	158.40	R11.25
0.7742	R15.13	R568 960.00	114	0.868	R80.85	0.997	R14.35	7.21	103.40	55	158.40	R11.25

0.7341	R14.99	R568 904.00	115	0.467	R77.04	0.318	R13.10	7.21	94.40	55	149.40	R10.69
0.7159	R14.93	R568 880.00	116	0.864	R80.81	0.153	R10.75	7.21	77.46	55	132.46	R10.73
0.9509	R17.12	R569 756.00	117	0.182	R58.14	0.201	R12.10	7.21	87.19	55	142.19	R8.66
0.5925	R14.74	R568 804.00	118	0.304	R66.73	0.9	R14.10	7.21	101.60	55	156.60	R9.81
0.55	R14.67	R568 776.00	119	0.998	R112.53	0.961	R14.35	7.21	103.40	55	158.40	R14.42
0.9635	R17.15	R569 768.00	120	0.627	R78.56	0.886	R14.10	7.21	101.60	55	156.60	R10.99
0.4972	R14.57	R568 736.00	121	0.838	R80.56	0.284	R12.10	7.21	87.19	55	142.19	R10.90
0.7974	R15.18	R568 980.00	122	0.571	R78.03	0.304	R12.10	7.21	87.19	55	142.19	R10.65
0.6259	R14.77	R568 816.00	123	0.52	R77.54	0.526	R13.60	7.21	98.00	55	153.00	R10.81
0.8901	R16.57	R569 536.00	124	0.308	R67.01	0.42	R13.35	7.21	96.20	55	151.20	R9.73
0.7662	R15.12	R568 956.00	125	0.847	R80.65	0.276	R12.10	7.21	87.19	55	142.19	R10.91
0.5257	R14.63	R568 760.00	126	0.145	R55.54	0.383	R13.35	7.21	96.20	55	151.20	R8.58
0.831	R15.27	R569 016.00	127	0.752	R79.75	0.858	R14.10	7.21	101.60	55	156.60	R11.11
0.9156	R17.23	R569 800.00	128	0.38	R72.08	0.207	R12.10	7.21	87.19	55	142.19	R10.05
0.9935	R17.24	R569 804.00	129	0.286	R65.46	0.823	R13.85	7.21	99.80	55	154.80	R9.64
0.8738	R15.89	R569 264.00	130	0.989	R110.28	0.505	R13.60	7.21	98.00	55	153.00	R14.09
0.7681	R15.12	R568 956.00	131	0.415	R74.55	0.522	R13.60	7.21	98.00	55	153.00	R10.51
0.7292	R14.97	R568 896.00	132	0.458	R76.96	0.542	R13.60	7.21	98.00	55	153.00	R10.76
0.9403	R17.28	R569 820.00	133	0.786	R80.07	0.644	R13.60	7.21	98.00	55	153.00	R11.07
0.7737	R15.13	R568 960.00	134	0.81	R80.30	0.404	R13.35	7.21	96.20	55	151.20	R11.05
0.5873	R14.74	R568 804.00	135	0.458	R76.96	0.484	R13.60	7.21	98.00	55	153.00	R10.76
0.9844	R17.31	R569 832.00	136	0.663	R78.90	0.15	R10.75	7.21	77.46	55	132.46	R10.54
0.545	R14.67	R568 776.00	137	0.628	R78.57	0.872	R14.10	7.21	101.60	55	156.60	R10.99
0.9556	R17.33	R569 840.00	138	0.201	R59.48	0.415	R13.35	7.21	96.20	55	151.20	R8.97
0.9609	R17.34	R569 844.00	139	0.816	R80.36	0.8	R13.85	7.21	99.80	55	154.80	R11.13
0.8978	R17.33	R569 840.00	140	0.516	R77.51	0.561	R13.60	7.21	98.00	55	153.00	R10.81
0.8776	R16.16	R569 372.00	141	0.198	R59.27	0.697	R13.85	7.21	99.80	55	154.80	R9.02
0.6164	R14.75	R568 808.00	142	0.731	R79.55	0.911	R14.10	7.21	101.60	55	156.60	R11.09
0.827	R15.27	R569 016.00	143	0.57	R78.02	0.461	R13.35	7.21	96.20	55	151.20	R10.83
0.8998	R17.33	R569 840.00	144	0.52	R77.54	0.981	R14.35	7.21	103.40	55	158.40	R10.92

0.9139	R17.40	R569 868.00	145	0.614	R78.44	0.079	R10.50	7.21	75.66	55	130.66	R10.46
0.7235	R14.96	R568 892.00	146	0.47	R77.07	0.677	R13.60	7.21	98.00	55	153.00	R10.77
0.9892	R17.42	R569 876.00	147	0.356	R70.39	0.697	R13.85	7.21	99.80	55	154.80	R10.14
0.6203	R14.76	R568 812.00	148	0.199	R59.34	0.602	R13.60	7.21	98.00	55	153.00	R8.99
0.8708	R15.60	R569 148.00	149	0.552	R77.85	0.768	R13.85	7.21	99.80	55	154.80	R10.88
0.8566	R15.40	R569 068.00	150	0.385	R72.44	0.116	R10.75	7.21	77.46	55	132.46	R9.89

II. UAV with Digital Camera Monte Carlo Analysis Data

Initial Cost				Operation Cost											
Phantom + Battery				Operator		Charge		Fuel Cost				Service and Repair			
Iteration	Probability	Cost	Total Initial Cost	Probability	Cost	Probability	Cost	Probability	Fuel Price	Fuel Factor	Cost (C)	Cost (C)	Running Cost (C)	Total Initial Cost	Total Operating Cost
1	0.13	R13.95	R560 055.75	0.69	R114.87	0.88	R1.02	0.65	R13.60	7.21	98.00	55	153.00	R565 217.25	R4.98
2	0.4	R14.42	R563 197.70	0.35	R100.79	0.35	R0.49	0.225	R12.10	7.21	87.19	55	142.19	R568 533.10	R4.44
3	0.06	R13.83	R559 253.55	0.89	R127.88	0.42	R0.53	0.826	R13.85	7.21	99.80	55	154.80	R564 370.65	R5.37
4	0.44	R14.47	R563 531.95	0.91	R135.58	0.76	R0.97	0.828	R13.85	7.21	99.80	55	154.80	R568 885.85	R5.61
5	0.26	R14.20	R561 727.00	0.21	R90.57	0.86	R1.01	0.203	R12.10	7.21	87.19	55	142.19	R566 981.00	R4.15
6	0.71	R14.92	R566 540.20	0.54	R110.73	0.77	R0.98	0.407	R13.35	7.21	96.20	55	151.20	R572 060.60	R4.84
7	0.82	R15.23	R568 612.55	0.37	R102.25	0.95	R1.47	0.859	R14.10	7.21	101.60	55	156.60	R574 247.65	R4.65
8	0.94	R18.31	R589 202.35	0.64	R113.49	0.78	R0.98	0.711	R13.85	7.21	99.80	55	154.80	R595 977.05	R4.95
9	0.62	R14.76	R565 470.60	0.68	R114.59	0.41	R0.53	0.67	R13.60	7.21	98.00	55	153.00	R570 931.80	R4.96
10	0.57	R14.73	R565 270.05	0.41	R105.17	0.57	R0.65	0.146	R10.75	7.21	77.46	55	132.46	R570 720.15	R4.47
11	0.87	R15.60	R571 086.00	0.77	R117.08	0.54	R0.62	0.724	R13.85	7.21	99.80	55	154.80	R576 858.00	R5.05
12	0.82	R15.23	R568 612.55	0.51	R109.90	0.49	R0.59	0.408	R13.35	7.21	96.20	55	151.20	R574 247.65	R4.80
13	0.49	R14.56	R564 133.60	0.56	R111.28	0.7	R0.82	0.954	R14.35	7.21	103.40	55	158.40	R569 520.80	R4.92
14	0.62	R14.76	R565 470.60	0.62	R112.94	0.42	R0.53	0.852	R14.10	7.21	101.60	55	156.60	R570 931.80	R4.94
15	0.33	R14.32	R562 529.20	0.56	R111.28	0.89	R1.02	0.418	R13.35	7.21	96.20	55	151.20	R567 827.60	R4.85
16	0.34	R14.35	R562 729.75	0.31	R97.87	0.95	R1.47	0.264	R12.10	7.21	87.19	55	142.19	R568 039.25	R4.38

17	0.44	R14.47	R563 531.95	0.82	R118.46	0.75	R0.97	0.085	R10.50	7.21	75.66	55	130.66	R568 885.85	R4.86
18	0.25	R14.19	R561 660.15	0.97	R158.65	0.65	R0.71	0.756	R13.85	7.21	99.80	55	154.80	R566 910.45	R6.29
19	0.82	R15.23	R568 612.55	0.87	R119.84	0.58	R0.65	0.965	R14.35	7.21	103.40	55	158.40	R574 247.65	R5.17
20	0.83	R15.27	R568 879.95	0.19	R89.11	0.62	R0.68	0.081	R10.50	7.21	75.66	55	130.66	R574 529.85	R3.98
21	0.76	R15.08	R567 609.80	0.8	R117.91	0.36	R0.49	0.259	R12.10	7.21	87.19	55	142.19	R573 189.40	R4.95
22	0.47	R14.54	R563 999.90	0.38	R102.98	0.96	R1.81	0.779	R13.85	7.21	99.80	55	154.80	R569 379.70	R4.67
23	0.64	R14.77	R565 537.45	0.21	R90.57	0.79	R0.98	0.485	R13.60	7.21	98.00	55	153.00	R571 002.35	R4.25
24	0.94	R18.31	R589 202.35	0.17	R87.65	0.9	R1.03	0.629	R13.60	7.21	98.00	55	153.00	R595 977.05	R4.17
25	0.88	R16.16	R574 829.60	0.94	R147.12	0.64	R0.70	0.832	R13.85	7.21	99.80	55	154.80	R580 808.80	R5.95
26	0.94	R18.31	R589 202.35	0.63	R113.21	0.53	R0.62	0.164	R12.10	7.21	87.19	55	142.19	R595 977.05	R4.81
27	0.89	R16.57	R577 570.45	0.99	R166.35	0.76	R0.97	0.521	R13.60	7.21	98.00	55	153.00	R583 701.35	R6.51
28	0.43	R14.47	R563 531.95	0.54	R110.73	0.35	R0.49	0.478	R13.60	7.21	98.00	55	153.00	R568 885.85	R4.84
29	0.93	R18.07	R587 597.95	0.77	R117.08	0.58	R0.65	0.775	R13.85	7.21	99.80	55	154.80	R594 283.85	R5.05
30	0.16	R14.03	R560 590.55	0.18	R88.38	0.95	R1.47	0.327	R13.10	7.21	94.40	55	149.40	R565 781.65	R4.17
31	0.7	R14.91	R566 473.35	0.79	R117.63	0.97	R2.15	0.851	R14.10	7.21	101.60	55	156.60	R571 990.05	R5.13
32	0.46	R14.51	R563 799.35	0.93	R143.27	0.87	R1.01	0.989	R14.35	7.21	103.40	55	158.40	R569 168.05	R5.88
33	0.31	R14.29	R562 328.65	0.92	R139.42	0.8	R0.99	0.312	R12.10	7.21	87.19	55	142.19	R567 615.95	R5.60
34	0.76	R15.08	R567 609.80	0.82	R118.46	0.89	R1.02	0.539	R13.60	7.21	98.00	55	153.00	R573 189.40	R5.09
35	0.87	R15.60	R571 086.00	0.74	R116.25	0.98	R2.50	0.272	R12.10	7.21	87.19	55	142.19	R576 858.00	R4.96
36	0.09	R13.91	R559 788.35	0.13	R84.73	0.58	R0.65	0.878	R14.10	7.21	101.60	55	156.60	R564 935.05	R4.11
37	0.39	R14.41	R563 130.85	0.2	R89.84	0.92	R1.03	0.974	R14.35	7.21	103.40	55	158.40	R568 462.55	R4.29
38	0.05	R13.78	R558 919.30	0.76	R116.80	1	R3.18	0.19	R12.10	7.21	87.19	55	142.19	R564 017.90	R4.99
39	0.17	R14.08	R560 924.80	0.34	R100.06	0.33	R0.47	0.639	R13.60	7.21	98.00	55	153.00	R566 134.40	R4.52
40	0.31	R14.29	R562 328.65	0.57	R111.56	0.89	R1.02	0.403	R13.35	7.21	96.20	55	151.20	R567 615.95	R4.86
41	0.2	R14.13	R561 259.05	0.93	R143.27	0.87	R1.01	0.171	R12.10	7.21	87.19	55	142.19	R566 487.15	R5.72
42	0.44	R14.47	R563 531.95	0.94	R147.12	0.81	R0.99	0.538	R13.60	7.21	98.00	55	153.00	R568 885.85	R5.94
43	0.03	R13.67	R558 183.95	0.96	R154.81	0.71	R0.85	0.208	R12.10	7.21	87.19	55	142.19	R563 241.85	R6.05
44	0.11	R13.92	R559 855.20	0.66	R114.04	0.44	R0.55	0.597	R13.60	7.21	98.00	55	153.00	R565 005.60	R4.94

45	0.98	R18.80	R592 478.00	0.44	R107.36	0.76	R0.97	0.358	R13.10	7.21	94.40	55	149.40	R599 434.00	R4.72
46	0.23	R14.18	R561 593.30	0.45	R108.09	0.81	R0.99	0.336	R13.10	7.21	94.40	55	149.40	R566 839.90	R4.74
47	0.26	R14.20	R561 727.00	0.75	R116.53	0.97	R2.15	0.479	R13.60	7.21	98.00	55	153.00	R566 981.00	R5.06
48	0.67	R14.83	R565 938.55	0.92	R139.42	0.56	R0.64	0.135	R10.75	7.21	77.46	55	132.46	R571 425.65	R5.49
49	0.01	R13.40	R556 379.00	0.16	R86.92	0.58	R0.65	0.619	R13.60	7.21	98.00	55	153.00	R561 337.00	R4.14
50	0.8	R15.20	R568 412.00	0.17	R87.65	0.49	R0.59	0.796	R13.85	7.21	99.80	55	154.80	R574 036.00	R4.17
51	0.51	R14.62	R564 534.70	0.78	R117.36	0.68	R0.76	0.814	R13.85	7.21	99.80	55	154.80	R569 944.10	R5.06
52	0.08	R13.88	R559 587.80	0.31	R97.87	0.69	R0.79	0.97	R14.35	7.21	103.40	55	158.40	R564 723.40	R4.52
53	0.11	R13.92	R559 855.20	0.34	R100.06	0.41	R0.53	0.996	R14.35	7.21	103.40	55	158.40	R565 005.60	R4.58
54	0.04	R13.69	R558 317.65	0.64	R113.49	0.75	R0.97	0.482	R13.60	7.21	98.00	55	153.00	R563 382.95	R4.94
55	0.71	R14.92	R566 540.20	0.37	R102.25	0.98	R2.50	0.425	R13.35	7.21	96.20	55	151.20	R572 060.60	R4.63
56	0.43	R14.47	R563 531.95	0.92	R139.42	0.77	R0.98	0.73	R13.85	7.21	99.80	55	154.80	R568 885.85	R5.73
57	0.98	R18.80	R592 478.00	0.41	R105.17	0.65	R0.71	0.28	R12.10	7.21	87.19	55	142.19	R599 434.00	R4.57
58	0.11	R13.92	R559 855.20	0.57	R111.56	0.7	R0.82	0.77	R13.85	7.21	99.80	55	154.80	R565 005.60	R4.89
59	0.59	R14.74	R565 336.90	0.93	R143.27	0.95	R1.47	0.32	R13.10	7.21	94.40	55	149.40	R570 790.70	R5.80
60	0.48	R14.55	R564 066.75	0.56	R111.28	0.43	R0.54	0.701	R13.85	7.21	99.80	55	154.80	R569 450.25	R4.88
61	0.68	R14.85	R566 072.25	0.46	R108.52	0.82	R1.00	0.919	R14.10	7.21	101.60	55	156.60	R571 566.75	R4.83
62	0.49	R14.56	R564 133.60	0.32	R98.60	0.5	R0.59	0.771	R13.85	7.21	99.80	55	154.80	R569 520.80	R4.50
63	0.3	R14.26	R562 128.10	0.41	R105.17	0.63	R0.69	0.724	R13.85	7.21	99.80	55	154.80	R567 404.30	R4.70
64	0.1	R13.91	R559 788.35	0.94	R147.12	0.37	R0.50	0.857	R14.10	7.21	101.60	55	156.60	R564 935.05	R5.96
65	0.72	R14.94	R566 673.90	0.22	R91.30	0.91	R1.03	0.456	R13.35	7.21	96.20	55	151.20	R572 201.70	R4.26
66	0.94	R18.31	R589 202.35	0.13	R84.73	0.96	R1.81	0.783	R13.85	7.21	99.80	55	154.80	R595 977.05	R4.12
67	0.23	R14.18	R561 593.30	0.17	R87.65	0.66	R0.71	0.239	R12.10	7.21	87.19	55	142.19	R566 839.90	R4.05
68	0.66	R14.81	R565 804.85	0.5	R109.62	0.42	R0.53	0.284	R12.10	7.21	87.19	55	142.19	R571 284.55	R4.70
69	0.27	R14.21	R561 793.85	0.58	R111.83	0.64	R0.70	0.469	R13.35	7.21	96.20	55	151.20	R567 051.55	R4.86
70	0.16	R14.03	R560 590.55	0.49	R109.35	0.49	R0.59	0.635	R13.60	7.21	98.00	55	153.00	R565 781.65	R4.80
71	0.66	R14.81	R565 804.85	0.19	R89.11	0.84	R1.00	0.454	R13.35	7.21	96.20	55	151.20	R571 284.55	R4.19
72	0.87	R15.60	R571 086.00	0.65	R113.77	0.66	R0.71	0.777	R13.85	7.21	99.80	55	154.80	R576 858.00	R4.96

73	0.39	R14.41	R563 130.85	0.47	R108.79	0.81	R0.99	0.651	R13.60	7.21	98.00	55	153.00	R568 462.55	R4.80
74	0.33	R14.32	R562 529.20	0.9	R131.73	0.53	R0.62	0.892	R14.10	7.21	101.60	55	156.60	R567 827.60	R5.50
75	0.73	R14.97	R566 874.45	0.71	R115.42	0.64	R0.70	0.465	R13.35	7.21	96.20	55	151.20	R572 413.35	R4.97
76	0.09	R13.91	R559 788.35	0.18	R88.38	0.65	R0.71	0.155	R10.75	7.21	77.46	55	132.46	R564 935.05	R3.98
77	0.5	R14.59	R564 334.15	0.2	R89.84	0.93	R1.04	0.141	R10.75	7.21	77.46	55	132.46	R569 732.45	R4.03
78	0.99	R19.01	R593 881.85	0.36	R101.52	0.32	R0.47	0.203	R12.10	7.21	87.19	55	142.19	R600 915.55	R4.46
79	0.79	R15.15	R568 077.75	0.3	R97.14	0.6	R0.67	0.718	R13.85	7.21	99.80	55	154.80	R573 683.25	R4.46
80	0.39	R14.41	R563 130.85	0.7	R115.15	0.48	R0.58	0.961	R14.35	7.21	103.40	55	158.40	R568 462.55	R5.03
81	0.52	R14.62	R564 534.70	0.84	R119.01	0.76	R0.97	0.768	R13.85	7.21	99.80	55	154.80	R569 944.10	R5.12
82	0.81	R15.22	R568 545.70	0.62	R112.94	0.35	R0.49	0.958	R14.35	7.21	103.40	55	158.40	R574 177.10	R4.96
83	0.77	R15.12	R567 877.20	0.14	R85.46	0.38	R0.51	0.108	R10.75	7.21	77.46	55	132.46	R573 471.60	R3.88
84	0.76	R15.08	R567 609.80	0.75	R116.53	0.63	R0.69	0.078	R10.50	7.21	75.66	55	130.66	R573 189.40	R4.80
85	0.39	R14.41	R563 130.85	0.34	R100.06	0.87	R1.01	0.121	R10.75	7.21	77.46	55	132.46	R568 462.55	R4.33
86	0.56	R14.69	R565 002.65	0.23	R92.03	0.5	R0.59	0.073	R10.50	7.21	75.66	55	130.66	R570 437.95	R4.06
87	0.65	R14.79	R565 671.15	0.89	R127.88	0.91	R1.03	0.479	R13.60	7.21	98.00	55	153.00	R571 143.45	R5.37
88	0.59	R14.74	R565 336.90	0.32	R98.60	0.92	R1.03	0.765	R13.85	7.21	99.80	55	154.80	R570 790.70	R4.51
89	0.83	R15.27	R568 879.95	0.86	R119.57	0.89	R1.02	0.758	R13.85	7.21	99.80	55	154.80	R574 529.85	R5.14
90	0.95	R18.40	R589 804.00	0.97	R158.65	0.4	R0.52	0.598	R13.60	7.21	98.00	55	153.00	R596 612.00	R6.27
91	0.42	R14.45	R563 398.25	0.35	R100.79	0.39	R0.51	0.502	R13.60	7.21	98.00	55	153.00	R568 744.75	R4.54
92	0.77	R15.12	R567 877.20	0.76	R116.80	1	R3.18	0.995	R14.35	7.21	103.40	55	158.40	R573 471.60	R5.16
93	0.96	R18.48	R590 338.80	0.71	R115.42	0.98	R2.50	0.196	R12.10	7.21	87.19	55	142.19	R597 176.40	R4.93
94	0.74	R15.04	R567 342.40	0.19	R89.11	0.35	R0.49	0.883	R14.10	7.21	101.60	55	156.60	R572 907.20	R4.23
95	0.74	R15.04	R567 342.40	0.31	R97.87	0.6	R0.67	0.669	R13.60	7.21	98.00	55	153.00	R572 907.20	R4.46
96	0.82	R15.23	R568 612.55	0.25	R93.49	0.45	R0.56	0.944	R14.10	7.21	101.60	55	156.60	R574 247.65	R4.36
97	0.74	R15.04	R567 342.40	0.16	R86.92	0.93	R1.04	0.873	R14.10	7.21	101.60	55	156.60	R572 907.20	R4.18
98	0.87	R15.60	R571 086.00	0.32	R98.60	0.47	R0.57	0.099	R10.50	7.21	75.66	55	130.66	R576 858.00	R4.26
99	0.18	R14.09	R560 991.65	0.48	R109.07	0.79	R0.98	0.845	R14.10	7.21	101.60	55	156.60	R566 204.95	R4.84
100	0.12	R13.94	R559 988.90	0.19	R89.11	0.82	R1.00	0.912	R14.10	7.21	101.60	55	156.60	R565 146.70	R4.25

101	0.9	R17.33	R582 651.05	0.95	R150.96	0.41	R0.53	0.166	R12.10	7.21	87.19	55	142.19	R589 063.15	R5.93
102	0.74	R15.04	R567 342.40	0.89	R127.88	0.33	R0.47	0.58	R13.60	7.21	98.00	55	153.00	R572 907.20	R5.35
103	0.7	R14.91	R566 473.35	0.89	R127.88	0.7	R0.82	0.986	R14.35	7.21	103.40	55	158.40	R571 990.05	R5.41
104	0.53	R14.64	R564 668.40	0.97	R158.65	0.78	R0.98	0.387	R13.35	7.21	96.20	55	151.20	R570 085.20	R6.26
105	0.61	R14.75	R565 403.75	0.89	R127.88	0.6	R0.67	0.339	R13.10	7.21	94.40	55	149.40	R570 861.25	R5.32
106	0.45	R14.48	R563 598.80	0.65	R113.77	0.38	R0.51	0.381	R13.35	7.21	96.20	55	151.20	R568 956.40	R4.91
107	0.17	R14.08	R560 924.80	0.39	R103.71	0.88	R1.02	0.106	R10.75	7.21	77.46	55	132.46	R566 134.40	R4.44
108	0.43	R14.47	R563 531.95	0.13	R84.73	0.36	R0.49	0.386	R13.35	7.21	96.20	55	151.20	R568 885.85	R4.05
109	0.25	R14.19	R561 660.15	0.62	R112.94	0.54	R0.62	0.987	R14.35	7.21	103.40	55	158.40	R566 910.45	R4.96
110	0.68	R14.85	R566 072.25	0.35	R100.79	0.47	R0.57	0.103	R10.50	7.21	75.66	55	130.66	R571 566.75	R4.32
111	0.12	R13.94	R559 988.90	0.52	R110.17	0.69	R0.79	0.14	R10.75	7.21	77.46	55	132.46	R565 146.70	R4.63
112	0.27	R14.21	R561 793.85	0.99	R166.35	0.76	R0.97	0.576	R13.60	7.21	98.00	55	153.00	R567 051.55	R6.51
113	0.59	R14.74	R565 336.90	0.68	R114.59	0.86	R1.01	0.264	R12.10	7.21	87.19	55	142.19	R570 790.70	R4.86
114	0.29	R14.25	R562 061.25	0.94	R147.12	0.61	R0.68	0.359	R13.10	7.21	94.40	55	149.40	R567 333.75	R5.89
115	0.44	R14.47	R563 531.95	0.7	R115.15	0.82	R1.00	0.677	R13.60	7.21	98.00	55	153.00	R568 885.85	R4.99
116	0.48	R14.55	R564 066.75	0.84	R119.01	0.75	R0.97	0.162	R12.10	7.21	87.19	55	142.19	R569 450.25	R4.99
117	0.63	R14.77	R565 537.45	0.91	R135.58	0.91	R1.03	0.572	R13.60	7.21	98.00	55	153.00	R571 002.35	R5.60
118	0.29	R14.25	R562 061.25	0.77	R117.08	0.66	R0.71	0.627	R13.60	7.21	98.00	55	153.00	R567 333.75	R5.04
119	0.8	R15.20	R568 412.00	0.87	R119.84	0.34	R0.48	0.876	R14.10	7.21	101.60	55	156.60	R574 036.00	R5.15
120	0.46	R14.51	R563 799.35	0.2	R89.84	0.46	R0.56	0.868	R14.10	7.21	101.60	55	156.60	R569 168.05	R4.26
121	0.88	R16.16	R574 829.60	0.88	R124.04	0.45	R0.56	0.461	R13.35	7.21	96.20	55	151.20	R580 808.80	R5.22
122	0.34	R14.35	R562 729.75	0.54	R110.73	0.49	R0.59	0.671	R13.60	7.21	98.00	55	153.00	R568 039.25	R4.84
123	0.21	R14.14	R561 325.90	0.36	R101.52	0.61	R0.68	0.44	R13.35	7.21	96.20	55	151.20	R566 557.70	R4.55
124	0.18	R14.09	R560 991.65	0.72	R115.70	0.63	R0.69	0.381	R13.35	7.21	96.20	55	151.20	R566 204.95	R4.98
125	0.1	R13.91	R559 788.35	0.41	R105.17	0.69	R0.79	0.248	R12.10	7.21	87.19	55	142.19	R564 935.05	R4.58
126	0.69	R14.86	R566 139.10	0.64	R113.49	0.39	R0.51	0.096	R10.50	7.21	75.66	55	130.66	R571 637.30	R4.70
127	0.79	R15.15	R568 077.75	0.77	R117.08	0.93	R1.04	0.226	R12.10	7.21	87.19	55	142.19	R573 683.25	R4.94
128	0.07	R13.84	R559 320.40	0.29	R96.41	0.96	R1.81	0.515	R13.60	7.21	98.00	55	153.00	R564 441.20	R4.45

129	0.51	R14.62	R564 534.70	0.72	R115.70	0.53	R0.62	0.926	R14.10	7.21	101.60	55	156.60	R569 944.10	R5.03
130	0.34	R14.35	R562 729.75	0.69	R114.87	0.92	R1.03	0.339	R13.10	7.21	94.40	55	149.40	R568 039.25	R4.94
131	0.02	R13.58	R557 582.30	0.97	R158.65	0.58	R0.65	0.523	R13.60	7.21	98.00	55	153.00	R562 606.90	R6.27
132	0.8	R15.20	R568 412.00	0.78	R117.36	0.85	R1.01	0.847	R14.10	7.21	101.60	55	156.60	R574 036.00	R5.09
133	0.65	R14.79	R565 671.15	0.69	R114.87	0.83	R1.00	0.88	R14.10	7.21	101.60	55	156.60	R571 143.45	R5.01
134	0.33	R14.32	R562 529.20	0.74	R116.25	0.34	R0.48	0.374	R13.35	7.21	96.20	55	151.20	R567 827.60	R4.99
135	0.59	R14.74	R565 336.90	0.2	R89.84	0.76	R0.97	0.387	R13.35	7.21	96.20	55	151.20	R570 790.70	R4.21
136	0.32	R14.31	R562 462.35	0.7	R115.15	0.88	R1.02	0.528	R13.60	7.21	98.00	55	153.00	R567 757.05	R4.99
137	0.24	R14.19	R561 660.15	0.53	R110.45	0.85	R1.01	0.909	R14.10	7.21	101.60	55	156.60	R566 910.45	R4.88
138	0.68	R14.85	R566 072.25	0.49	R109.35	0.39	R0.51	0.964	R14.35	7.21	103.40	55	158.40	R571 566.75	R4.85
139	0.6	R14.74	R565 336.90	0.68	R114.59	0.66	R0.71	0.21	R12.10	7.21	87.19	55	142.19	R570 790.70	R4.85
140	0.7	R14.91	R566 473.35	0.48	R109.07	0.79	R0.98	0.419	R13.35	7.21	96.20	55	151.20	R571 990.05	R4.79
141	0.57	R14.73	R565 270.05	0.83	R118.74	0.88	R1.02	0.516	R13.60	7.21	98.00	55	153.00	R570 720.15	R5.09
142	0.29	R14.25	R562 061.25	0.45	R108.09	0.38	R0.51	0.255	R12.10	7.21	87.19	55	142.19	R567 333.75	R4.65
143	0.83	R15.27	R568 879.95	0.44	R107.36	0.48	R0.58	0.474	R13.60	7.21	98.00	55	153.00	R574 529.85	R4.74
144	0.83	R15.27	R568 879.95	0.87	R119.84	0.75	R0.97	0.638	R13.60	7.21	98.00	55	153.00	R574 529.85	R5.13
145	0.22	R14.17	R561 526.45	0.57	R111.56	0.44	R0.55	0.26	R12.10	7.21	87.19	55	142.19	R566 769.35	R4.76
146	0.98	R18.80	R592 478.00	0.43	R106.63	0.39	R0.51	0.306	R12.10	7.21	87.19	55	142.19	R599 434.00	R4.61
147	0.54	R14.66	R564 802.10	0.24	R92.76	0.93	R1.04	0.308	R12.10	7.21	87.19	55	142.19	R570 226.30	R4.21
148	0.16	R14.03	R560 590.55	0.96	R154.81	0.6	R0.67	0.752	R13.85	7.21	99.80	55	154.80	R565 781.65	R6.18
149	0.02	R13.58	R557 582.30	0.14	R85.46	0.73	R0.91	0.931	R14.10	7.21	101.60	55	156.60	R562 606.90	R4.14
150	0.8	R15.20	R568 412.00	0.54	R110.73	0.93	R1.04	0.305	R12.10	7.21	87.19	55	142.19	R574 036.00	R4.75

III. Traditional Inspection Monte Carlo Analysis Data

Initial Cost			Vehicle Operating Cost						
			Fuel Cost				Service and Repair		
Iteration	Probability	Cost	Probability	Fuel Price	Fuel factor	Cost (C)	Cost (C)	Running Cost (C)	Total Cost
1	0.143	R194.09	0.216	R12.10	7.21	87.19	55	142.19	R11.13
2	0.983	R334.10	0.978	R14.35	7.21	103.40	55	158.40	R18.29
3	0.185	R203.86	0.37	R13.35	7.21	96.20	55	151.20	R11.70
4	0.857	R282.99	0.097	R10.50	7.21	75.66	55	130.66	R15.46
5	0.19	R205.02	0.78	R13.85	7.21	99.80	55	154.80	R11.80
6	0.641	R272.75	0.841	R13.85	7.21	99.80	55	154.80	R15.19
7	0.326	R236.65	0.965	R14.35	7.21	103.40	55	158.40	R13.42
8	0.736	R277.25	0.828	R13.85	7.21	99.80	55	154.80	R15.41
9	0.364	R245.49	0.624	R13.60	7.21	98.00	55	153.00	R13.80
10	0.353	R242.93	0.308	R12.10	7.21	87.19	55	142.19	R13.57
11	0.668	R274.03	0.257	R12.10	7.21	87.19	55	142.19	R15.12
12	0.346	R241.30	0.345	R13.10	7.21	94.40	55	149.40	R13.56
13	0.133	R191.77	0.653	R13.60	7.21	98.00	55	153.00	R11.12
14	0.797	R280.14	0.766	R13.85	7.21	99.80	55	154.80	R15.56
15	0.842	R282.27	0.867	R14.10	7.21	101.60	55	156.60	R15.68
16	0.967	R326.10	0.622	R13.60	7.21	98.00	55	153.00	R17.83
17	0.601	R270.85	0.423	R13.35	7.21	96.20	55	151.20	R15.05
18	0.702	R275.64	0.425	R13.35	7.21	96.20	55	151.20	R15.29
19	0.168	R199.91	0.302	R12.10	7.21	87.19	55	142.19	R11.42
20	0.808	R280.66	0.832	R13.85	7.21	99.80	55	154.80	R15.58
21	0.484	R265.31	0.578	R13.60	7.21	98.00	55	153.00	R14.80
22	0.564	R269.10	0.2	R12.10	7.21	87.19	55	142.19	R14.88
23	0.885	R285.10	0.725	R13.85	7.21	99.80	55	154.80	R15.80
24	0.455	R263.93	0.704	R13.85	7.21	99.80	55	154.80	R14.74

25	0.261	R221.53	0.243	R12.10	7.21	87.19	55	142.19	R12.50
26	0.653	R273.32	0.297	R12.10	7.21	87.19	55	142.19	R15.09
27	0.418	R258.05	0.291	R12.10	7.21	87.19	55	142.19	R14.32
28	0.943	R314.10	0.506	R13.60	7.21	98.00	55	153.00	R17.23
29	0.457	R264.03	0.215	R12.10	7.21	87.19	55	142.19	R14.62
30	0.218	R211.53	0.376	R13.35	7.21	96.20	55	151.20	R12.09
31	0.446	R264.56	0.728	R13.85	7.21	99.80	55	154.80	R14.78
32	0.545	R268.20	0.881	R14.10	7.21	101.60	55	156.60	R14.98
33	0.919	R302.10	0.843	R14.10	7.21	101.60	55	156.60	R16.67
34	0.981	R333.10	0.275	R12.10	7.21	87.19	55	142.19	R18.08
35	0.29	R228.28	0.389	R13.35	7.21	96.20	55	151.20	R12.93
36	0.775	R279.10	0.588	R13.60	7.21	98.00	55	153.00	R15.48
37	0.329	R237.35	0.317	R13.10	7.21	94.40	55	149.40	R13.36
38	0.555	R268.67	0.152	R10.75	7.21	77.46	55	132.46	R14.76
39	0.645	R272.94	0.806	R13.85	7.21	99.80	55	154.80	R15.19
40	0.743	R277.58	0.711	R13.85	7.21	99.80	55	154.80	R15.43
41	0.385	R250.37	0.344	R13.10	7.21	94.40	55	149.40	R14.01
42	0.527	R267.35	0.692	R13.85	7.21	99.80	55	154.80	R14.92
43	0.289	R228.05	0.797	R13.85	7.21	99.80	55	154.80	R12.95
44	0.974	R329.60	0.247	R12.10	7.21	87.19	55	142.19	R17.90
45	0.638	R272.61	0.625	R13.60	7.21	98.00	55	153.00	R15.16
46	0.139	R193.16	0.065	R10.50	7.21	75.66	55	130.66	R10.96
47	0.277	R225.26	0.462	R13.35	7.21	96.20	55	151.20	R12.77
48	0.244	R217.58	0.529	R13.60	7.21	98.00	55	153.00	R12.41
49	0.496	R265.88	0.802	R13.85	7.21	99.80	55	154.80	R14.84
50	0.337	R239.21	0.084	R10.50	7.21	75.66	55	130.66	R13.27
51	0.315	R234.09	0.096	R10.50	7.21	75.66	55	130.66	R13.01
52	0.873	R283.74	0.688	R13.85	7.21	99.80	55	154.80	R15.74
53	0.237	R215.95	0.77	R13.85	7.21	99.80	55	154.80	R12.35
54	0.513	R266.68	0.13	R10.75	7.21	77.46	55	132.46	R14.66

55	0.257	R220.60	0.581	R13.60	7.21	98.00	55	153.00	R12.56
56	0.53	R267.49	0.06	R10.50	7.21	75.66	55	130.66	R14.68
57	0.629	R272.18	0.854	R14.10	7.21	101.60	55	156.60	R15.18
58	0.359	R244.33	0.348	R13.10	7.21	94.40	55	149.40	R13.71
59	0.883	R284.10	0.228	R12.10	7.21	87.19	55	142.19	R15.63
60	0.991	R338.10	0.294	R12.10	7.21	87.19	55	142.19	R18.33
61	0.434	R261.77	0.645	R13.60	7.21	98.00	55	153.00	R14.62
62	0.851	R282.70	0.807	R13.85	7.21	99.80	55	154.80	R15.68
63	0.594	R270.52	0.649	R13.60	7.21	98.00	55	153.00	R15.06
64	0.302	R231.07	0.766	R13.85	7.21	99.80	55	154.80	R13.10
65	0.603	R270.95	0.153	R10.75	7.21	77.46	55	132.46	R14.87
66	0.128	R190.60	0.953	R14.35	7.21	103.40	55	158.40	R11.11
67	0.859	R283.08	0.277	R12.10	7.21	87.19	55	142.19	R15.58
68	0.798	R280.19	0.692	R13.85	7.21	99.80	55	154.80	R15.56
69	0.594	R270.52	0.25	R12.10	7.21	87.19	55	142.19	R14.95
70	0.937	R311.10	0.744	R13.85	7.21	99.80	55	154.80	R17.10
71	0.25	R218.98	0.822	R13.85	7.21	99.80	55	154.80	R12.50
72	0.952	R318.60	0.315	R12.10	7.21	87.19	55	142.19	R17.35
73	0.68	R274.60	0.722	R13.85	7.21	99.80	55	154.80	R15.28
74	0.674	R274.31	0.094	R10.50	7.21	75.66	55	130.66	R15.02
75	0.664	R273.84	0.095	R10.50	7.21	75.66	55	130.66	R15.00
76	0.575	R269.62	0.482	R13.60	7.21	98.00	55	153.00	R15.01
77	0.259	R221.07	0.505	R13.60	7.21	98.00	55	153.00	R12.58
78	0.449	R265.26	0.946	R14.10	7.21	101.60	55	156.60	R14.83
79	0.736	R277.25	0.485	R13.60	7.21	98.00	55	153.00	R15.39
80	0.865	R283.36	0.176	R12.10	7.21	87.19	55	142.19	R15.59
81	0.97	R327.60	0.254	R12.10	7.21	87.19	55	142.19	R17.80
82	0.89	R287.60	0.478	R13.60	7.21	98.00	55	153.00	R15.91
83	0.62	R271.75	0.655	R13.60	7.21	98.00	55	153.00	R15.12
84	0.825	R281.47	0.847	R14.10	7.21	101.60	55	156.60	R15.64

85	0.953	R319.10	0.497	R13.60	7.21	98.00	55	153.00	R17.48
86	0.358	R244.09	0.899	R14.10	7.21	101.60	55	156.60	R13.77
87	0.286	R227.35	0.108	R10.75	7.21	77.46	55	132.46	R12.69
88	0.974	R329.60	0.946	R14.10	7.21	101.60	55	156.60	R18.05
89	0.251	R219.21	0.15	R10.75	7.21	77.46	55	132.46	R12.29
90	0.934	R309.60	0.198	R12.10	7.21	87.19	55	142.19	R16.90
91	0.979	R332.10	0.134	R10.75	7.21	77.46	55	132.46	R17.93
92	0.964	R324.60	0.233	R12.10	7.21	87.19	55	142.19	R17.65
93	0.277	R225.26	0.169	R12.10	7.21	87.19	55	142.19	R12.68
94	0.193	R205.72	0.271	R12.10	7.21	87.19	55	142.19	R11.71
95	0.61	R271.28	0.734	R13.85	7.21	99.80	55	154.80	R15.11
96	0.516	R266.82	0.962	R14.35	7.21	103.40	55	158.40	R14.93
97	0.281	R226.19	0.941	R14.10	7.21	101.60	55	156.60	R12.88
98	0.533	R267.63	0.193	R12.10	7.21	87.19	55	142.19	R14.80
99	0.432	R261.30	0.578	R13.60	7.21	98.00	55	153.00	R14.60
100	0.586	R270.14	0.975	R14.35	7.21	103.40	55	158.40	R15.09
101	0.274	R224.56	0.213	R12.10	7.21	87.19	55	142.19	R12.65
102	0.734	R277.16	0.904	R14.10	7.21	101.60	55	156.60	R15.42
103	0.264	R222.23	0.646	R13.60	7.21	98.00	55	153.00	R12.64
104	0.731	R277.01	0.191	R12.10	7.21	87.19	55	142.19	R15.27
105	0.381	R249.44	0.94	R14.10	7.21	101.60	55	156.60	R14.04
106	0.166	R199.44	0.293	R12.10	7.21	87.19	55	142.19	R11.39
107	0.153	R196.42	0.98	R14.35	7.21	103.40	55	158.40	R11.40
108	0.751	R277.96	0.511	R13.60	7.21	98.00	55	153.00	R15.43
109	0.641	R272.75	0.224	R12.10	7.21	87.19	55	142.19	R15.06
110	0.324	R236.19	0.469	R13.35	7.21	96.20	55	151.20	R13.32
111	0.895	R290.10	0.617	R13.60	7.21	98.00	55	153.00	R16.03
112	0.93	R307.60	0.871	R14.10	7.21	101.60	55	156.60	R16.95
113	0.81	R280.76	0.625	R13.60	7.21	98.00	55	153.00	R15.57
114	0.243	R217.35	0.516	R13.60	7.21	98.00	55	153.00	R12.40

115	0.5	R266.07	0.212	R12.10	7.21	87.19	55	142.19	R14.73
116	0.605	R271.04	0.362	R13.10	7.21	94.40	55	149.40	R15.05
117	0.995	R340.10	0.678	R13.60	7.21	98.00	55	153.00	R18.53
118	0.641	R272.75	0.395	R13.35	7.21	96.20	55	151.20	R15.15
119	0.892	R288.60	0.71	R13.85	7.21	99.80	55	154.80	R15.98
120	0.532	R267.58	0.628	R13.60	7.21	98.00	55	153.00	R14.91
121	0.598	R270.71	0.1	R10.50	7.21	75.66	55	130.66	R14.84
122	0.841	R282.23	0.607	R13.60	7.21	98.00	55	153.00	R15.64
123	0.45	R265.49	0.827	R13.85	7.21	99.80	55	154.80	R14.82
124	0.246	R218.05	0.844	R14.10	7.21	101.60	55	156.60	R12.47
125	0.584	R270.05	0.309	R12.10	7.21	87.19	55	142.19	R14.92
126	0.547	R268.29	0.95	R14.35	7.21	103.40	55	158.40	R15.00
127	0.213	R210.37	0.812	R13.85	7.21	99.80	55	154.80	R12.07
128	0.625	R271.99	0.996	R14.35	7.21	103.40	55	158.40	R15.18
129	0.646	R272.99	0.61	R13.60	7.21	98.00	55	153.00	R15.18
130	0.855	R282.89	0.315	R12.10	7.21	87.19	55	142.19	R15.57
131	0.194	R205.95	0.357	R13.10	7.21	94.40	55	149.40	R11.79
132	0.347	R241.53	0.11	R10.75	7.21	77.46	55	132.46	R13.40
133	0.683	R274.74	0.093	R10.50	7.21	75.66	55	130.66	R15.04
134	0.806	R280.57	0.728	R13.85	7.21	99.80	55	154.80	R15.58
135	0.319	R235.02	0.46	R13.35	7.21	96.20	55	151.20	R13.26
136	0.563	R269.05	0.153	R10.75	7.21	77.46	55	132.46	R14.78
137	0.375	R248.05	0.573	R13.60	7.21	98.00	55	153.00	R13.93
138	0.548	R268.34	0.219	R12.10	7.21	87.19	55	142.19	R14.84
139	0.339	R239.67	0.207	R12.10	7.21	87.19	55	142.19	R13.41
140	0.335	R238.74	0.908	R14.10	7.21	101.60	55	156.60	R13.50
141	0.862	R283.22	0.152	R10.75	7.21	77.46	55	132.46	R15.49
142	0.331	R237.81	0.784	R13.85	7.21	99.80	55	154.80	R13.44
143	0.152	R196.19	0.389	R13.35	7.21	96.20	55	151.20	R11.32
144	0.605	R271.04	0.666	R13.60	7.21	98.00	55	153.00	R15.08

145	0.234	R215.26	0.676	R13.60	7.21	98.00	55	153.00	R12.29
146	0.419	R258.28	0.636	R13.60	7.21	98.00	55	153.00	R14.44
147	0.354	R243.16	0.576	R13.60	7.21	98.00	55	153.00	R13.69
148	0.472	R264.74	0.256	R12.10	7.21	87.19	55	142.19	R14.66
149	0.677	R274.45	0.289	R12.10	7.21	87.19	55	142.19	R15.14
150	0.292	R228.74	0.577	R13.60	7.21	98.00	55	153.00	R12.97

Appendix C: Image Processing Program Code

The code of the image processing program can be found at my supervisor Mr Chris Jurgens. He can be contacted to provide the code. The image processing program can be used as a runnable JAR file if the user has the software package, Java runtime environment installed.